Budget of nitrous acid (HONO) and its impacts on atmospheric oxidation capacity at an urban site in the fall season of Guangzhou, China

Yihang Yu[1,2,†], Peng Cheng[1,2,5,*,†], Huirong Li[1,2], Wenda Yang[1,2], Baobin Han[1,2], Wei Song[3], Weiwei Hu[3], Xinming Wang[3], Bin Yuan[4,5], Min Shao[4,5], Zhijiong Huang[4], Zhen Li[4], Junyu Zheng[4,5], Haichao Wang[6] and Xiaofang Yu[1,2]

[1]Institute of Mass Spectrometry and Atmospheric Environment, Jinan University, Guangzhou 510632, China
[2]Guangdong Provincial Engineering Research Center for Online Source Apportionment System of Air Pollution, Guangzhou 510632, China
[3]State Key Laboratory of Organic Geochemistry, Guangzhou Institute of Geochemistry, Chinese Academy of Sciences, Guangzhou 510640, China
[4]Institute for Environmental and Climate Research, Jinan University, Guangzhou 511443, China
[5]Guangdong-Hongkong-Macau Joint Laboratory of Collaborative Innovation for Environmental Quality, Guangzhou 511443, China
[6]School of Atmospheric Sciences, Sun Yat-Sen University, Zhuhai, China.

†These authors contribute equally to this paper.

Correspondence to: Peng Cheng (chengp@jnu.edu.cn)

Abstract. Nitrous acid (HONO) can produce hydroxyl radicals (OH) by photolysis and plays an important role in atmospheric photochemistry. Over the years, high concentrations of HONO have been observed in the Pearl River Delta region (PRD) of China, which may be one reason for the elevated atmospheric oxidation capacity. A comprehensive atmospheric observation campaign was conducted at an urban site in Guangzhou from 27 September to 9 November 2018. During the period, HONO was measured from 0.02 to 4.43 ppbv with an average of 0.74 ± 0.70 ppbv. The emission ratios (HONO/NOx) of 0.9 ± 0.4% were derived from 11 fresh plumes. The primary emission rates of HONO at night were calculated to be between 0.04 ± 0.02 ppbv h^{-1} and 0.30 ± 0.15 ppbv h^{-1} based on a high-resolution emission inventory. The HONO formation rate by the homogeneous reaction of OH + NO at night was 0.26 ± 0.08 ppbv h^{-1}, which can be seen as secondary results from primary emission. They were both much higher than the increase rate of HONO (0.02 ppbv h^{-1}) during night. The soil emission rate of HONO at night was calculated to be 0.019 ± 0.001 ppbv h^{-1}. Assuming dry deposition as the dominant removal process of HONO at night, a deposition velocity of at least ~ ~~2.5~~ 1.8 cm s^{-1} is required to balance the direct emissions and OH + NO reaction. Correlation analysis shows that NH_3 and relative humidity (RH) may participate in the heterogeneous transformation from NO_2 to HONO at night. In the daytime, the average primary emission P_{emis} was 0.12 ± 0.01 ppbv h^{-1}, and the homogeneous reaction P_{OH+NO} was 0.79 ± 0.61 ppbv h^{-1}, larger than the unknown sources $P_{Unknown}$ (0.65 ± 0.46 ppbv h^{-1}). These results suggest primary emissions as a key factor affecting HONO at our site, both during daytime and nighttime. Similar to previous studies, the daytime unknown source of HONO, $P_{Unknown,}$ appeared to be

related to the photo-enhanced conversion of NO_2. The daytime average OH production rates by photolysis of HONO was 3.7 × 10^6 cm^{-3} s^{-1}, lower than that from $O^1D + H_2O$ at 4.9 × 10^6 cm^{-3} s^{-1}. Simulations of OH and O_3 with the Master Chemical Mechanism (MCM) box model suggested strong enhancement effect of HONO on OH and O_3 by 59% and 68.8%, respectively, showing a remarkable contribution of HONO to the atmospheric oxidation in the fall season of Guangzhou.

Keywords: HONO; Atmospheric oxidation capacity; Budget analysis; Heterogeneous reaction

1 Introduction

As a primary source of hydroxyl radical (OH), HONO has attracted scientific researchers' great interest. The photolysis of HONO (Reaction R1) can generate a substantial amount of OH, which is a primary atmosphere oxidant that is responsible for oxidizing and removing of most natural and anthropogenic trace gases. Additionally, OH radicals can initiate the oxidation of the volatile organic compounds (VOC) to produce hydroperoxyl radicals (HO_2) and organic peroxy radicals (RO_2). These free radicals can further lead to the formation of ozone (O_3) in the presence of nitrogen oxides (NOx) (Xue et al., 2016; Finlayson-Pitts and Pitts, 2000; Hofzumahaus et al., 2009; Lelieveld et al., 2016; Tan et al., 2018). Up to 33–92% OH formation can be attributed to HONO photolysis in both rural and urban sites (Kleffmann et al., 2005; Michoud et al., 2012; Tan et al., 2017; Xue et al., 2020; Hendrick et al., 2014). However, the detailed formation mechanisms of HONO are still not well understood and the observed HONO concentrations cannot be completely explained by current research (Sörgel et al., 2011a; Kleffmann et al., 2005; Sarwar et al., 2008; Liu et al., 2019a; Lee et al., 2016; Liu et al., 2020c).

$$HONO + h\nu \rightarrow OH + NO \ (300\ nm < \lambda < 405\ nm) \quad (R1)$$

HONO sources generally include direct emissions, homogeneous reactions and heterogeneous reactions. HONO can be directly emitted into the troposphere from combustion processes such as biomass burning, vehicle exhaust, domestic heating, and industrial exhaust (Liu et al., 2019b; Neuman et al., 2016; Nie et al., 2015; Kramer et al., 2020). The emission ratios of HONO/NOx of traffic sources have been estimated in the range of 0.3%–0.85% through tunnel experiments considering various engine types (Kirchstetter et al., 1996; Kurtenbach et al., 2001; Kramer et al., 2020). Soil nitrite formed through the processes of biological nitrification and denitrification, were proposed to be a prominent HONO source in the troposphere (Maljanen et al., 2013; Oswald et al., 2013; Wu et al., 2019; Su et al., 2011). Subsequently, biological soil crusts (biocrusts) were also found to release HONO (Weber et al., 2015; Porada et al., 2019; Meusel et al., 2018). In addition, an acid displacement mechanism has also been suggested to contribute substantial fraction of daytime HONO formation (VandenBoer et al., 2015). The reaction between NO and OH is considered an important pathway of HONO formation when OH and NO concentrations are relatively high (Alicke et al., 2002; Li et al., 2012; Pagsberg et al., 1997; Qin et al., 2009; Wong et al., 2011), whereas this pathway often cannot explain the observed HONO concentrations, especially during

daytime (Tang et al., 2015; Li et al., 2010; Czader et al., 2012; Tong et al., 2016). Bejan et al. (2006) studied the HONO formation by the photolysis of different gaseous nitrophenols and proposed that the photolysis of nitrophenols can partly explain the observed HONO formation in the urban atmosphere. ~~Li et al. (2008) suggested that the homogeneous reaction between water vapor (H_2O) and electronically excited NO_2 ($\lambda > 420$ nm) can form OH and HONO. While the reaction rate and yield of this reaction are still under discussion (Carr et al., 2009), and this formation mechanism can only marginally contribute to the formation of atmospheric HONO (Amedro et al., 2011; Crowley and Carl, 1997; Sörgel et al., 2011a; Wong et al., 2011; Dillon and Crowley, 2018)~~. Zhang and Tao (2010) proposed that HONO can form through homogeneous nucleation of NH_3, NO_2 and H_2O. However, this reaction has not yet been observed in field experiments nor tested by laboratory studies. Li et al. (2014b) proposed that the reaction of NO_2 with $HO_2 \cdot H_2O$ could be a gas-phase source of HONO in the lower troposphere. But Ye et al. (2015) estimated the HONO yield of the reaction of NO_2 with $HO_2 \cdot H_2O$ was only 3%. Additionally, heterogeneous reactions on different kinds of surfaces have also been found to be possible significant HONO sources, including heterogeneous reactions of NO_2 on ground surfaces (Meusel et al., 2016; VandenBoer et al., 2013), building surfaces (Acker et al., 2006; Indarto, 2012), ocean surfaces (Wen et al., 2019; Wojtal et al., 2011; Yang et al., 2021a), soil surfaces (Laufs et al., 2017; Kleffmann et al., 2003; Yang et al., 2021b) and vegetation surfaces (Stutz et al., 2002; Marion et al., 2021), etc. Photosensitized reduction reaction of NO_2 on organic surfaces (such as humic acids and aromatics) has been considered as an effective pathway to generate HONO (George et al., 2005; Stemmler et al., 2006; Liu et al., 2020a; Ammar et al., 2010; Brigante et al., 2008; Cazoir et al., 2014; Sosedova et al., 2011). The heterogeneous conversion of NO_2 to HONO on humid surfaces have also been studied (Finlayson-Pitts et al., 2003; Ammann et al., 1998; Ndour et al., 2008) and this conversion can be further promoted by ambient NH_3 and SO_2 (Ge et al., 2019; Wang et al., 2016; Xu et al., 2019; Li et al., 2018b; Wang et al., 2021). In addition, HONO can also be formed by heterogeneous conversion of NO_2 on secondary organic aerosols and fresh soot particles (Arens et al., 2001; Ziemba et al., 2010), but the contributions and mechanisms are still under discussion (Arens et al., 2001; Aubin and Abbatt, 2007; Bröske et al., 2003; Qin et al., 2009). Both field observations and laboratory studies found that the photolysis of adsorbed HNO_3 and particulate nitrate (NO_3^-) made an important contribution to HONO formation (Ye et al., 2016; Ye et al., 2017; Zhou et al., 2003; Zhou et al., 2002b; Zhou et al., 2011; Ziemba et al., 2010). However, Laufs and Kleffmann (2016) obtained a very low HNO_3 photolysis frequency in laboratory, almost two orders of magnitude lower than the result by Zhou et al. (2003).

The Pearl River Delta (PRD) region is one of the biggest city clusters in the world with dense population and large anthropogenic emissions. Rapid economic development and urbanization have led to severe deterioration of air quality in this region, which was characterized by atmospheric "compound pollution" with concurrent high fine particulate matter ($PM_{2.5}$) and ozone (O_3) (Tang, 2004; Chan and Yao, 2008; Yue et al., 2010; Wang et al., 2017b; Xue et al., 2014; Zheng et al., 2010). While O_3 has been increasing along with reduced $PM_{2.5}$ over recent years in the region (Li et al., 2014a; Liao et al., 2020; Wang et al., 2009; Zhong et al., 2013; Lu et al., 2018), and has become the dominant factor of the air quality index exceeding the national standard (Feng et al., 2019), indicating the enhancement of atmospheric oxidation capacity. By far

two comprehensive atmospheric observations were conducted in the PRD region to detect OH radicals. High concentrations of OH radicals were observed both times, especially in the first time it was the highest ever-reported, which cannot be explained by the current knowledge of atmospheric chemistry (Hofzumahaus et al., 2009). Substantial level of HONO was suggested to be the major source of the OH–HO_2–RO_2 radical system in above two campaigns (Lu et al., 2012; Tan et al., 2019a). Moreover, high concentrations of HONO have also been confirmed in other observations in this area during last two decades ~~Numerous studies have observed high concentrations of atmospheric HONO in Guangzhou~~ (Hu et al., 2002; Su et al., 2008b; Su et al., 2008a; Qin et al., 2009; Li et al., 2012; Shao et al., 2004). Fast OH production through HONO photolysis may be a key factor for the increasing atmospheric oxidation capacity and ozone concentration in this area.

In this work, we performed continuous measurements of HONO, along with trace gases, photolysis frequencies and meteorological conditions at an urban site in Guangzhou from 27 September to 9 November 2018, as part of the field campaign named "Particles, Radicals, Intermediates from oxiDation of primary Emissions in Greater Bay Area" (PRIDE-GBA2018). Benefiting from numerous prior field observational studies in the PRD region, our study stands in a strong position to ensure high quality of data acquisition and analysis of HONO, along with a full suite of other chemical species, providing a unique and valuable opportunity to refine our knowledge of HONO sources and sinks, as well as the role of HONO in the photochemistry of O_3 and OH in such a region with extensive air pollution as well as rigorous emission control over recent years. A high resolution (3 km × 3 km) NOx emission inventory for the Guangzhou city (Huang et al., 2021) was used to estimate the primary emission rates of NOx and HONO, which would reduce the uncertainty of HONO primary emission rate. By analysing our observational data, both nighttime HONO formation pathways and daytime HONO budgets have been investigated in this study. The contribution of HONO photolysis to OH production has been calculated and compared with that of O_3 photolysis and ozonolysis of alkenes. The impact of HONO on atmospheric oxidation capacity and O_3 formation is further investigated using a chemical box model based on Master Chemical Mechanism (MCMv3.3.1).

2 Experiment

2.1 Observation site

The sampling site (23.14° N, 113.36° E) is located in the Guangzhou Institute of Geochemistry Chinese Academy of Sciences (GIGCAS). The instruments were deployed in the cabin on the rooftop of a seven-story building (~ 40 m above the ground). The site is surrounded by residential communities and schools, with no industrial manufacturers or power plants around, representing a typical urban environment in the PRD region. The south China Expressway and Guangyuan Expressway, both with heavy traffic loading, are located at west and south of the site, with distances of about 300 m. As a result, the site often experienced local emissions from traffic. The location and surroundings of the site are shown in Fig. S1.

2.2 Measurements

HONO was measured by a custom-built LOPAP (LOng Path Absorption Photometer) (Heland et al., 2001; Kleffmann et al., 2006). More information about our custom-built LOPAP (including principle, quality assurance/quality control, instrument parameters and intercomparison) are introduced in supplement information. ~~HONO was measured by a custom-built LOPAP (LOng Path Absorption Photometer) based on wet chemical sampling and photometric detection (Heland et al., 2001). Ambient air is sampled into an external sampling unit consisting of two similar stripping coils in series. Almost all of the HONO and a small fraction of interfering substances (PAN, HNO_3, NO_2, etc.) are absorbed in solution in the first stripping coil, while in the second stripping coil only the interfering species are absorbed. To minimize the potential interferences, we assume the interferences absorbed in the first and the second coil are the same, so the real HONO concentration in the atmosphere is determined by subtracting the measured signal of the second coil from the measured signal of the first coil. The absorption solution R1 is a mixture reagent of 1 L hydrochloric acid (HCl) (37 % volume fraction) and 100 g sulfanilamide dissolved in 9 L pure water. The dye solution R2, 2 g n (1 naphtyl) ethylendiamine dihydrchloride (NEDA) dissolved in 10 L pure water, is then reacted with the absorption solution from two stripping coils pumped by a peristaltic pump to form colored azo dye. The light absorbing colored azo dye is then pumped through a debubbler by the peristaltic pump and flows into the detection unit, which consists of two liquid waveguide capillary cells (World Precision Instrument, LWCC), one LED light source (Ocean Optics), two miniature spectrometers (Ocean Optics, Maya2000Pro) and several optical fibers. To correct for the small zero-drifts in the instrument's baseline, the zero measurements were conducted every 12 h by introducing zero air (highly pure nitrogen) at a flow rate of 1 L min^{-1}. During the instrument's operation, the instrument calibration was performed every week using the standard sodium nitrite ($NaNO_2$) solution. The detection limit, time resolution and uncertainty of the measurement were 5 pptv, 15 min and 8 %, respectively. More detailed information of LOPAP instrument can be found in previous studies (Heland et al., 2001; Kleffmann et al., 2006; Kleffmann et al., 2002)~~.

In addition to HONO, ambient VOCs were measured using a TH-300B On-Line VOCs Monitoring System involving detection technology of ultralow temperature preconcentration coupled with gas chromatography-mass spectrometry (GC/MS) with the time resolution of 1 h. NOx (NO + NO_2) was measured by a nitrogen oxides analyzer (Thermo Scientific, Model 42i), which used a NO-NO_x chemiluminescence detector equipped with a molybdenum-based converter with the time resolution and detection limit of 1 min and 1 ppbv respectively. It should be noted that the molybdenum oxide (MoO) converters may also convert some NOz (= NOy - NOx) (e.g., HONO, peroxyacetyl nitrate (PAN), HNO_3, and so on.) species to NO and hence could overestimate the ambient NO_2 concentrations. The degree of overestimation depends on both air mass age and the composition of NOy. At our site that was greatly affected by fresh emissions, the relative interferences of NOz to NO_2 have been estimated to be around 10%, which is closed to the results of Xu et al. (2013) and negligible for our discussion of HONO budget. O_3 was measured by an O_3 analyzer (Thermo Scientific, Model 49i) via ultraviolet absorption method with the time resolution and detection limit of 1 min and 1 ppbv respectively. SO_2 was measured by SO_2 analyzer

(Thermo Scientific, Model 43i) via pulsed fluorescence method with the time resolution and detection limit of 1 min and 1 ppbv respectively. CO was measured by a CO analyzer (Thermo Scientific, Model 48i) with the time resolution and detection limit of 1 min and 0.1 ppmv respectively. NH_3 was measured by laser absorption spectroscopy (PICARRO, G2508) with the time resolution and detection limit of 1 min and 1 ppbv respectively. Gaseous HNO_3 was detected by a Time-Of-Flight Chemical Ionization Mass Spectrometer (Aerodyne Research Inc., TOF-CIMS) with a time resolution of 1 min. And particulate nitrate (NO_3^-) was measured by Time-Of-Flight Accelerator Mass Spectrometry (Aerodyne Research Inc., TOF-AMS) with a time resolution of 1 min. $PM_{2.5}$ was measured by a Beta Attenuation Monitor (MET One Instruments Inc., BAM-1020) with the time resolution and detection limit of 1 h and 4.0 μg m^{-3} respectively. The meteorological data, including temperature (T), relative humidity (RH) and wind speed and direction (WS, WD) were recorded by Vantage Pro2 Weather Station (Davis Instruments Inc., Vantage Pro2) with the time resolution of 1 min. Photolysis frequencies including J(HONO), J(NO_2), J(H_2O_2) and J(O^1D) were measured by a filter radiometry (Focused Photonics Inc., PFS-100) with a time resolution of 1 min.

2.3 Box model

To evaluate the influence of HONO chemistry on the atmospheric oxidation capacity, a zero dimensional box model (Framework for 0-Dimensional Atmospheric Modeling–F0AM) based on the Master Chemical Mechanism (MCMv3.3.1) (Wolfe et al., 2016; Jenkin et al., 2003; Jenkin et al., 2015) was applied to calculate the concentrations of O_3 and OH radicals. The Master Chemical Mechanism describes atmospheric gas-phase organic chemistry in detail which has been widely used in atmospheric chemistry modelling. Kinetic rate coefficients were derived from the MCM v3.3.1 website (http://mcm.leeds.ac.uk/MCM). The model was implemented in MATLAB 2012. In this work, the boundary layer diurnal cycle has been modified and the dilution factor k_{dil} was set at 86400^{-1} s. The solar zenith angle (SZA) ~~solar altitude~~ was calculated based on longitude, latitude and time of the observation. Photolysis rate correction coefficient j_{corr} was set to 1. The model simulation was constrained by hourly averaged measurement data, including HONO, NO, NO_2, CO, SO_2, VOC species (listed in Table S2), and temperature, water vapor, wind speed, wind direction, pressure and photolysis frequencies J(NO_2), J(HONO), J(O^1D) and J(H_2O_2). Other non-measured photolysis frequencies were calculated according to Eq. (1) (Jenkin et al., 1997), and then scaled by the measured J(NO_2):

$$J_i = L_i \cos(\chi)^{M_i} \exp(-N_i \sec(\chi)) \quad (1)$$

where χ represents the solar zenith angle (SZA); L_i, M_i and N_i are the photolysis parameters under clear sky conditions which were taken from Jenkin et al. (1997). The heterogeneous processes as well as deposition of chemical species were not considered in this model. The simulation results were evaluated by comparing against the measurements, and index of agreement (IOA), a statistical parameter was employed for the evaluation (Jeon et al., 2018; Xing et al., 2019; Li et al., 2010). Two simulations with and without HONO constrained by measured values were conducted to examine the impact of HONO on OH and O_3 formation.

3 Results and discussion

3.1 Data overview

The time series of meteorological parameters and pollutants during the campaign are shown in Fig. 1. The HONO concentrations ranged from 0.02 to 4.43 ppbv with an average of 0.74 ± 0.70 ppbv. Table 1 summarizes the HONO observations reported in PRD region since 2002. HONO appears to have shown a decreasing trend in Guangzhou, as improvement of air quality in Guangzhou was witnessed during the past decade. Spikes of NO occurred frequently, even up to 134.8 ppbv, as a result of traffic emissions from two major roads near the site. The concentrations of NO_2, SO_2, NH_3 and $PM_{2.5}$ ranged from 5.4–102.0 ppbv, 0–6.3 ppbv, 2.8–7.8 ppbv and 4–109 μg m^{-3} respectively with the average values of 50.8 ± 17.2 ppbv, 1.9 ± 1.2 ppbv, 6.3 ± 2.7 ppbv, and 36 ± 16 μg m^{-3} respectively. The O_3 concentrations ranged from 0.3–149.8 ppbv with an average peak concentration of 73.9 ± 28.4 ppbv. During the observation, the temperature ranged from 17 °C to 30 °C with an average of 24 ± 3 °C, and the relative humidity ranged from 28% to 97% with an average of 70 ± 17%. The average wind speed was 6.8 ± 4.5 m s^{-1}, while the maximum wind speed was 22.7 m s^{-1}. There was a pollution period from 8th to 10th October with elevated $PM_{2.5}$ (60 ± 12 μg m^{-3}) and HONO (0.94 ± 0.58 ppbv). By contrast, from 29 October to 3 November, efficient ventilation driven by strong winds (> 11 m s^{-1}) led to low levels of most pollutants in this period, with average concentrations of $PM_{2.5}$ and HONO at 28 ± 11 μg m^{-3} and 0.56 ± 0.34 ppbv, respectively.

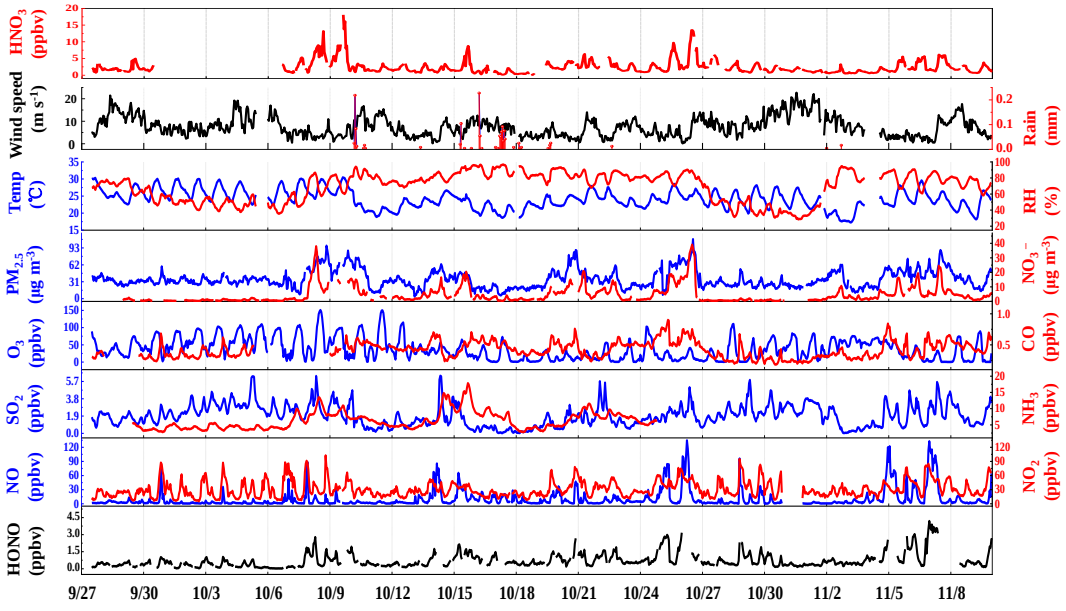

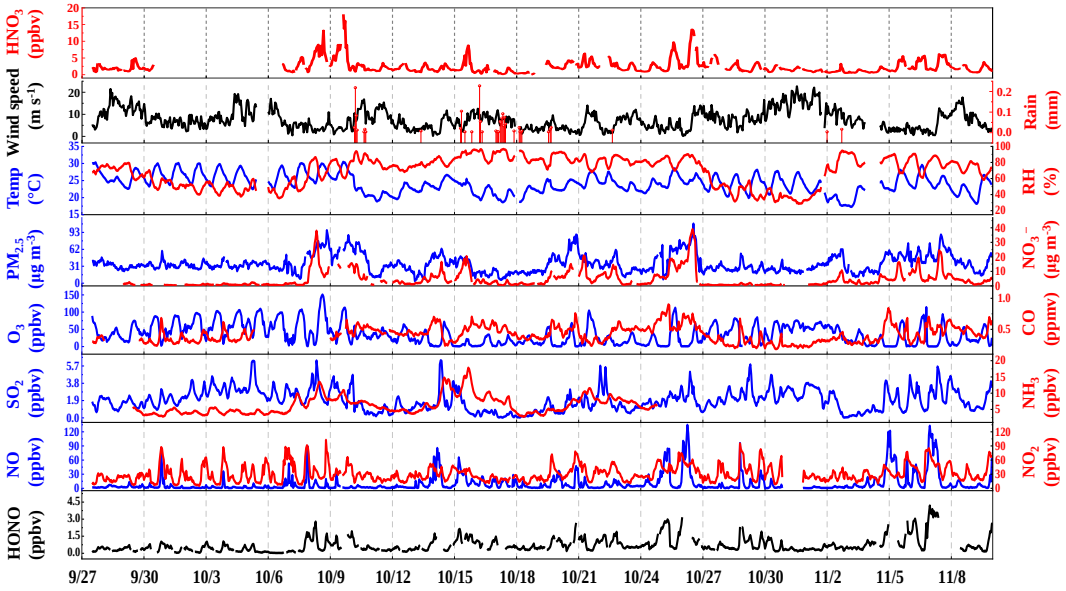

Figure 1. Temporal variations of meteorological and pollutants during the observation period.

Table 1. Overview of the ambient HONO, NO_2 and NOx measurement, as well as the ratios of HONO/NO_2 in the PRD region ordered chronologically. Data from Guangzhou are in italic.

Location	Date	HONO (ppbv)	HONO (ppbv)		NO_2 (ppbv)		NOx (ppbv)		HONO/NO_2		Reference
			Night	Day	Night	Day	Night	Day	Night	Day	
Guangzhou (China)	*Jul 2002*	*1.89*	~~	~~	~~	~~	~~	~~	~~	~~	*1*
	Nov 2002	*1.52*	~~	~~	~~	~~	~~	~~	~~	~~	
Xinken (China)	*Oct–Nov 2004*	*1.20*	*1.30*	*0.80*	*34.8*	*30.0*	*37.8*	*40.0*	*0.037*	*0.027*	*2*
Back Garden (China)	*Jul 2006*	*0.93*	*0.95*	*0.24*	*16.5*	*4.5*	*20.9*	*5.5*	*0.057*	*0.053*	*3*
Guangzhou (China)	*Jul 2006*	*2.80*	*3.50*	*2.00*	*20.0*	*30.0*	~~	~~	*0.175*	*0.067*	*4*
Guangzhou (China)	*Oct 2015*	*1.64*	*2.25*	*0.90*	*40.5*	*27.3*	*57.9*	*39.8*	*0.060*	*0.030*	*5*
Guangzhou (China)	*Jul 2016*	*1.03*	*1.27*	*0.70*	*35.0*	*25.9*	*66.3*	*52.1*	*0.040*	*0.070*	*6*
This work	*Sep–Nov 2018*	*0.74*	*0.91*	*0.44*	*36.9*	*23.3*	*47.7*	*30.1*	*0.026*	*0.022*	
Jiangmen (China)	Oct–Nov 2008	0.60	~~	0.48	~~	~~	~~	9.1	~~	~~	7
Hong Kong (China)	Aug 2011	0.66	0.66	0.70	21.8	18.1	29.3	29.3	0.031	0.042	8
	Nov 2011	0.93	0.95	0.89	27.2	29.0	37.2	40.6	0.034	0.030	
	Feb 2012	0.91	0.88	0.92	22.2	25.8	37.8	48.3	0.036	0.035	
	May 2012	0.35	0.33	0.40	14.7	15.0	19.1	21.1	0.022	0.030	
Hong Kong (China)	Sep–Dec 2012	0.13	~~	~~	~~	~~	~~	~~	~~	~~	9
Heshan (China)	Oct 2013	1.57	~~	~~	~~	~~	~~	~~	~~	~~	~~9~~10
Heshan (China)	Oct–Nov 2014	1.40	1.78	0.77	19.3	17.9	21.5	22.7	0.093	0.055	~~10~~11
Hong Kong (China)	Mar–May 2015	3.30	2.86	3.91	~~	~~	~~	~~	~~	~~	~~11~~12
Heshan (China)	Jan 2017	2.70	3.10	2.30	~~	~~	~~	~~	0.116	0.089	13

References：1. Hu et al. (2002); 2. Su et al. (2008a) and (Su et al., 2008b); 3. Li et al. (2012) and Su (2008); 4. Qin et al. (2009); 5. Tian et al. (2018); 6. Yang et al. (2017a); 7. Yang (2014); 8. Xu et al. (2015); 9. Zha et al. (2014); ~~9~~10. Yue et al. (2016); ~~10~~11. Liu (2017); ~~11~~12. Yun et al. (2017). 13. (Yun, 2018)

The time series of photolysis frequencies J(HONO), J(O^1D) and J(NO_2) in the whole observation period are shown in Fig. S~~2~~3. The maximum values of J(HONO), J(O^1D) and J(NO_2) are 1.58 × 10^{-3} s^{-1}, 2.54 × 10^{-5} s^{-1} and 9.31 × 10^{-3} s^{-1}, respectively. These J values tracked a similar diurnal pattern, reaching a maximum at noon with high solar radiation and decreasing to zero at night.

The diurnal variations of HONO, NO_2, HONO/NO_2, and NO are shown in Fig. 2. A daytime trough and a night-time peak of HONO were observed, as typically seen in cities and rural sites (Lee et al., 2016; Xue et al., 2020; Villena et al., 2011; Yang et al., 2021c). The observed high HONO concentration around 0.5 ppbv at daytime implies strong HONO production to balance its rapid loss through photolysis. NO_2 showed a similar diurnal pattern. It is worth noting that the diurnal variation of NO was quite similar to that of HONO, implying the potential association between them. Additionally, the observed large amount of NO (10.8 ± 17.2 ppbv) at night indicates strong primary emission near the site. As an indicator of NO_2 to HONO conversion, the ratio of HONO/NO_2 rose at night and decreased after sunrise due to photolysis, ranging from ~~1.4~~0.2% to ~~3.0~~9.1% with an average of 2.3 ± 1.3%, which is lower than most previous field observations in PRD region (Li et al., 2012; Qin et al., 2009; Xu et al., 2015), and is typical for relatively fresh plumes. Previous many field observations also reported low values of HONO/NO_2 ranging from 2% to 10% in freshly polluted air masses (Febo et al., 1996; Lammel and Cape, 1996; Sörgel et al., 2011b; Stutz et al., 2004; Zhou et al., 2007; Su et al., 2008a). The relatively stable and low value of HONO/NO_2 in nighttime seems to indicate the low contribution of heterogeneous reactions of NO_2 to HONO concentrations.

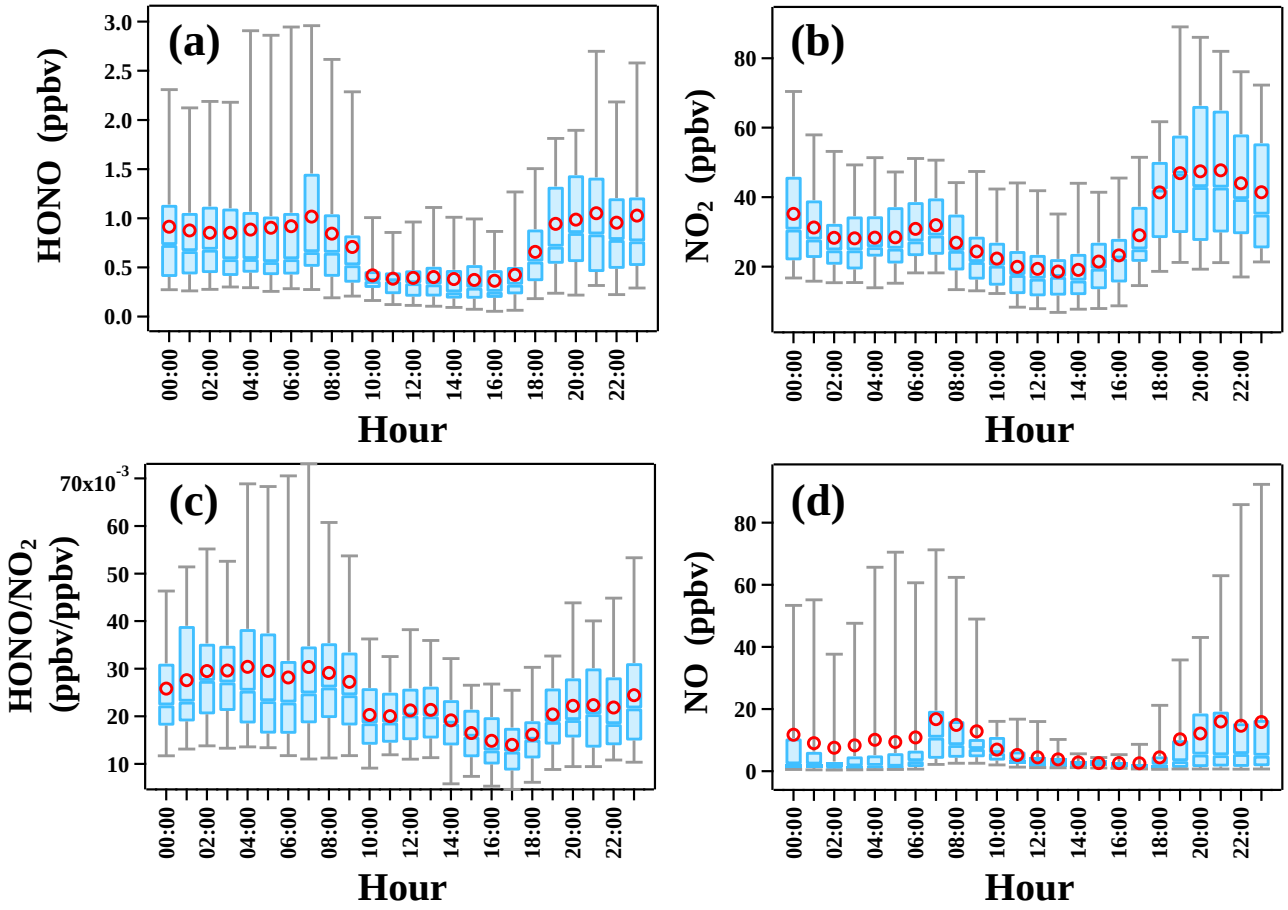

Figure 2. Diurnal profiles of HONO, NO_2, NO and HONO/NO_2 during the observation period. The blue line in the box and red circle refer to the median and mean, respectively. Boxes represent 25% to 75% of the data, and whiskers 95% of the data. The box plots presented in this study is generated by an Igor Pro-based computer program, Histbox (Wu et al., 2018).

3.2 Nocturnal HONO formation and sources

3.2.1 Direct emissions

As noted in Sect. 1, the site was expected to receive substantial direct emission of HONO from two major roads nearby. We obtained the emitted HONO/NOx ratios in fresh plumes defined with the following criteria (Xu et al., 2015):

(a) NOx > 49.7 ppbv (highest 25% of NOx data);

(b) NO/NOx > 0.8;

(c) good correlation between NOx and HONO ($R^2 > 0.70$, $P < 0.05$);

(d) short duration of plumes (< 2 h);

(e) global radiation < 10 W m^{-2} ($J(NO_2)$ < 0.25 × 10^{-3} s^{-1}).

During the campaign, 11 fresh plumes were identified to satisfy criteria (a)–(e) (see Table S~~1~~3). Two cases among them are shown in Fig. S~~3~~4. The HONO/NOx ratios in these selected plumes varied from 0.1% to 1.5% with an average value of 0.9 ± 0.4%, which is comparable to the average value of 1.2% measured in Hong Kong (Xu et al., 2015), 1.0% observed in Hong Kong (Yun et al., 2017), 0.79% measured in Nanjing (Liu et al., 2019b) and 0.69% observed in Changzhou (Shi et al., 2020b). It should be noted that the emission factor derived in this study is based on field observation and the screening criterion for fresh air mass is NO/NOx > 0.8, while the fresh air mass was characterized by NO/NOx > 0.9 in the tunnel experiments conducted by Kurtenbach et al. (2001), so the air masses we selected were still slightly aged and the emission factor derived in this study is slightly overestimated.

To evaluate ~~calculate~~ the primary emission ~~P_{emis}~~, three methods have been used in previous studies (Liu et al., 2019b; Liu et al., 2020b; Meng et al., 2020). In method (1), ~~P_{emis}~~ $HONO_{emis}$ (the primary emission's contribution to HONO concentration) is equal to the product of emission coefficient K and observed NOx concentration (Cui et al., 2018; Huang et al., 2017) (see Eq. (~~1~~2)). This method ignores the sink of NOx and HONO, as well as transport and convection. On this basis, the observed NOx is equal to the accumulation of NOx emission, and HONO emission is linearly related to NOx concentration. However, ubiquitous loss of NOx would increase the uncertainty of this method, especially during daytime. In method (2), primary emission rate P_{emis} is equal to the product of emission coefficient K and [ΔNOx], the increase of NOx concentration during Δt (Liu et al., 2019b; Zheng et al., 2020) (see Eq. (~~2~~3)). The promise of this method is similar to method (1), and it can only be used when NOx is increasing. As expected, a decrease in NOx would yield a negative HONO emission rate, which is unrealistic. In method (3), P_{emis} is equal to the product of emission coefficient K and NOx*, the NOx emission from source emission inventory (Michoud et al., 2014; Su et al., 2008b) (see Eq. (~~3~~4)). This method adheres to the definition of HONO emission rate, assuming that the primary sources are evenly mixed in a specific area. It is desirable that emission inventory data with high spatial and temporal resolution are used to obtain an accurate estimate.

~~$P_{emis} = K \times NOx$~~ $[HONO_{emis}] = K \times [NOx]$ (~~1~~2)

$P_{emis} = K \times [\Delta NOx]$ (~~2~~3)

$P_{emis} = K \times NOx^*$ (~~3~~4)

$P_{HONO} = \frac{[HONO]_{t2} - [HONO]_{t1}}{t_2 - t_1}$ (5)

In this study, we first used NOx emission rate from a high-resolution emission inventory (Huang et al., 2021) to calculate emission rate of HONO P_{emis} at night (18:00–6:00). The NOx emission rate was extracted from a 3 km × 3 km grid cell centred around our site. As a comparison, we also used the 2017 NOx emission inventory of Guangzhou city to repeat the

calculation. The two inventories are primarily different in spatial resolution. The high-resolution 3 km × 3 km data is expected to better represent local traffic emissions, whereas the city-level emission inventory represents the total emission. Since we cannot quantify the relative contribution of the local and regional emissions to this site, two results are used to represent upper and lower limits of the contribution of primary emissions to HONO. The nighttime height of the boundary layer is assuming to 200 m according to the previous study by Fan et al. (2008).

The observed HONO production/accumulation rate P_{HONO} is calculated by Eq. (5), where $[HONO]_{t1}$ and $[HONO]_{t2}$ represent the HONO concentration at 18:00 and 6:00 Local Time, respectively. Then an average P_{HONO} of 0.02 ppbv h^{-1} can be derived. Hourly HONO primary emission rates calculated with the two inventories are shown in Fig. 3. P_{emis} calculated with the high-resolution emission data （3 km × 3 km）shows a steep downward trend from 18:00 (0.56 ppbv h^{-1}) to 4:00 (0.14 ppbv h^{-1}), followed by an upward trend from 4:00 (0.14 ppbv h^{-1}) to 6:00 (0.25 ppbv h^{-1}). The average of P_{emis} is 0.30 ± 0.15 ppbv h^{-1}, far larger than the average accumulating rate of HONO at night (0.02 ppbv h^{-1}) derived from observed HONO variation. By contrast, P_{emis} with the city level emission data (Guangzhou) is much lower (0.04 ± 0.02 ppbv h^{-1}) and varied smoothly throughout the night~~, but is still larger than the observed HONO accumulation rate~~. Similar results have been obtained at urban sites (Liu et al., 2020b; Liu et al., 2020c) and a suburban site (Michoud et al., 2014), while the result at a rural site is much lower (Su et al., 2008b). The lower limit of the calculated P_{emis} is still larger than the observed HONO accumulation rate. Considering the uncertainty of the inventories (-25%–28%), P_{emis} may be overestimated or underestimated to the same extent. Nevertheless, ~~D~~direct emission of HONO ~~appears to be~~ is a large HONO source at night along with other sources of HONO that remain to be considered. Furthermore, a large sink of HONO was necessary to explain the observed trend of HONO.

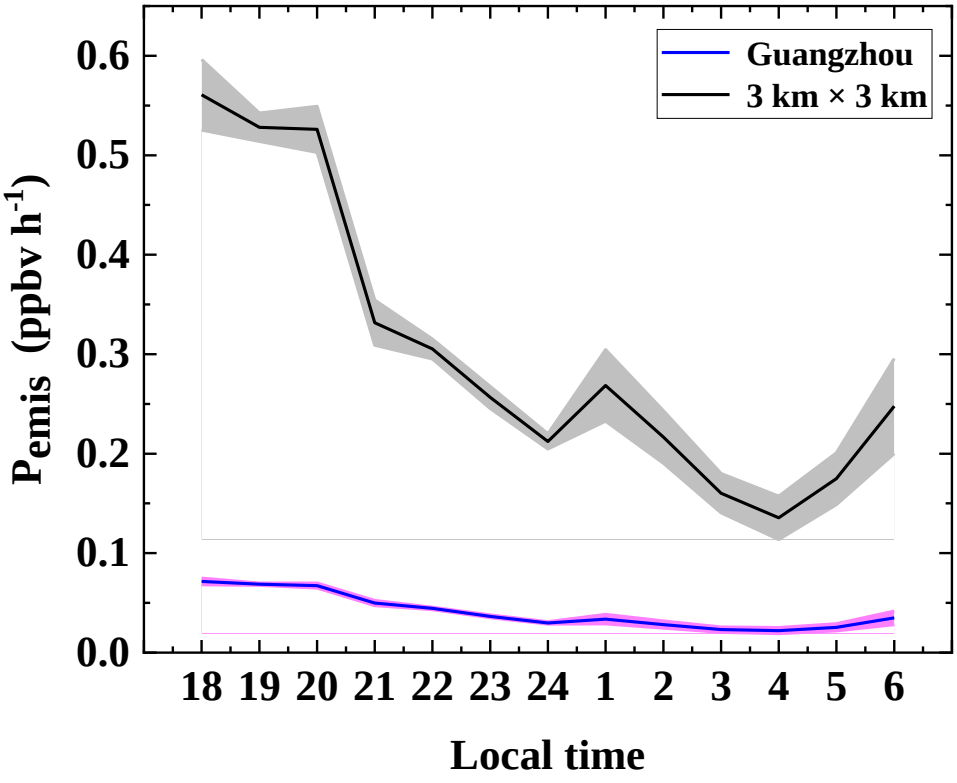
Guangzhou
3 km × 3 km
P_{emis} (ppbv h^{-1})
0.0
0.1
0.2
0.3
0.4
0.5
0.6
18 19 20 21 22 23 24 1 2 3 4 5 6
Local time

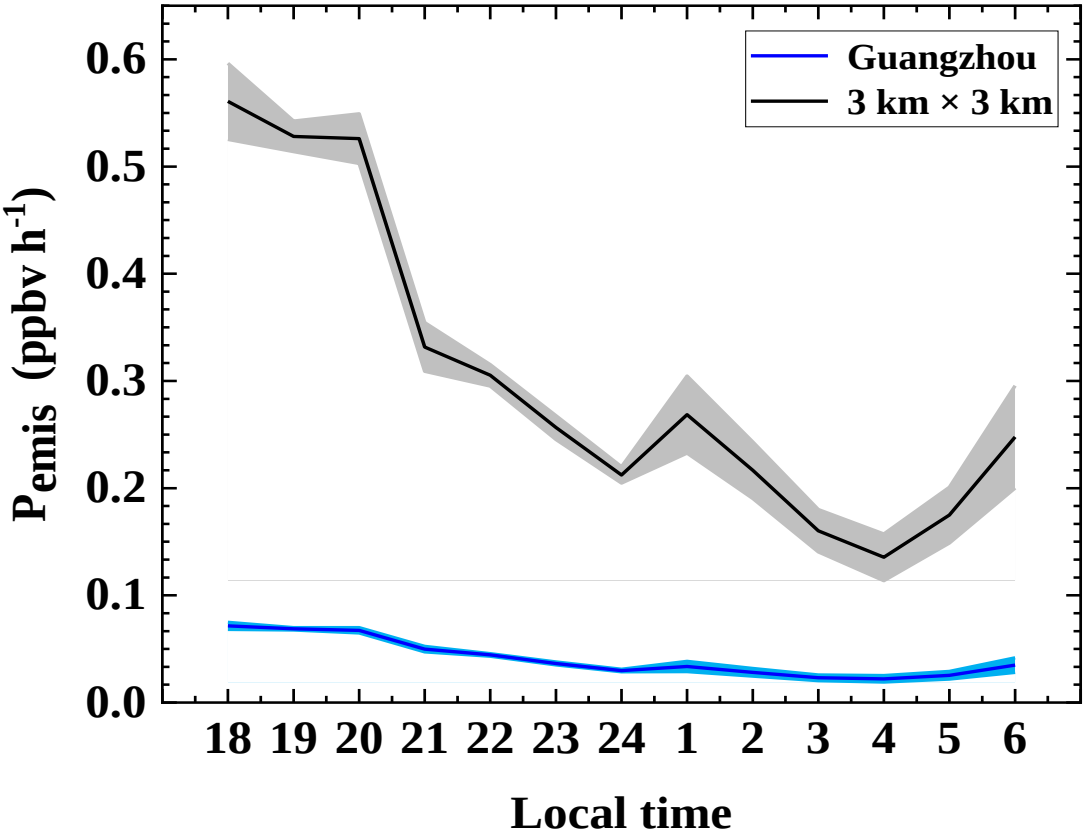

Figure 3. The nocturnal variation of HONO primary emission rates. The black and blue lines represent the HONO primary emission rates calculated by the 2017 NOx emission source inventory of the 3 km × 3 km grid cell centred on the Guangzhou Institute of Geochemistry and the 2017 NOx emission source inventory of Guangzhou city respectively. The coloured areas represent 1 – σ standard deviations.

Method (1) is also adopted here to calculate $[HONO]_{emis}$ ~~P_{emis}~~, and ~~P_{emis}~~$[HONO]_{emis}$/HONO can simply represent the primary emission's contribution to HONO. ~~The ratio of P_{emis}/HONO is 47 %, much higher than previous estimates in Shanghai (12.5 %) (Cui et al., 2018), Ji'nan (18 %) (Li et al., 2018a), Xi'an (23.6 %) (Huang et al., 2017) and Hong Kong (35.2 %) (Xu et al., 2015). It is possible that the observation site in this study is more strongly affected by primary emission from vehicle exhaust compared to those previous studies.~~ We summarized $[HONO]_{emis}$/[HONO] ratios obtained from urban sites in China (Table S4). The values varied at a wide range from 12% to 52%, and the difference of 2 times or more existed in different seasons at the same site. These indicate the complexity of the impact of source emissions on observation site. The ratio of $[HONO]_{emis}$/[HONO] at our site is at a high level of 47%, indicating that the site during the campaign is more strongly affected by primary emission from vehicle exhaust compared to most previous studies.

In addition to traffic emissions, we also estimated the HONO emission rate from soil P_{soil} (ppbv h^{-1}) according to Eq. (6~~4~~):

$$P_{soil} = \frac{\alpha F_{soil}}{H} \quad (6~~4~~)$$

where F_{soil} is the emission flux (g m^{-2} s^{-1}); H is the height of boundary layer (H, m) and was assumed to be 200 m (Fan et al., 2008); α is the conversion factor ($\alpha = \frac{1 \times 10^9 \times 3600 \times R \times T}{M \times P} = \frac{2.99 \times 10^{13} \times T}{M \times P}$); T is the temperature (K); M is the molecular weight (g mol^{-1}) and P is the atmospheric pressure (Pa). HONO emission flux from soil depends on the temperature, water content and nitrogen nutrient content of soil, which have been considered according to the parameters reported in the literature (Oswald et al., 2013)~~, assuming the site is surrounded by grassland. The water content was set at 35–45%.~~ Since grassland, coniferous forest and tropical rain forest are the typical plants in Guangzhou city area (Wu et al., 2015) and their emission fluxes are comparable (Oswald et al., 2013), emission flux from grassland was adopted to represent the soil HONO emission in Guangzhou. The average nighttime P_{soil} varied from 0.011 to 0.035 ppbv h^{-1}, with a mean value of 0.019 ± 0.001 ppbv h^{-1}. It is comparable to the lower limit of primary emission rate of 0.04 ± 0.02 ppbv h^{-1}.

3.2.2 NO + OH homogeneous reaction

The reaction between NO and OH acts as the principle homogenous HONO source. It can contribute a substantial fraction to HONO formation when NO and OH concentrations are high (Alicke et al., 2003; Liu et al., 2019b; Wong et al., 2011; Tong et al., 2015). Taking the homogeneous Reactions R2 and R3 into account, the net HONO homogeneous production rate can be calculated by following Eq. (7~~5~~):

$$NO + OH \rightarrow HONO \quad (R2)$$

$$HONO + OH \rightarrow NO_2 + H_2O \quad (R3)$$

$$P_{net} = k_{NO+OH}[NO][OH] - k_{HONO+OH}[HONO][OH] \quad (7~~5~~)$$

In Eq. (5~~7~~), k_{NO+OH} (7.2×10^{-12} cm^3 s^{-1}) and $k_{HONO+OH}$ (5.0×10^{-12} cm^3 s^{-1}) are the reaction rate constants of the Reactions R2 and R3 at 298 K, respectively (Li et al., 2012). Since the OH concentration was not measured, an average nighttime value of 1.0×10^6 cm^{-3} measured in Heshan in the PRD region in autumn of 2014 was assumed (Liu, 2017). As shown in Fig. 4, the variation of P_{net} is highly similar to NO, for the concentration of NO was 10 times larger than HONO. And the average value of P_{net} is 0.26 ± 0.08 ppbv h^{-1}, leading to a cumulative HONO contribution of 3.24 ppbv. However, the measured HONO only increased 0.26 ppbv in this period. It suggests that, (1) the reaction between NO and OH is adequate to explain the HONO increase in the whole night, even though other sources like NO_2 heterogeneous conversion might still exist; (2) except for HONO + OH, the strength of HONO sink should be at least 0.30~~0.25~~ ppbv h^{-1}, 5~~5~~6 times larger than that obtained by Li et al. (2012) and comparable to that by Hao et al. (2020).

We carried out sensitivity tests using one tenth, twice and half of assumed OH concentration (1.0×10^6 cm^{-3}) (Lou et al., 2010). As is shown in Table S5~~2~~, within the range of nighttime OH concentration, the cumulative production of the homogeneous reaction of NO + OH in this study are all larger than the averaged measured accumulation of HONO, indicating that taking a value within the range of the observed nighttime OH concentration will not affect the conclusion of this study.

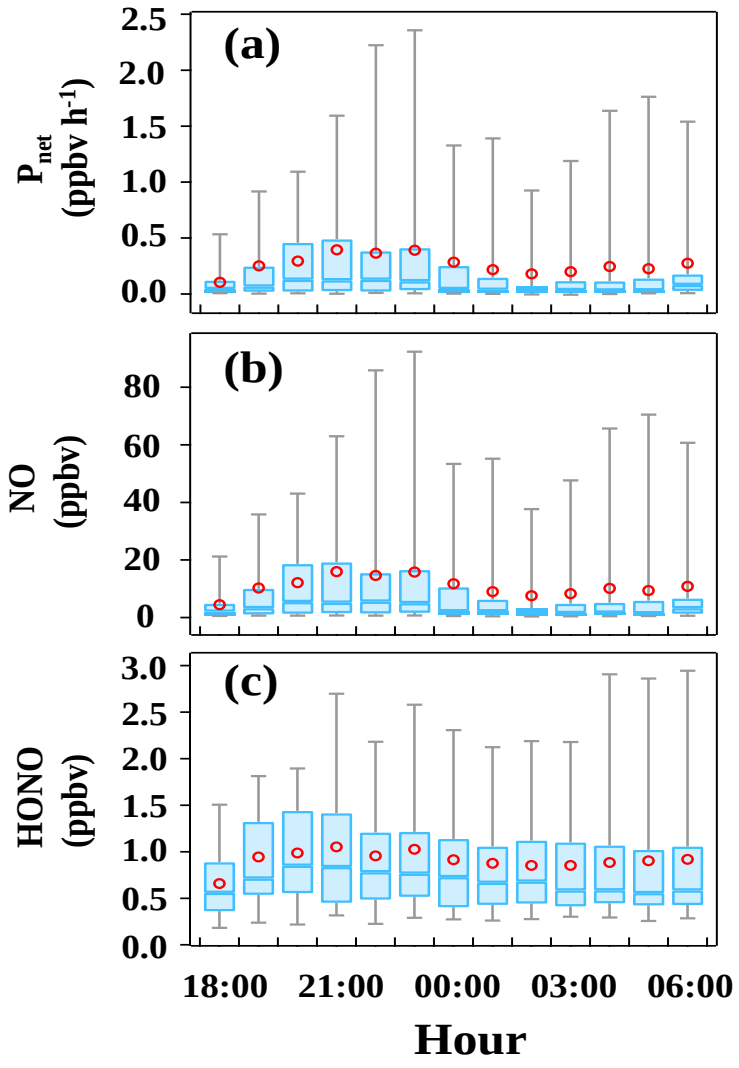

Figure 4. The mean nocturnal variation of P_{net}, HONO and NO. The blue line in the box and red circle refer to the median and mean, respectively. Boxes represent 25% to 75% of the data, and whiskers 95% of the data.

3.2.3 NO_2 to HONO heterogeneous conversion

Our analysis so far suggests that direct emissions and the homogeneous reaction between NO and OH are more than sufficient to explain the growth of HONO concentration through the night. The relatively high ~~good~~ correlation (R^2 = 0.5927) between HONO and NO is in line with this finding ~~provides further evidence~~(Fig. 5 (a)). In addition, correlation analysis was conducted to explore possible pathways of heterogeneous NO_2 to HONO conversion at night (18:00–6:00).

The ratio of HONO/NO_2 has often been used to indicate the heterogeneous conversion efficiency of NO_2 to HONO (Lammel and Cape, 1996; Stutz et al., 2002), for being less influenced by transport processes or convection. Figure 5 (c) shows a weak correlation (R^2 = 0.0638) between HONO/NO_2 and $PM_{2.5}$, suggesting that the formation of HONO on aerosol surfaces might not be the main pathway (Kalberer et al., 1999; Kleffmann et al., 2003; Wong et al., 2011; Zhang et al., 2009; Sörgel et al., 2011a; VandenBoer et al., 2013). Because the surface area of ground (including vegetation surface, building surface and soil, etc.) is generally larger than the surface area of aerosols (Zhang et al., 2016), some studies suggested that the heterogeneous reaction of NO_2 and water vapor on ground surfaces was the main source of HONO (Harrison and Kitto, 1994; Li et al., 2012; Wong et al., 2012). Furthermore, the correlations between HONO/NO_2 and NH_3 and RH are 0.3746 and 0.2381, respectively, and the correlation further improved between HONO/NO_2 and the product of NH_3 and RH (R^2 = 0.4597). Some studies proposed that NH_3 can decrease the free-energy barrier in hydrolysis of NO_2 thus enhance the HONO formation (Xu et al., 2019; Li et al., 2018b; Zhang and Tao, 2010; Wang et al., 2021).

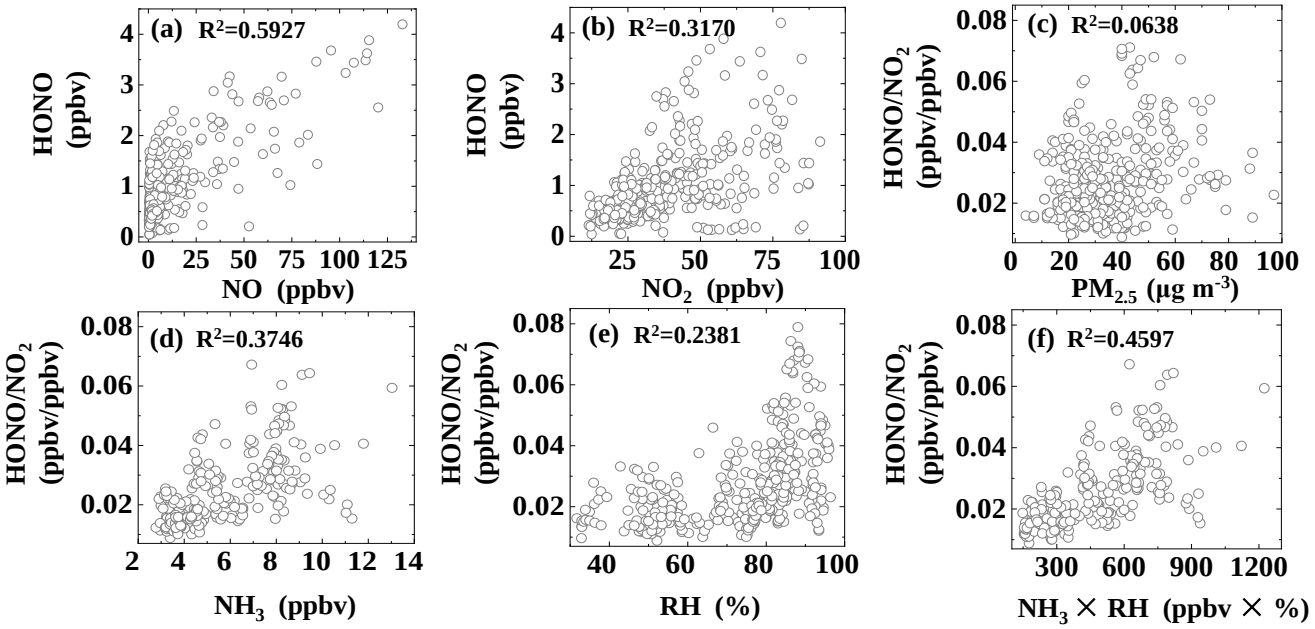

Figure 5. Correlations between HONO, HONO/NO_2 and various parameters during the time interval of 18:00–6:00.

In Fig. 6, we further explored the RH effect by focusing on high $HONO/NO_2$ values, i.e., the 5 highest $HONO/NO_2$ values for 5% RH intervals (Stutz et al., 2004). When RH was lower than 87.5%, $HONO/NO_2$ increased with RH, which is in accordance with the reaction kinetics of disproportionation reaction of NO_2 and H_2O. Furthermore, the slope of linear fitting between $HONO/NO_2$ and RH was much smaller for RH range of 30% ~ 70% (slope = 0.04%; $R^2 = 0.5202$) than for the RH range of 70% ~ 87.5% (slope = 0.25%, $R^2 = 0.8767$). Similar piecewise correlations between $HONO/NO_2$ and RH have been found in previous studies (Qin et al., 2009; Zhang et al., 2019b), which have been interpreted as evidence for the non-linear dependence of NO_2-to-HONO conversion efficiency on RH. Once the relative humidity exceeded 87.5%, NO_2-to-HONO conversion appeared to be inhibited by RH (slope = - 0.32%; $R^2 = 0.9750$). A possible explanation is that the number of water layers formed on various surfaces increased rapidly with RH, resulting in effective uptake of HONO and making the surface inaccessible or less reactive to NO_2. Previous studies also found fast growth of aqueous layers when RH over 70% for glass (Saliba et al., 2001) and over 80% for stone (Stutz et al., 2004). The tipping point inferred from ambient observations appear to vary across locales, likely reflecting the different composition of the ground surfaces, e.g., 60% for Chengdu (Yang et al., 2021c), 65–70% for Beijing (Wang et al., 2017a), 70% for Back Garden (Li et al., 2012), 75% for Shanghai (Wang et al., 2013), and 85% for Xi'an (Huang et al., 2017).

In sum, our correlation analysis for $HONO/NO_2$ suggests that nighttime heterogenous conversion of NO_2 into HONO at our site might be related to NH_3 and water vapor, whereas aerosol surfaces appeared unimportant.

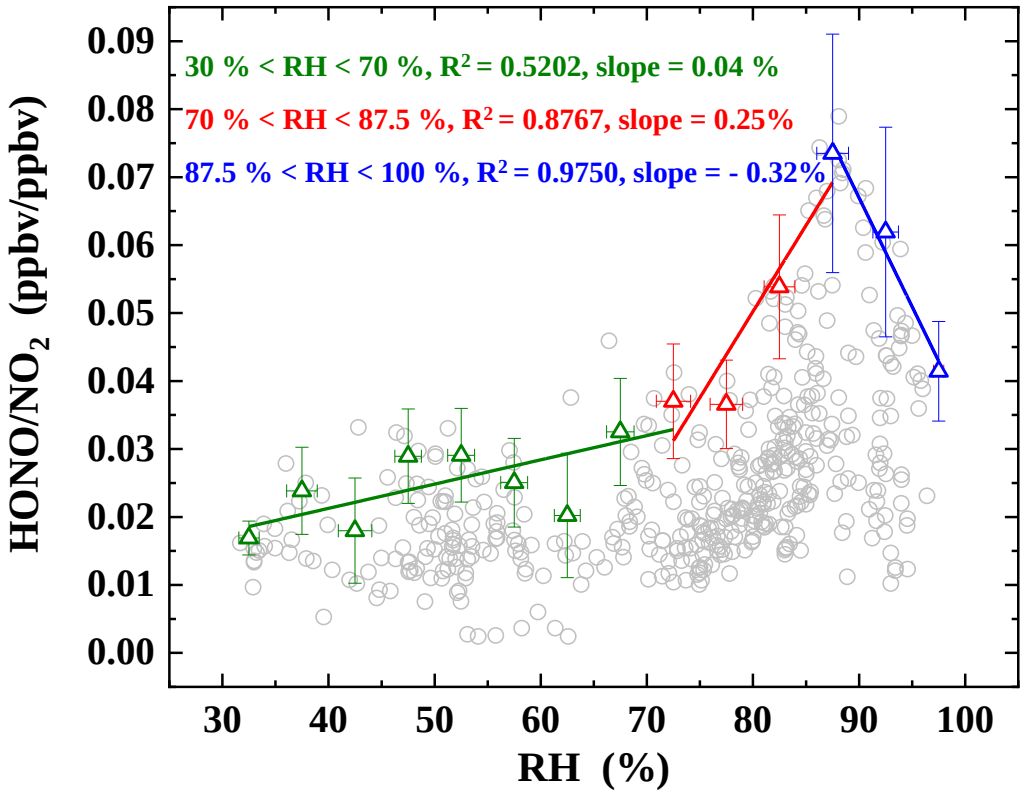

Figure 6. Scatter plot of $HONO/NO_2$ ratio against RH during nighttime from 18:00 to 6:00. Triangles are the average of top-5 $HONO/NO_2$ values in each 5% RH interval.

3.2.4 Removal of HONO through dry deposition

As discussed in Sect. 3.2.2, a sink of at least ~~0.25~~0.30 ppbv h^{-1} is required to balance the nighttime HONO production. Since the reactions of HONO + OH and HONO + HONO are negligible (Kaiser and Wu, 1977; Mebel et al., 1998), it is conceivable that HONO is mainly removed through deposition on the ground. HONO dry deposition velocity V_d can be estimated with Eq. (~~8~~6) :

$$\frac{d[HONO]}{dt} = P_{emis} + P_{soil} + P_{net} - \frac{V_d \times [HONO]}{H} \quad (~~8~~6)$$

The average deposition velocity V_d between 18:00–6:00 was calculated to be 1.8~~2.5~~ cm s^{-1}, which is within the range of prior researches (0.077~~0.5–6~~3 cm s^{-1}) (Harrison and Kitto, 1994; Harrison et al., 1996; Spindler et al.; Stutz et al., 2002; Li et al., 2012), and also consistent to the results derived from the HONO uptake coefficient on soil and ground (Donaldson et al.,

2014; VandenBoer et al., 2013). It should be noted that heterogeneous conversion of NO_2-HONO has not been taken into account, so 1.8~~2.5~~ cm s^{-1} is the lower limit of dry deposition velocity. High RH at night probably increased the amount of adsorbed water on the ground surfaces and facilitates dry deposition of HONO.

In sum, primary emission from vehicle exhaust (between 0.04 ± 0.02 ppbv h^{-1} and 0.30 ± 0.15 ppbv h^{-1}) and the homogeneous reaction of OH + NO (0.26 ± 0.08 ppbv h^{-1}) were major sources of HONO at night. Nighttime soil emission rate was calculated to be 0.019 ± 0.001 ppbv h^{-1}, which is comparable to the observed nocturnal increase rate of HONO (0.02 ppbv h^{-1}), further indicating the importance of direct emissions. Additionally, contribution from NO_2 heterogeneous reactions on surfaces should not be ruled out. To balance the nighttime HONO budget by assuming dry deposition to be the principal loss process, a dry deposition rate of at least 1.8 cm s^{-1} is required.

3.3 Daytime HONO budget and unknown sources analysis

In this section, we concentrate on the daytime chemistry of HONO by a detailed budget analysis. The time variation of HONO concentration at our site can be related to its sources and sinks as follows:

$$\frac{\partial[HONO]}{\partial t} = P_{HONO} - L_{HONO} = (P_{OH+NO} + P_{Unknown} + P_{emis} + P_{soil} + T_V + T_H) - (L_{OH+HONO} + L_{Phot} + L_{Dep}) \quad (~~7~~9)$$

where ∂[HONO]/∂t represents the time variation of HONO; P_{HONO} and L_{HONO} are the sources and sinks of HONO, respectively; P_{OH+NO} and $L_{OH+HONO}$ are the homogeneous HONO formation and loss rates in Reactions R2 and R3, respectively; $P_{Unknown}$ is the HONO production rate from unknown sources; T_V and T_H are two terms representing vertical and horizontal transport processes, respectively; $L_{Phot~~o~~}$ denotes the photolysis loss rate of HONO, which can be calculated with $L_{Phot~~o~~}$ = J(HONO) × [HONO]; L_{Dep} represents the deposition loss rate of HONO and can be calculated as $L_{D~~o~~ep} = V_d \times$ [HONO]/H, where V_d is the deposition velocity of HONO and H is the daytime mixing height. Assuming a daytime V_d of 1.6 cm s^{-1} (Hou et al., 2016; Li et al., 2011) and an daytime mixing height (H) of 1000 m (Liao et al., 2018; Song et al., 2019), the average $L_{D~~o~~ep}$ is 0.003 ± 0.001 ppbv h^{-1}, three orders of magnitude smaller than $L_{Phot~~o~~}$ and therefore can be ignored in the following discussion.

OH was not measured and was calculated with a parameterized approach based on strong correlation between observed OH radicals and J(O^1D). The parameterization was first proposed by Rohrer and Berresheim (2006) and has been applied by several studies in China (Lu et al., 2013; Lu et al., 2012; Lu et al., 2014). In this study, OH was estimated with observed J(O^1D) along with parameters from fitting the observed OH radicals and J(O^1D) data in Guangzhou Back Garden by Lu et al. (2012). The daytime maximum OH concentration was estimated to be 1.3 × 10^7 cm^{-3}, which is slightly smaller than the daily

peak values of 1.5–2.6×10^7 cm^{-3} observed in summer of Guangzhou by Lu et al. (2012). And the estimated daily average OH concentration is 6.7 × 10^6 cm^{-3}, close to 7.5 × 10^6 cm^{-3} measured in the PRD region in autumn of 2014 by Yang et al. (2017b). Daytime P_{emis} was calculated based on the method (3) (mentioned in Sect. 3.2.1). Because the HONO lifetime was in the order of 20 min under typical daytime conditions (Stutz et al., 2000) and the transport distance is only a few kilometers, the NOx emission rate extracted from the 3 km × 3 km grid cell centred around sampling site is used to calculate the impact of primary emission on HONO.

To minimize interferences, we choose a period from 9:00 to 15:00 with intense solar radiation and a short HONO lifetime. Horizontal transport T_H was assumed negligible by selecting the cases with low wind speed (Su et al., 2008b; Yang et al., 2014). The magnitude of ~~V~~vertical transport T_V can be estimated by using a parameterization for dilution by background air according to (Dillon et al., 2002), i.e. $T_V = k_{(dilution)} \times ([HONO]-[HONO]_{background})$. Where $k_{(dilution)}$ is the dilution rate, $[HONO]_{background}$ represents the background HONO concentration. Assuming a $k_{(dilution)}$ of 0.23 h^{-1} (Dillon et al., 2002; Sörgel et al., 2011a), a $[HONO]_{background}$ value of 10 pptv (Zhang et al., 2009), and taking the mean noontime [HONO] value of 400 pptv in this study, a value of about 0.09 ppbv h^{-1} can be derived, which is much smaller than L_{Phot} and can be ignored in the following discussion. The average daytime HONO emission rate from soil P_{soil} varied from 0.002 to 0.007 with a mean value of 0.004 ± 0.001 ppbv h^{-1}, which is three orders of magnitude smaller than L_{Phot}~~o~~, and can also be ignored in the following discussion. As a result, $P_{Unknown}$ can be expressed by Eq. (~~8~~10), in which ∂[HONO]/∂t is substituted by Δ[HONO]/Δ~~d~~t.

$$\frac{\Delta[HONO]}{\Delta t} = (P_{OH+NO} + P_{emis} + P_{Unknown}) - (L_{OH+HONO} + L_{Phot}) \quad (~~8~~10)$$

Figure 7 shows the budget of HONO from 9:00 to 15:00. As expected, photolysis HONO L_{Photo} (1.58 ± 0.82 ppbv h^{-1}) is the main loss pathway in the day, followed by a small contribution by the homogeneous reaction of HONO + OH ($L_{OH+HONO}$, 0.07 ± 0.03 ppbv h^{-1}). Among the sources, P_{OH+NO} and $P_{Unknown}$ were comparable in magnitudes, with an average of 0.79 ± 0.61 ppbv h^{-1} and 0.65 ± 0.46 ppbv h^{-1}, respectively. $P_{Unknown}$ showed a photo-enhanced feature, reaching its maximum at 12:00 at 0.97 ppbv h^{-1}, similar to the observations in Xinken (Su et al., 2008b), Beijing (Yang et al., 2014), Wangdu (Liu et al., 2019a), Changzhou (Zheng et al., 2020) and Cyprus (Meusel et al., 2016). The average of $P_{Unknown}$ is comparable to the observation in Back Garden (0.77 ppbv h^{-1}) by Li et al. (2012), but smaller than those in Xinken (≈ 2.0 ppbv h^{-1}) by Su et al. (2008b) and Guangzhou city area (1.25 ppbv h^{-1}) by Yang et al. (2017a). Homogeneous reaction of NO + OH reached its maximum in the early morning, and contributed the most fraction in the whole day. Apparently, high NO concentrations at our site made P_{OH+NO} the biggest daytime source of HONO, exceeding $P_{Unknown}$, similar to other high-NOx sites such as Santiago de Chile (Elshorbany et al., 2009), London (Heard et al., 2004), Paris (Michoud et al., 2014), Beijing (Liu et al., 2021; Slater et al., 2020; Zhang et al., 2019b; Liu et al., 2020c), Taiwan (Lin et al., 2006) and Hebei (Xue et al., 2020). Next, we investigate possible factors relating to $P_{Unknown}$.

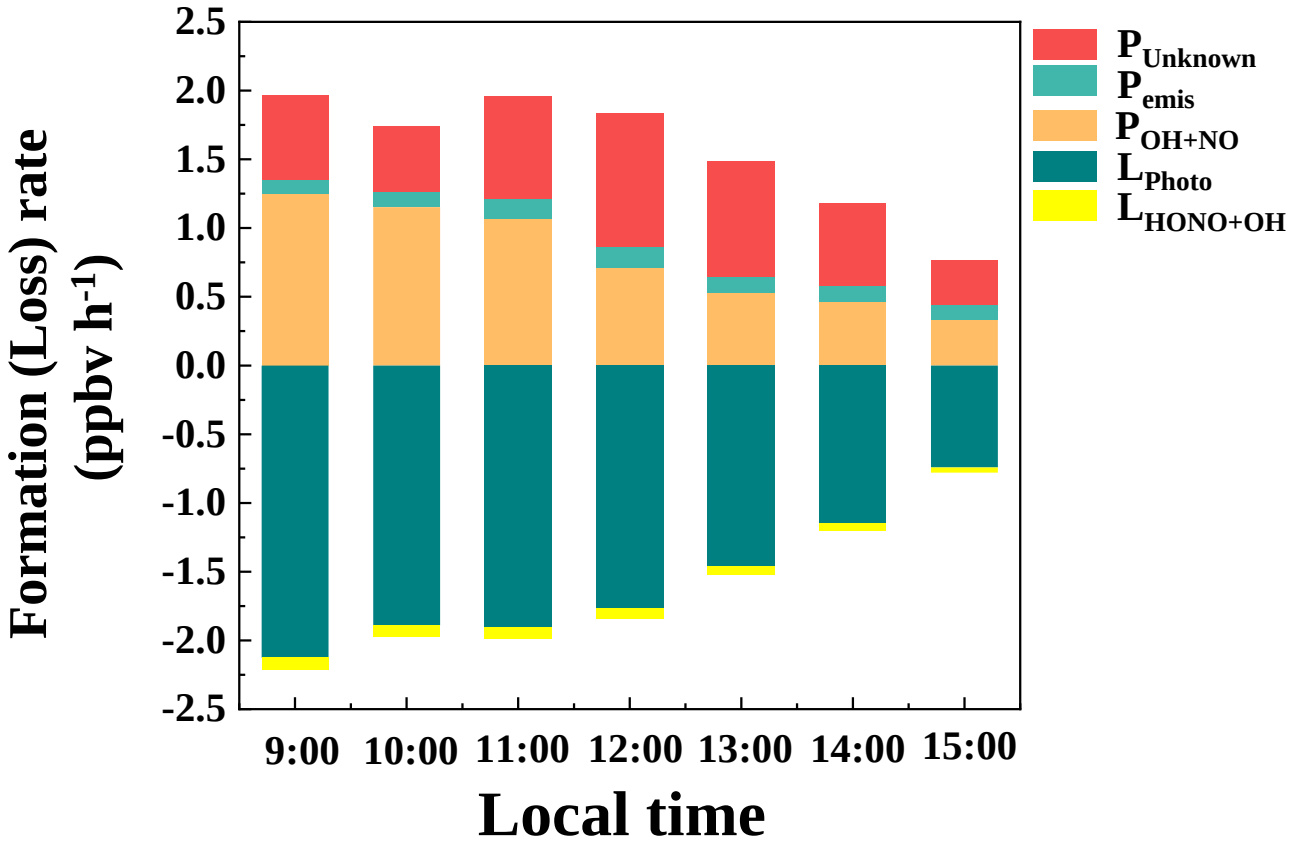

Figure 7. Items of the HONO budget (Eq. (~~8~~10)) in Guangzhou during the observation period.

Figure 8 shows the correlation between $P_{Unknown}$ and NO_2 and $J(NO_2)$ was 0.0681 and 0.2713, respectively. The correlation between $P_{Unknown}$ and $NO_2 \times J(NO_2)$ further improved to 0.4116, indicating that $P_{Unknown}$ may be related to the photo-enhanced reaction of NO_2 (Jiang et al., 2020; Li et al., 2018a; Liu et al., 2019a; Liu et al., 2019b; Su et al., 2008b; Zheng et al., 2020; Huang et al., 2017).

No correlation was found between $P_{Unknown}$ and $PM_{2.5}$ (R^2 = 0.00014), indicating that particulate matters may not be a key factor in daytime HONO production (Wong et al., 2012; Li et al., 2018a; Sörgel et al., 2011a; Wang et al., 2017a; Zheng et al., 2020). Meanwhile, the correlations between $P_{Unknown}$ and nitrate in PM_1 and the sum of gaseous nitric acid and nitrate in PM_1 were very low, with R^2 of 0.0348 and 0.0062 respectively. And the correlation between $P_{Unknown}$ and the product of nitrate and $J(NO_2)$ was also poor R^2 = 0.0007, which does not relate $P_{Unknown}$ to the photolysis of nitrate or gaseous nitric acid. Wang et al. (2016) and Ge et al. (2019) suggested that NH_3 can efficiently promote the reaction of NO_2 and SO_2 to form HONO and sulfate. However, we did not find good correlations for $P_{Unknown}$ vs. NH_3, $P_{Unknown}$ vs. SO_2, or $P_{Unknown}$ vs. $NH_3 \times SO_2$.

In summary, at our site with relatively strong traffic impact and high NO, NO + OH appears to be the largest daytime HONO source followed by an unknown photolytic source, which does not seem to be related to aerosols, nor the photolysis of nitrate/nitric acid, nor the reaction between NO_2, SO_2 and NH_3.

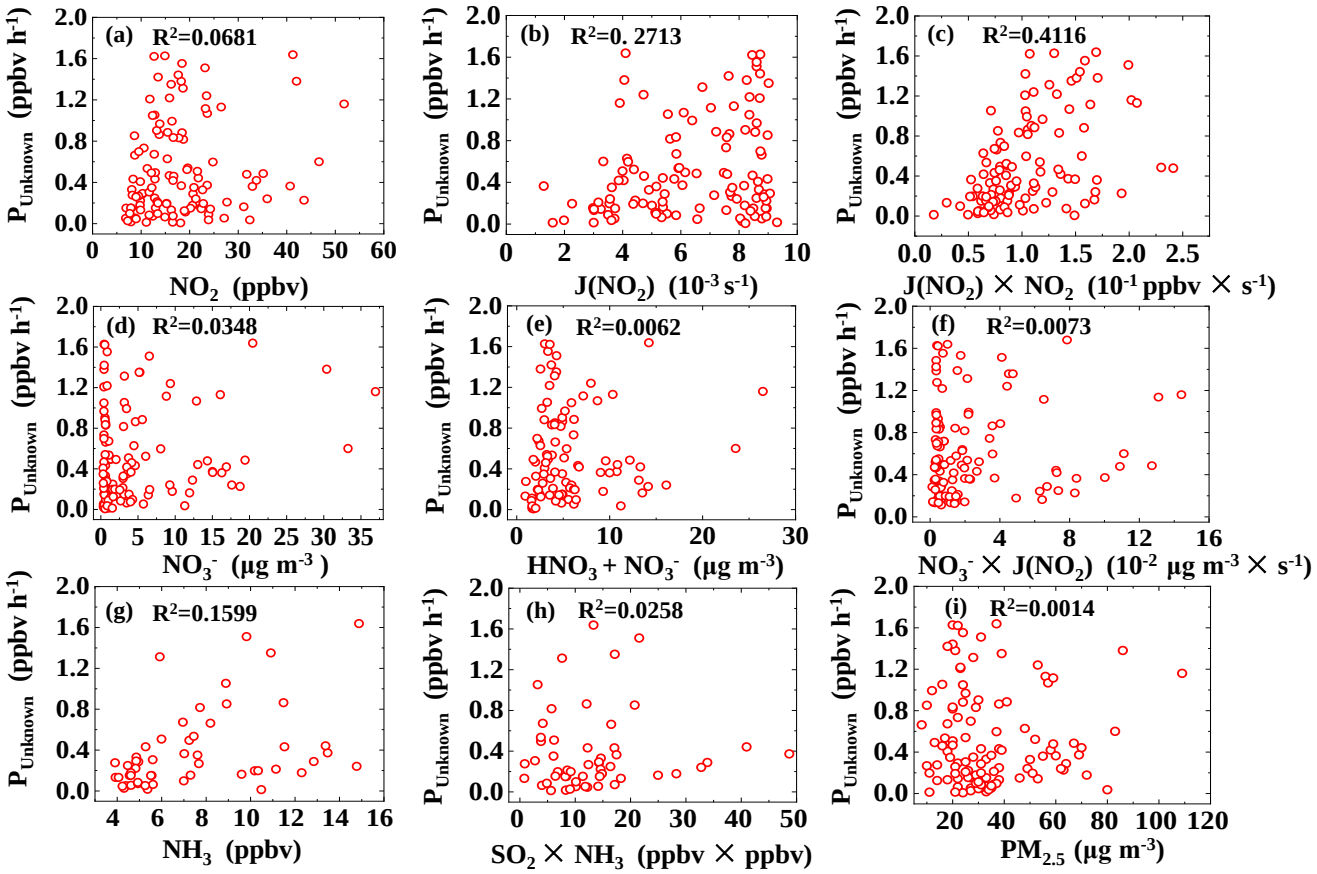

Figure 8. Correlations between daytime HONO unknown sources $P_{Unknown}$ and related parameters.

3.4 The contribution of HONO, ~~and~~ O_3 and ozonolysis of alkenes to OH

Photolysis of HONO and O_3 contribute dominant the primary source of OH radicals. Ozonolysis of alkenes was found to be important source of OH (Heard et al., 2004; Elshorbany et al., 2009; Tan et al., 2019b). Here we evaluated and compared the contribution of the three~~two~~ pathways. Other sources such as ~~ozonolysis reactions of alkenes and~~ the photolysis of peroxides, ~~are~~is usually not very significant in urban areas, especially during daytime, thus was ~~were~~ not considered in this study (Li et al., 2018a; Shi et al., 2020b). The contribution of HCHO photolysis to OH was also not considered due to the lack of measurement for HCHO. The OH radicals' production rate from HONO photolysis $P_{OH(HONO)}$ can be calculated from the

measured photolysis frequencies and the mixing ratios of HONO using Eq. (~~9~~11). The net OH radicals' production from HONO $P_{(HONO–OH)}$ can be calculated by subtracting the OH loss caused by Reactions R1 and R2 from $P_{OH(HONO)}$ (Eq. (~~10~~12)). The OH radicals' production rate from O_3 photolysis $P_{(O_3–OH)}$ can be calculated from Eq. (~~11~~13). Only part of $O(^1D)$ atoms, formed through the photolysis of O_3 at solar radiation below 320 nm (Reaction R4), can generate OH radicals by reacting with water vapor (Reaction R5) in the atmosphere, so we used the absolute mixing ratio of water vapor, which can be derived from the temperature and relative humidity data, to calculate the fraction of OH (Φ_{OH}) between Reactions R5 and R6. The reaction rate of $O(^1D)$ with N_2 and O_2 is 3.1×10^{-11} cm^3 s^{-1} and 4.0×10^{-11} cm^3 s^{-1} respectively (Seinfeld and Pandis, 2016). In Eq. (15), $k_{alkenes(i)+O_3}$ represents the reaction rate constant for the reaction of O_3 with alkene (i), and Y_{OH_i} represents the yield of OH from the gas-phase reaction of O_3 and alkene (i). Table S6 summarized the reaction rate constant of O_3 with alkenes at 298 K and the yields of OH.

$$P_{OH(HONO)} = J(HONO)[HONO] \quad (~~9~~11)$$

$$P_{(HONO–OH)} = P_{OH(HONO)} - k_{NO+OH}[NO][OH] - k_{HONO+OH}[HONO][OH] \quad (~~10~~12)$$

$$P_{(O_3–OH)} = 2\Phi_{OH}[O_3]J(O^1D) \quad (~~11~~13)$$

$$\Phi_{OH} = k_5[H_2O]/(k_5[H_2O]+k_6[M]) \quad (~~12~~14)$$

$$P_{(O_3+alkenes)–OH} = \sum k_{alkenes(i)+O_3}[alkenes(i)][O_3]\,Y_{OH_i} \quad (15)$$

$$O_3 + h\nu \rightarrow O(^1D) + O_2\ (\lambda < 320\ nm) \quad (R4)$$

$$O(^1D) + H_2O \rightarrow 2OH \quad (R5)$$

$$O(^1D) + M \rightarrow O(^3P) + M\ (M \text{ is } N_2 \text{ or } O_2) \quad (R6)$$

Figure 9 shows that $P_{(HONO–OH)}$ was larger than $P_{(O_3–OH)}$ before 10:00, while the latter became always higher with the solar radiation enhanced after 10:00. Both the two sources of OH reached their maximum around 12:00, while $P_{(O_3–OH)}$ was approximately two times of that of $P_{(HONO–OH)}$. On average, the OH production rates by photolysis of HONO and O_3 were 3.7×10^6 cm^{-3} s^{-1} and 4.9×10^6 cm^{-3} s^{-1}, respectively. In daytime, the sum of OH production rates by ozonolysis of alkenes was 3×10^5 cm^{-3} s^{-1}, which is much smaller than that of HONO and O_3. This value (3×10^5 cm^{-3} s^{-1}) was comparable to the results in previous studies (Kim et al., 2014; Ge et al., 2021; Martinez et al., 2003; Ren et al., 2003; Lee et al., 2016; Alicke et al., 2002; Kleffmann et al., 2005; Ren et al., 2013), but smaller than some other studies (Shi et al., 2020b; Zheng et al., 2020; Heard et al., 2004). Table 2 summarizes the OH production rate from HONO and O_3 photolysis from previous studies worldwide. It can be seen that $P_{(HONO–OH)}$ are larger than $P_{(O_3–OH)}$ in most of the observations, but sometimes the opposite is reported. Apparently, the relative importance of $P_{(HONO–OH)}$ and $P_{(O_3–OH)}$ strongly depends on the ratio of HONO/O_3. Especially in winter, photolysis of HONO tends to be the predominant OH source due to the low concentration of O_3 and water vapor.

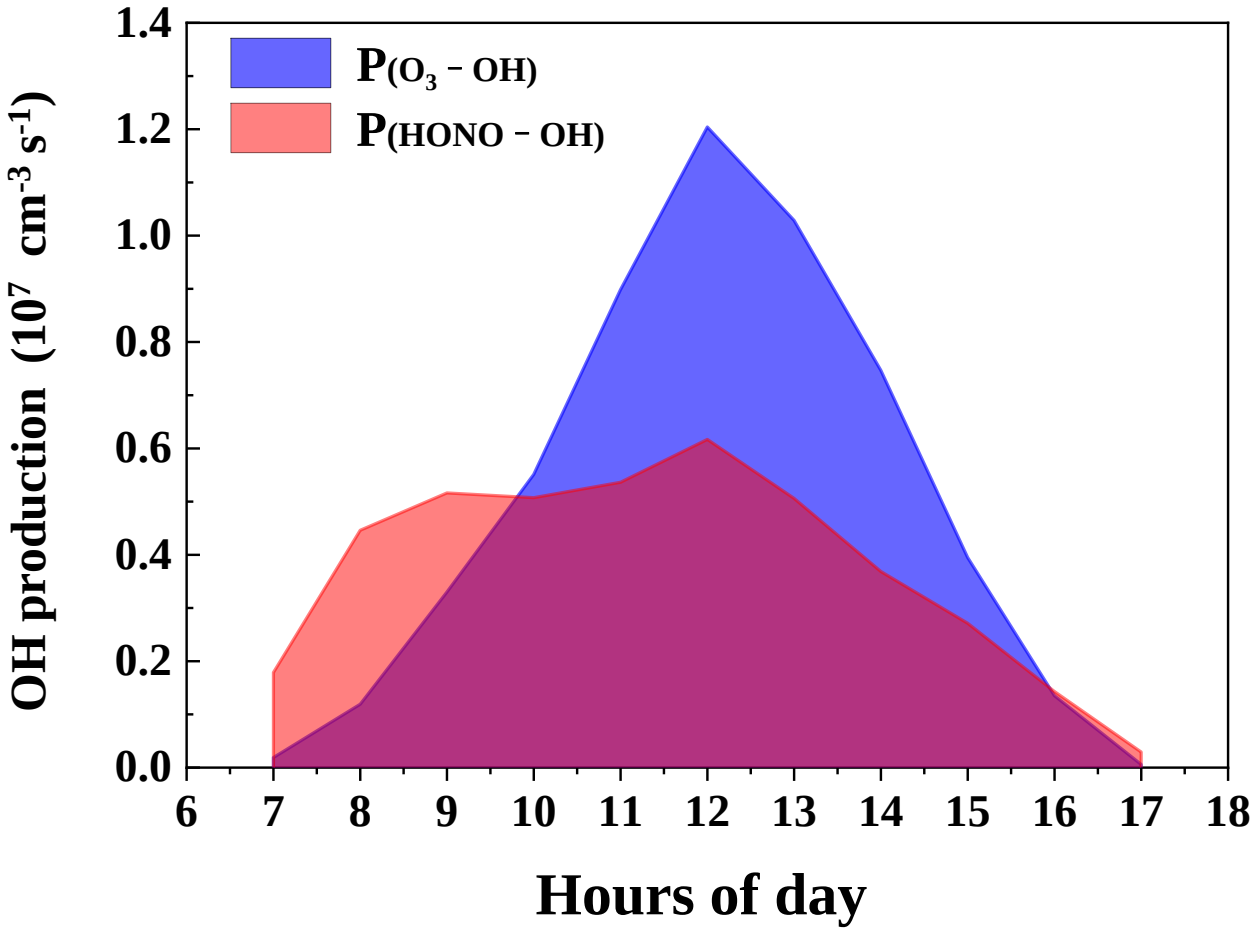
P(O3 – OH)
P(HONO – OH)
OH production (10^7 cm^-3 s^-1)
1.4
1.2
1.0
0.8
0.6
0.4
0.2
0.0
6
7
8
9
10
11
12
13
14
15
16
17
18
Hours of day

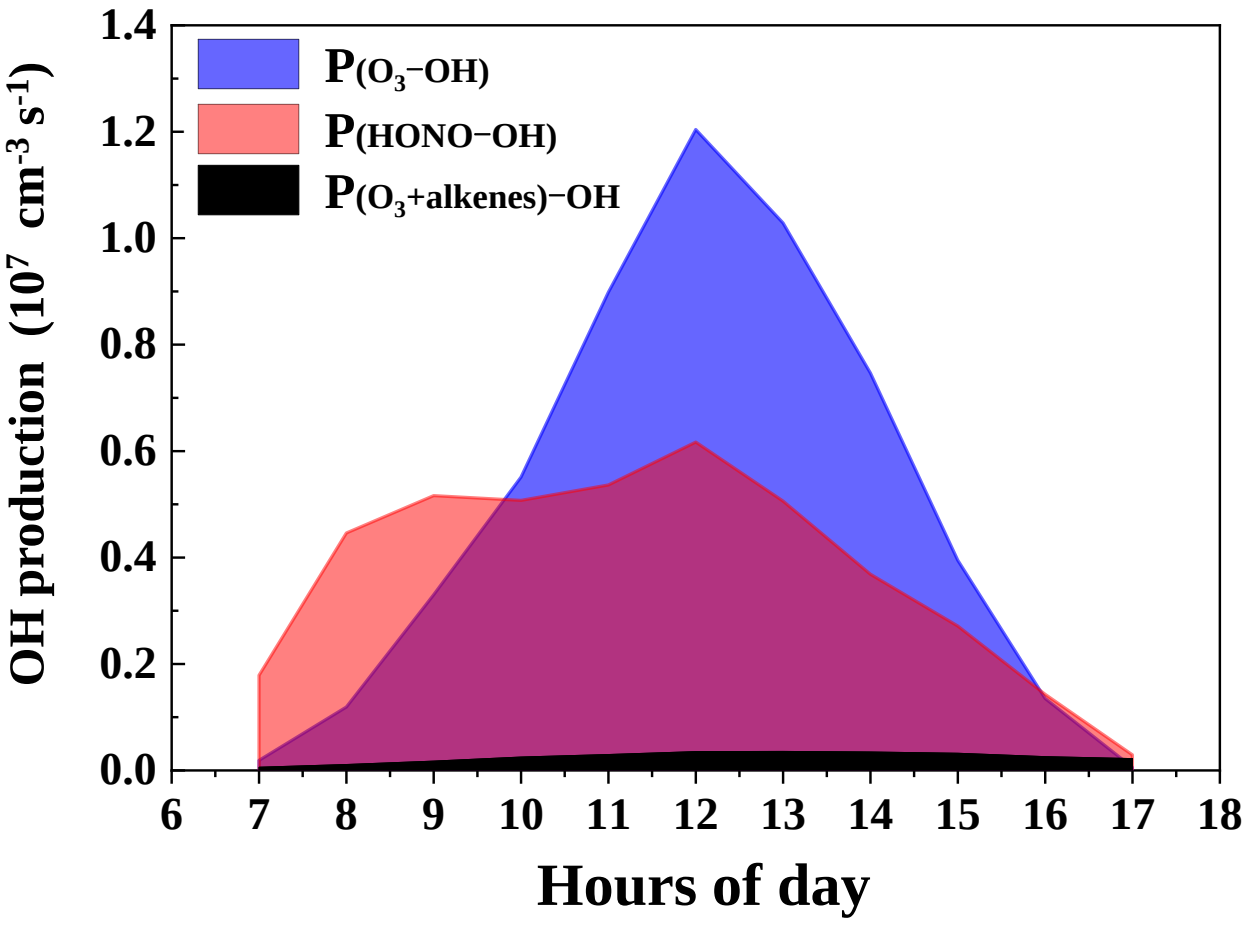

Figure 9. The yield and comparison of OH radicals by HONO, ~~and~~ O_3 and ozonolysis of alkenes.

Table 2. The OH production rates from HONO and O_3 photolysis in previous observations.

Location	Date	Season	$P_{(HONO-OH)}$ (ppbv h^{-1})	$P_{(O_3-OH)}$ (ppbv h^{-1})	Reference
New York, USA	Jun-Jul 1998	Summer	0.10	0.22	1
Nashville, USA	Jun-Jul 1999	Summer	0.29	0.33	2
Birmingham, UK	Jan-Feb 2000	Winter	0.45	0.01	3
New York, USA	Jun-Aug 2001	Summer	0.81	0.19	4
Santiago, Chile	May-Jun 2005	Winter	2.90	0.01	5
	Mar 2005	Summer	1.70	0.13	
El Arenosillo, Spain	Dec 2008	Winter	0.11	0.09	6
Colorado, USA	Feb-Mar 2011	Winter	0.45	0.04	7
Beijing, China	Sep-Oct 2004	Autumn	1.31	0.18	8
Xinken, China	Oct-Nov 2004	Autumn	3.66	0.88	9
Back Garden, China	Jul 2006	Summer	1.32	2.20	10
Yufa, China	Aug 2006	Summer	1.68	0.38	11
Tung Chung, China	Aug 2011	Summer	1.50	0.90	12
Wangdu, China	June 2014	Summer	1.68	1.20	13
Hong Kong, China	Mar-May 2015	Spring	6.40	a	14
Changzhou, China	Dec 2015	Winter	1.04	0.36	15
Guangzhou, China	Oct 2015	Autumn	1.24	0.41	16
	Jul 2016	Summer	0.71	0.44	
Ji'nan, China	Aug 2016	Summer	1.88	0.63	17
Changzhou, China	Apr 2017	Spring	1.66	2.78	18
Mount Tai, China	Dec 2017	Winter	0.52	0.02	19
	Mar-Apr 2018	Spring	0.51	0.18	
Nanjing, China	Nov-Nov 2017/2018	A year	1.16	0.41	20
Gucheng, China	Jan-Feb 2018	Winter	1.40	0.01	21
Guangzhou, China	Sep-Nov 2018	Autumn	0.54	0.72	22

a: far less than $P_{(HONO-OH)}$.

Reference: 1. Zhou et al. (2002a); 2. Martinez et al. (2003); 3. Heard et al. (2004); 4. Ren et al. (2003); 5. Elshorbany et al. (2010); 6. Sörgel et al. (2011a); 7. Kim et al. (2014) ; 8. An et al. (2009); 9. Su et al. (2008b); 10. Su (2008); 11. Yang et al. (2014); 12. Xue et al.

(2016); 13. Liu et al. (2019a); 14. Yun et al. (2017); 15. Zheng et al. (2020); 16. Yang et al. (2017a); 17. Li et al. (2018a); 18. Shi et al. (2020a); 19. Jiang et al. (2020); 20. Liu et al. (2019b); 21. (Li in preparation); 22. This study

3.5 Box model simulation of HONO impact on atmospheric oxidation capacity

Atmospheric oxidation capacity refers to the total removal rates of CO and VOCs by major oxidants (e.g., OH, NO_3 and O_3) (Elshorbany et al., 2010; Xue et al., 2016; Tan et al., 2019b). As the primary oxidant in the atmosphere, the OH concentration is widely used to quantitatively describe the atmospheric oxidation capacity (Zheng et al., 2020; Liu et al., 2021; Shi et al., 2020b; Zhang et al., 2019a). And ozone is another indicator of atmospheric oxidation capacity. A box model (MCMv3.3.1) was conducted to simulate OH and O_3 concentrations with and without HONO constrained with observational data. Figure S45 shows the time series of measured and simulated O_3 concentrations. The model performance was evaluated to be good by the index of agreement (IOA) (see Supplementary infomation). It should be noted that the box model ignores the influence of transport and convection, so the simulated O_3 concentration does not represent the actual O_3 concentration in the atmosphere.

The time series of simulation results of O_3 and OH can be found in Fig. S56. Figure 10 shows diurnal variations of simulated O_3 and OH with and without HONO constrained. Daytime maximum OH concentration with HONO (6.1×10^6 cm^{-3}) was simulated to be 59% higher than the simulation without HONO (3.9×10^6 cm^{-3}), and the daily maximum concentration of O_3 with HONO (43.2 ppbv) was simulated to be 68.8% higher than the simulation without HONO (25.6 ppbv). These results are both within the range of prior studies (Elshorbany et al., 2012; Fu et al., 2019; Gil et al., 2021; Liu et al., 2021; Malkin et al., 2016; Xue et al., 2020; Yang et al., 2021a; Yun et al., 2017; Zhang et al., 2016), suggesting a strong HONO enhancement effect on atmospheric oxidation capacity. In addition, the impact of HONO on O_3 appeared two hours later than on OH, likely reflecting that HO_2 and RO_2, which are key proxy radicals in O_3 production were not significantly higher during early morning hours, despite higher HONO and OH.

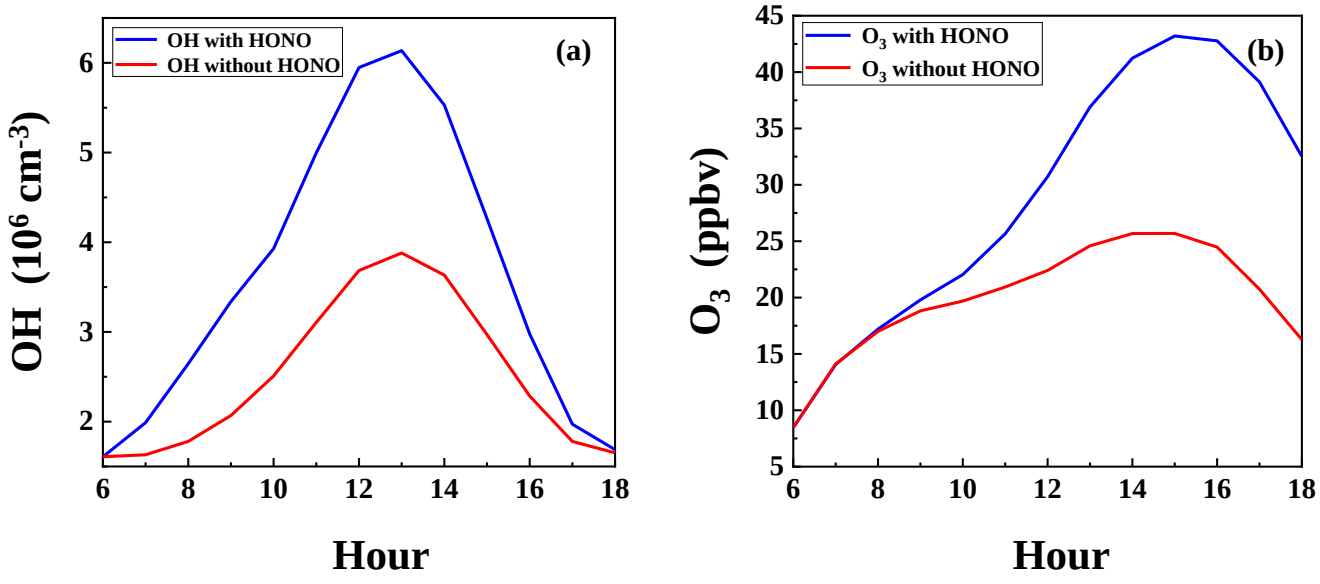

Figure 10. The diurnal variations of simulated O_3 and OH output with and without the HONO constrained in model.

4 Conclusions

Nitrous acid (HONO) was measured with a custom-built LOPAP instrument, along with meteorological parameters and other atmospheric constituents at an urban site in Guangzhou in Pearl River Delta from 27 September to 9 November 2018. The HONO concentrations varied from 0.02 to 4.43 ppbv with an average of 0.74 ± 0.70 ppbv. Compared to prior measurements in Guangzhou, a decreasing trend of HONO can be seen along with improved air quality in the city over the past decade. The emission ratios (HONO/NOx) were derived from an analysis of 11 fresh plumes, varying from 0.1% to 1.5% with an average value of 0.9% ± 0.4%. Using this estimated emission ratio and an estimate of NOx emission rate extracted from a grid cell around our site in a high-resolution (3 km × 3 km) NOx emission inventory, we estimated a primary HONO emission rate of 0.30 ± 0.15 ppbv h^{-1}, which turned out far larger (almost by an order of magnitude) than what would be estimated with a city-level NOx emission estimate, which does not adequately represent NOx emission rate specifically for the observation site. Thus, for future analysis of HONO data to properly estimate direct emission of HONO, we suggest that high quality emission data be used to reduce uncertainty. This is especially crucial for a site that receives nearby traffic emissions like ours. HONO produced by the homogeneous reaction of OH + NO at night was 0.26 ± 0.08 ppbv h^{-1}, which can be seen as secondary results from primary emission. They were both much higher than the observed increase rate of HONO (0.02 ppbv h^{-1}) during the night. Nighttime soil emission rate was calculated to be 0.019 ± 0.001 ppbv h^{-1}, which is comparable to the observed increase rate of HONO during night, thus further demonstrating the importance of direct emissions. In order to balance the nighttime HONO budget and assuming dry deposition to be the principle loss process, a dry deposition rate of at least ~~2.5~~1.8 cm s^{-1} is required. Correlation analysis shows that the heterogeneous reaction of NO_2

related to NH_3 and RH may contribute to the nighttime HONO formation. Daytime HONO budget analysis revealed that in order to sustain the observed HONO concentration around 450 pptv despite fast photolysis of HONO, an additional unknown source production rate ($P_{Unkonwn}$) of 0.65 ± 0.46 ppbv h^{-1} was needed, in addition to the primary emission P_{emis} at 0.12 ± 0.01 ppbv h^{-1}, and the homogenous reaction source P_{OH+NO} at 0.79 ± 0.61 ppbv h^{-1}. It is worth noting that the homogenous HONO source by NO + OH appeared to be a stronger source of HONO than the unknown source ($P_{Unkonwn}$), because of high levels of NO at our site. Correlation analysis between $P_{Unknown}$ and proxies of different mechanisms showed that $P_{Unknown}$ appeared to be photo-enhanced, and yet the mechanism remains unclear. Aerosols should not be as important as ground as a heterogenous reaction media, as very weak correlation between $P_{Unknown}$ and $PM_{2.5}$. Moreover, no correlations were found between $P_{Unknown}$ and nitrate/HNO_3, NH_3, SO_2. We assessed the role of HONO in the production of OH and O_3 by calculating OH production rate as well as by simulating the chemistry with a box model (MCMv3.3.1). The average net formation rate of OH attributed to HONO, ~~and~~ O_3 and ozonolysis of alkenes was 3.7×10^6 cm^{-3} s^{-1} 4.9×10^6 cm^{-3} s^{-1} and 3×10^5 cm^{-3} s^{-1}, respectively. Box model simulations confirmed strong HONO enhancement effect on OH and O_3 by 59% and 68.8%, respectively.

Data availability

HONO data, other trace gases data and meteorological data are available upon request from the corresponding author.

Contribution

Yihang Yu: Validation, Formal analysis, Writing - Original Draft, Visualization. **Peng Cheng:** Conceptualization, Methodology, Writing - Review & Editing, Supervision, Project administration, Funding acquisition. **Huirong Li:** Validation, Formal analysis, Investigation, Data Curation. **Wenda Yang:** Software, Investigation, Data Curation. **Baobin Han:** Investigation. **Wei Song:** Resources. **Weiwei Hu:** Resources. **Xinming Wang:** Resources. **Bin Yuan:** Resources. **Min Shao:** Resources. **Zhijiong Huang:** Resources. **Zhen Li:** Resources. **Junyu Zheng:** Resources. **Haichao Wang:** Writing - Review & Editing. **Xiaofang Yu:** Investigation.

Competing interests

The authors declare that they have no conflict of interest.

Acknowledgments

This work was funded by the National Key Research and Development Program of China (grant nos. 2018YFC0213904, 2017YFC0210104), Science and Technology Plan Projects in Guangzhou (grant no. 201804010115), the Guangdong Natural Science Funds for Distinguished Young Scholar (grant no. 2018B030306037), the Guangdong Innovative and Entrepreneurial Research Team Program (grant no. 2016ZT06N263), and the Special Fund Project for Science and Technology Innovation Strategy of Guangdong Province (grant no. 2019B121205004).

References

Acker, K., Febo, A., Trick, S., Perrino, C., Bruno, P., Wiesen, P., Möller, D., Wieprecht, W., Auel, R., Giusto, M., Geyer, A., Platt, U., and Allegrini, I.: Nitrous acid in the urban area of Rome, Atmospheric Environment, 40, 3123-3133, https://doi.org/10.1016/j.atmosenv.2006.01.028, 2006.

Alicke, B., Platt, U., and Stutz, J.: Impact of nitrous acid photolysis on the total hydroxyl radical budget during the Limitation of Oxidant Production/Pianura Padana Produzione di Ozono study in Milan, Journal of Geophysical Research: Atmospheres, 107, 8196, https://doi.org/10.1029/2000JD000075, 2002.

Alicke, B., Geyer, A., Hofzumahaus, A., Holland, F., Konrad, S., Pätz, H. W., Schäfer, J., Stutz, J., Volz-Thomas, A., and Platt, U.: OH formation by HONO photolysis during the BERLIOZ experiment, Journal of Geophysical Research: Atmospheres, 108, 8247, https://doi.org/10.1029/2001JD000579, 2003.

Ammann, M., Kalberer, M., Jost, D. T., Tobler, L., Rössler, E., Piguet, D., Gäggeler, H. W., and Baltensperger, U.: Heterogeneous production of nitrous acid on soot in polluted air masses, Nature, 395, 157-160, https://doi.org/10.1038/25965, 1998.

Ammar, R., Monge, M. E., George, C., and D'Anna, B.: Photoenhanced NO_2 Loss on Simulated Urban Grime, ChemPhysChem, 11, 3956-3961, https://doi.org/10.1002/cphc.201000540, 2010.

An, J., Zhang, W., and Qu, Y.: Impacts of a strong cold front on concentrations of HONO, HCHO, O_3, and NO_2 in the heavy traffic urban area of Beijing, Atmospheric Environment, 43, 3454-3459, https://doi.org/10.1016/j.atmosenv.2009.04.052, 2009.

Arens, F., Gutzwiller, L., Baltensperger, U., Gäggeler, H. W., and Ammann, M.: Heterogeneous Reaction of NO_2 on Diesel Soot Particles, Environmental Science & Technology, 35, 2191-2199, https://doi.org/10.1021/es000207s, 2001.

Aubin, D. G., and Abbatt, J. P. D.: Interaction of NO_2 with Hydrocarbon Soot: Focus on HONO Yield, Surface Modification, and Mechanism, The Journal of Physical Chemistry A, 111, 6263-6273, https://doi.org/10.1021/jp068884h, 2007.

Bejan, I., Abd-el-Aal, Y., Barnes, I., Benter, T., Bohn, B., Wiesen, P., and Kleffmann, J.: The photolysis of ortho-nitrophenols: a new gas phase source of HONO, Phys Chem Chem Phys, 8, 2028-2035, http://dx.doi.org/10.1039/B516590C, 2006.

Brigante, M., Cazoir, D., D'Anna, B., George, C., and Donaldson, D. J.: Photoenhanced Uptake of NO_2 by Pyrene Solid Films, The Journal of Physical Chemistry A, 112, 9503-9508, https://doi.org/10.1021/jp802324g, 2008.

Bröske, R., Kleffmann, J., and Wiesen, P.: Heterogeneous conversion of NO_2 on secondary organic aerosol surfaces: A possible source of nitrous acid (HONO) in the atmosphere?, Atmos. Chem. Phys., 3, 469-474, https://doi.org/10.5194/acp-3-469-2003, 2003.

Cazoir, D., Brigante, M., Ammar, R., D'Anna, B., and George, C.: Heterogeneous photochemistry of gaseous NO_2 on solid fluoranthene films: A source of gaseous nitrous acid (HONO) in the urban environment, Journal of Photochemistry and Photobiology A: Chemistry, 273, 23-28, https://doi.org/10.1016/j.jphotochem.2013.07.016, 2014.

Chan, C. K., and Yao, X.: Air pollution in mega cities in China, Atmospheric Environment, 42, 1-42, https://doi.org/10.1016/j.atmosenv.2007.09.003, 2008.

Cui, L., Li, R., Zhang, Y., Meng, Y., Fu, H., and Chen, J.: An observational study of nitrous acid (HONO) in Shanghai, China: The aerosol impact on HONO formation during the haze episodes, Science of The Total Environment, 630, 1057-1070, https://doi.org/10.1016/j.scitotenv.2018.02.063, 2018.

Czader, B. H., Rappenglück, B., Percell, P., Byun, D. W., Ngan, F., and Kim, S.: Modeling nitrous acid and its impact on ozone and hydroxyl radical during the Texas Air Quality Study 2006, Atmos. Chem. Phys., 12, 6939-6951, https://doi.org/10.5194/acp-12-6939-2012, 2012.

Dillon, M. B., Lamanna, M. S., Schade, G. W., Goldstein, A. H., and Cohen, R. C.: Chemical evolution of the Sacramento urban plume: Transport and oxidation, Journal of Geophysical Research: Atmospheres, 107, ACH 3-1-ACH 3-15, https://doi.org/10.1029/2001JD000969, 2002.

Donaldson, M. A., Berke, A. E., and Raff, J. D.: Uptake of Gas Phase Nitrous Acid onto Boundary Layer Soil Surfaces, Environmental Science & Technology, 48, 375-383, https://doi.org/10.1021/es404156a, 2014.

Elshorbany, Y. F., Kurtenbach, R., Wiesen, P., Lissi, E., Rubio, M., Villena, G., Gramsch, E., Rickard, A. R., Pilling, M. J., and Kleffmann, J.: Oxidation capacity of the city air of Santiago, Chile, Atmos. Chem. Phys., 9, 2257-2273, https://doi.org/10.5194/acp-9-2257-2009, 2009.

Elshorbany, Y. F., Kleffmann, J., Kurtenbach, R., Lissi, E., Rubio, M., Villena, G., Gramsch, E., Rickard, A. R., Pilling, M. J., and Wiesen, P.: Seasonal dependence of the oxidation capacity of the city of Santiago de Chile, Atmospheric Environment, 44, 5383-5394, https://doi.org/10.1016/j.atmosenv.2009.08.036, 2010.

Elshorbany, Y. F., Steil, B., Brühl, C., and Lelieveld, J.: Impact of HONO on global atmospheric chemistry calculated with an empirical parameterization in the EMAC model, Atmos. Chem. Phys., 12, 9977-10000, https://doi.org/10.5194/acp-12-9977-2012, 2012.

Fan, S., Wang, B., Tesche, M., Engelmann, R., Althausen, A., Liu, J., Zhu, W., Fan, Q., Li, M., Ta, N., Song, L., and Leong, K.: Meteorological conditions and structures of atmospheric boundary layer in October 2004 over Pearl River Delta area, Atmospheric Environment, 42, 6174-6186, https://doi.org/10.1016/j.atmosenv.2008.01.067, 2008.

Febo, A., Perrino, C., and Allegrini, I.: Measurement of nitrous acid in milan, italy, by doas and diffusion denuders, Atmospheric Environment, 30, 3599-3609, https://doi.org/10.1016/1352-2310(96)00069-6, 1996.

Feng, Y., Ning, M., Lei, Y., Sun, Y., Liu, W., and Wang, J.: Defending blue sky in China: Effectiveness of the "Air Pollution Prevention and Control Action Plan" on air quality improvements from 2013 to 2017, Journal of Environmental Management, 252, 109603, https://doi.org/10.1016/j.jenvman.2019.109603, 2019.

Finlayson-Pitts, B. J., and Pitts, J. N.: CHAPTER 4 - Photochemistry of Important Atmospheric Species, in: Chemistry of the Upper and Lower Atmosphere, edited by: Finlayson-Pitts, B. J., and Pitts, J. N., Academic Press, San Diego, 86-129, 2000.

Finlayson-Pitts, B. J., Wingen, L. M., Sumner, A. L., Syomin, D., and Ramazan, K. A.: The heterogeneous hydrolysis of NO_2 in laboratory systems and in outdoor and indoor atmospheres: An integrated mechanism, Physical Chemistry Chemical Physics, 5, 223-242, https://doi.org/10.1039/B208564J, 2003.

Fu, X., Wang, T., Zhang, L., Li, Q., Wang, Z., Xia, M., Yun, H., Wang, W., Yu, C., Yue, D., Zhou, Y., Zheng, J., and Han, R.: The significant contribution of HONO to secondary pollutants during a severe winter pollution event in southern China, Atmos. Chem. Phys., 19, 1-14, https://doi.org/10.5194/acp-19-1-2019, 2019.

Ge, S., Wang, G., Zhang, S., Li, D., Xie, Y., Wu, C., Yuan, Q., Chen, J., and Zhang, H.: Abundant NH_3 in China Enhances Atmospheric HONO Production by Promoting the Heterogeneous Reaction of SO_2 with NO_2, Environ Sci Technol, 53, 14339-14347, https://doi.org/10.1021/acs.est.9b04196, 2019.

Ge, Y., Shi, X., Ma, Y., Zhang, W., Ren, X., Zheng, J., and Zhang, Y.: Seasonality of nitrous acid near an industry zone in the Yangtze River Delta region of China: Formation mechanisms and contribution to the atmospheric oxidation capacity, Atmospheric Environment, 254, 118420, https://doi.org/10.1016/j.atmosenv.2021.118420, 2021.

George, C., Strekowski, R. S., Kleffmann, J., Stemmler, K., and Ammann, M.: Photoenhanced uptake of gaseous NO_2 on solid organic compounds: a photochemical source of HONO?, Faraday Discuss, 130, 195-210; discussion 241-164, 519-124, http://dx.doi.org/10.1039/B417888M, 2005.

Gil, J., Kim, J., Lee, M., Lee, G., Ahn, J., Lee, D. S., Jung, J., Cho, S., Whitehill, A., Szykman, J., and Lee, J.: Characteristics of HONO and its impact on O_3 formation in the Seoul Metropolitan Area during the Korea-US Air Quality study, Atmospheric Environment, 247, 118182, https://doi.org/10.1016/j.atmosenv.2020.118182, 2021.

Hao, Q., Jiang, N., Zhang, R., Yang, L., and Li, S.: Characteristics, sources, and reactions of nitrous acid during winter at an urban site in the Central Plains Economic Region in China, Atmos. Chem. Phys., 20, 7087-7102, https://doi.org/10.5194/acp-20-7087-2020, 2020.

Harrison, R. M., and Kitto, A.-M. N.: Evidence for a surface source of atmospheric nitrous acid, Atmospheric Environment, 28, 1089-1094, https://doi.org/10.1016/1352-2310(94)90286-0, 1994.

Harrison, R. M., Peak, J. D., and Collins, G. M.: Tropospheric cycle of nitrous acid, Journal of Geophysical Research: Atmospheres, 101, 14429-14439, https://doi.org/10.1029/96JD00341, 1996.

Heard, D. E., Carpenter, L. J., Creasey, D. J., Hopkins, J. R., Lee, J. D., Lewis, A. C., Pilling, M. J., Seakins, P. W., Carslaw, N., and Emmerson, K. M.: High levels of the hydroxyl radical in the winter urban troposphere, Geophysical Research Letters, 31, https://doi.org/10.1029/2004GL020544, 2004.

Heland, J., Kleffmann, J., Kurtenbach, R., and Wiesen, P.: A New Instrument To Measure Gaseous Nitrous Acid (HONO) in the Atmosphere, Environmental Science & Technology, 35, 3207-3212, https://doi.org/10.1021/es000303t, 2001.

Hendrick, F., Müller, J. F., Clémer, K., Wang, P., De Mazière, M., Fayt, C., Gielen, C., Hermans, C., Ma, J. Z., Pinardi, G., Stavrakou, T., Vlemmix, T., and Van Roozendael, M.: Four years of ground-based MAX-DOAS observations of HONO and NO_2 in the Beijing area, Atmos. Chem. Phys., 14, 765-781, https://doi.org/10.5194/acp-14-765-2014, 2014.

Hofzumahaus, A., Rohrer, F., Lu, K., Bohn, B., Brauers, T., Chang, C.-C., Fuchs, H., Holland, F., Kita, K., Kondo, Y., Li, X., Lou, S., Shao, M., Zeng, L., Wahner, A., and Zhang, Y.: Amplified Trace Gas Removal in the Troposphere, Science, 324, 1702-1704, https://doi.org/10.1126/science.1164566, 2009.

Hou, S., Tong, S., Ge, M., and An, J.: Comparison of atmospheric nitrous acid during severe haze and clean periods in Beijing, China, Atmospheric Environment, 124, 199-206, https://doi.org/10.1016/j.atmosenv.2015.06.023, 2016.

Hu, M., Zhou, F., Shao, K., Zhang, Y., Tang, X., and Slanina, J.: Diurnal variations of aerosol chemical compositions and related gaseous pollutants in Beijing and Guangzhou, J Environ Sci Health A Tox Hazard Subst Environ Eng, 37, 479-488, https://doi.org/10.1081/ESE-120003229, 2002.

Huang, R. J., Yang, L., Cao, J., Wang, Q., Tie, X., Ho, K. F., Shen, Z., Zhang, R., Li, G., Zhu, C., Zhang, N., Dai, W., Zhou, J., Liu, S., Chen, Y., Chen, J., and O'Dowd, C. D.: Concentration and sources of atmospheric nitrous acid (HONO) at an urban site in Western China, Science of The Total Environment, 593-594, 165-172, https://doi.org/10.1016/j.scitotenv.2017.02.166, 2017.

Huang, Z., Zhong, Z., Sha, Q., Xu, Y., Zhang, Z., Wu, L., Wang, Y., Zhang, L., Cui, X., Tang, M., Shi, B., Zheng, C., Li, Z., Hu, M., Bi, L., Zheng, J., and Yan, M.: An updated model-ready emission inventory for Guangdong Province by incorporating big data and mapping onto multiple chemical mechanisms, Science of The Total Environment, 769, 144535, https://doi.org/10.1016/j.scitotenv.2020.144535, 2021.

Indarto, A.: Heterogeneous reactions of HONO formation from NO_2 and HNO_3: a review, Research on Chemical Intermediates, 38, 1029-1041, https://doi.org/10.1007/s11164-011-0439-z, 2012.

Jenkin, M. E., Saunders, S. M., and Pilling, M. J.: The tropospheric degradation of volatile organic compounds: a protocol for mechanism development, Atmospheric Environment, 31, 81-104, https://doi.org/10.1016/S1352-2310(96)00105-7, 1997.

Jenkin, M. E., Saunders, S. M., Wagner, V., and Pilling, M. J.: Protocol for the development of the Master Chemical Mechanism, MCM v3 (Part B): tropospheric degradation of aromatic volatile organic compounds, Atmos. Chem. Phys., 3, 181-193, https://doi.org/10.5194/acp-3-181-2003, 2003.

Jenkin, M. E., Young, J. C., and Rickard, A. R.: The MCM v3.3.1 degradation scheme for isoprene, Atmos. Chem. Phys., 15, 11433-11459, https://doi.org/10.5194/acp-15-11433-2015, 2015.

Jeon, W., Choi, Y., Souri, A. H., Roy, A., Diao, L., Pan, S., Lee, H. W., and Lee, S. H.: Identification of chemical fingerprints in long-range transport of burning induced upper tropospheric ozone from Colorado to the North Atlantic Ocean, Science of The Total Environment, 613-614, 820-828, https://doi.org/10.1016/j.scitotenv.2017.09.177, 2018.

Jiang, Y., Xue, L., Gu, R., Jia, M., Zhang, Y., Wen, L., Zheng, P., Chen, T., Li, H., Shan, Y., Zhao, Y., Guo, Z., Bi, Y., Liu, H., Ding, A., Zhang, Q., and Wang, W.: Sources of nitrous acid (HONO) in the upper boundary layer and lower free troposphere of the North China Plain: insights from the Mount Tai Observatory, Atmos. Chem. Phys., 20, 12115-12131, https://doi.org/10.5194/acp-20-12115-2020, 2020.

Kaiser, E. W., and Wu, C. H.: A kinetic study of the gas phase formation and decomposition reactions of nitrous acid, The Journal of Physical Chemistry, 81, 1701-1706, https://doi.org/10.1021/j100533a001, 1977.

Kalberer, M., Ammann, M., Arens, F., Gäggeler, H. W., and Baltensperger, U.: Heterogeneous formation of nitrous acid (HONO) on soot aerosol particles, Journal of Geophysical Research: Atmospheres, 104, 13825-13832, https://doi.org/10.1029/1999JD900141, 1999.

Kim, S., VandenBoer, T. C., Young, C. J., Riedel, T. P., Thornton, J. A., Swarthout, B., Sive, B., Lerner, B., Gilman, J. B., Warneke, C., Roberts, J. M., Guenther, A., Wagner, N. L., Dubé, W. P., Williams, E., and Brown, S. S.: The primary and recycling sources of OH during the NACHTT-2011 campaign: HONO as an important OH primary source in the wintertime, Journal of Geophysical Research: Atmospheres, 119, 6886-6896, https://doi.org/10.1002/2013JD019784, 2014.

Kirchstetter, T. W., Harley, R. A., and Littlejohn, D.: Measurement of Nitrous Acid in Motor Vehicle Exhaust, Environmental Science & Technology, 30, 2843-2849, https://doi.org/10.1021/es960135y, 1996.

Kleffmann, J., Kurtenbach, R., Lörzer, J., Wiesen, P., Kalthoff, N., Vogel, B., and Vogel, H.: Measured and simulated vertical profiles of nitrous acid—Part I: Field measurements, Atmospheric Environment, 37, 2949-2955, https://doi.org/10.1016/S1352-2310(03)00242-5, 2003.

Kleffmann, J., Gavriloaiei, T., Hofzumahaus, A., Holland, F., Koppmann, R., Rupp, L., Schlosser, E., Siese, M., and Wahner, A.: Daytime formation of nitrous acid: A major source of OH radicals in a forest, Geophysical Research Letters, 32, https://doi.org/10.1029/2005GL022524, 2005.

Kleffmann, J., Lörzer, J. C., Wiesen, P., Kern, C., Trick, S., Volkamer, R., Rodenas, M., and Wirtz, K.: Intercomparison of the DOAS and LOPAP techniques for the detection of nitrous acid (HONO), Atmospheric Environment, 40, 3640-3652, https://doi.org/10.1016/j.atmosenv.2006.03.027, 2006.

Kramer, L. J., Crilley, L. R., Adams, T. J., Ball, S. M., Pope, F. D., and Bloss, W. J.: Nitrous acid (HONO) emissions under real-world driving conditions from vehicles in a UK road tunnel, Atmos. Chem. Phys., 20, 5231-5248, https://doi.org/10.5194/acp-20-5231-2020, 2020.

Kurtenbach, R., Becker, K. H., Gomes, J. A. G., Kleffmann, J., Lörzer, J. C., Spittler, M., Wiesen, P., Ackermann, R., Geyer, A., and Platt, U.: Investigations of emissions and heterogeneous formation of HONO in a road traffic tunnel, Atmospheric Environment, 35, 3385-3394, https://doi.org/10.1016/S1352-2310(01)00138-8, 2001.

Lammel, G., and Cape, J. N.: Nitrous acid and nitrite in the atmosphere, Chemical Society Reviews, 25, 361-369, http://dx.doi.org/10.1039/CS9962500361, 1996.

Laufs, S., and Kleffmann, J.: Investigations on HONO formation from photolysis of adsorbed HNO_3 on quartz glass surfaces, Phys Chem Chem Phys, 18, 9616-9625, https://doi.org/10.1039/C6CP00436A, 2016.

Laufs, S., Cazaunau, M., Stella, P., Kurtenbach, R., Cellier, P., Mellouki, A., Loubet, B., and Kleffmann, J.: Diurnal fluxes of HONO above a crop rotation, Atmos. Chem. Phys., 17, 6907-6923, https://doi.org/10.5194/acp-17-6907-2017, 2017.

Lee, J. D., Whalley, L. K., Heard, D. E., Stone, D., Dunmore, R. E., Hamilton, J. F., Young, D. E., Allan, J. D., Laufs, S., and Kleffmann, J.: Detailed budget analysis of HONO in central London reveals a missing daytime source, Atmos. Chem. Phys., 16, 2747-2764, https://doi.org/10.5194/acp-16-2747-2016, 2016.

Lelieveld, J., Gromov, S., Pozzer, A., and Taraborrelli, D.: Global tropospheric hydroxyl distribution, budget and reactivity, Atmos. Chem. Phys., 16, 12477-12493, https://doi.org/10.5194/acp-16-12477-2016, 2016.

Li, D., Xue, L., Wen, L., Wang, X., Chen, T., Mellouki, A., Chen, J., and Wang, W.: Characteristics and sources of nitrous acid in an urban atmosphere of northern China: Results from 1-yr continuous observations, Atmospheric Environment, 182, 296-306, https://doi.org/10.1016/j.atmosenv.2018.03.033, 2018a.

Li, G., Lei, W., Zavala, M., Volkamer, R., Dusanter, S., Stevens, P., and Molina, L. T.: Impacts of HONO sources on the photochemistry in Mexico City during the MCMA-2006/MILAGO Campaign, Atmos. Chem. Phys., 10, 6551-6567, https://doi.org/10.5194/acp-10-6551-2010, 2010.

Li, H., Cheng, P., Yu, Y., and Yang, W.: Nitrous acid (HONO) budget analysis at a rural site in the North China Plain during snowy days, in preparation.

Li, J., Lu, K., Lv, W., Li, J., Zhong, L., Ou, Y., Chen, D., Huang, X., and Zhang, Y.: Fast increasing of surface ozone concentrations in Pearl River Delta characterized by a regional air quality monitoring network during 2006–2011, Journal of Environmental Sciences, 26, 23-36, https://doi.org/10.1016/S1001-0742(13)60377-0, 2014a.

Li, L., Duan, Z., Li, H., Zhu, C., Henkelman, G., Francisco, J. S., and Zeng, X. C.: Formation of HONO from the NH_3 promoted hydrolysis of NO_2 dimers in the atmosphere, Proceedings of the National Academy of Sciences, 115, 7236-7241, https://doi.org/10.1073/pnas.1807719115, 2018b.

Li, X., Brauers, T., Häseler, R., Bohn, B., Fuchs, H., Hofzumahaus, A., Holland, F., Lou, S., Lu, K. D., Rohrer, F., Hu, M., Zeng, L. M., Zhang, Y. H., Garland, R. M., Su, H., Nowak, A., Wiedensohler, A., Takegawa, N., Shao, M., and Wahner, A.: Exploring the atmospheric chemistry of nitrous acid (HONO) at a rural site in Southern China, Atmos. Chem. Phys., 12, 1497-1513, https://doi.org/10.5194/acp-12-1497-2012, 2012.

Li, X., Rohrer, F., Hofzumahaus, A., Brauers, T., Häseler, R., Bohn, B., Broch, S., Fuchs, H., Gomm, S., Holland, F., Jäger, J., Kaiser, J., Keutsch, F. N., Lohse, I., Lu, K., Tillmann, R., Wegener, R., Wolfe, G. M., Mentel, T. F., Kiendler-Scharr, A., and Wahner, A.: Missing Gas-Phase Source of HONO Inferred from Zeppelin Measurements in the Troposphere, Science, 344, 292-296, https://doi.org/10.1126/science.1248999, 2014b.

Li, Y., An, J., Min, M., Zhang, W., Wang, F., and Xie, P.: Impacts of HONO sources on the air quality in Beijing, Tianjin and Hebei Province of China, Atmospheric Environment, 45, 4735-4744, https://doi.org/10.1016/j.atmosenv.2011.04.086, 2011.

Liao, B., Huang, J., Wang, C., Weng, J., Li, L., Cai, H., and D, W.: Comparative analysis on the boundary layer features of haze processes and cleaning process in Guangzhou, China Environmental Science, 38, 4432-4443, DOI:10.19674/j.cnki.issn1000-6923.2018.0496, 2018.

Liao, W., Wu, L., Zhou, S., Wang, X., and Chen, D.: Impact of Synoptic Weather Types on Ground-Level Ozone Concentrations in Guangzhou, China, Asia-Pacific Journal of Atmospheric Sciences, https://doi.org/10.1007/s13143-020-00186-2, 2020.

Lin, Y.-C., Cheng, M.-T., Ting, W.-Y., and Yeh, C.-R.: Characteristics of gaseous HNO_2, HNO_3, NH_3 and particulate ammonium nitrate in an urban city of Central Taiwan, Atmospheric Environment, 40, 4725-4733, https://doi.org/10.1016/j.atmosenv.2006.04.037, 2006.

Liu, J., Deng, H., Li, S., Jiang, H., Mekic, M., Zhou, W., Wang, Y., Loisel, G., Wang, X., and Gligorovski, S.: Light-Enhanced Heterogeneous Conversion of NO_2 to HONO on Solid Films Consisting of Fluorene and Fluorene/Na_2SO_4: An Impact on Urban and Indoor Atmosphere, Environ Sci Technol, 54, 11079-11086, https://doi.org/10.1021/acs.est.0c02627, 2020a.

Liu, J., Liu, Z., Ma, Z., Yang, S., Yao, D., Zhao, S., Hu, B., Tang, G., Sun, J., Cheng, M., Xu, Z., and Wang, Y.: Detailed budget analysis of HONO in Beijing, China: Implication on atmosphere oxidation capacity in polluted megacity, Atmospheric Environment, 244, 117957, https://doi.org/10.1016/j.atmosenv.2020.117957, 2021.

Liu, Y.: Observations and parameterized modelling of ambient nitrous acid (HONO) in the megacity areas of the eastern China, Ph.D. thsis. College of Environmental Sciences and Engineering, Peking University, China, 2017.

Liu, Y., Lu, K., Li, X., Dong, H., Tan, Z., Wang, H., Zou, Q., Wu, Y., Zeng, L., Hu, M., Min, K. E., Kecorius, S., Wiedensohler, A., and Zhang, Y.: A Comprehensive Model Test of the HONO Sources Constrained to Field Measurements at Rural North China Plain, Environ Sci Technol, https://doi.org/10.1021/acs.est.8b06367, 2019a.

Liu, Y., Nie, W., Xu, Z., Wang, T., Wang, R., Li, Y., Wang, L., Chi, X., and Ding, A.: Semi-quantitative understanding of source contribution to nitrous acid (HONO) based on 1 year of continuous observation at the SORPES station in eastern China, Atmos. Chem. Phys., 19, 13289-13308, https://doi.org/10.5194/acp-19-13289-2019, 2019b.

Liu, Y., Ni, S., Jiang, T., Xing, S., Zhang, Y., Bao, X., Feng, Z., Fan, X., Zhang, L., and Feng, H.: Influence of Chinese New Year overlapping COVID-19 lockdown on HONO sources in Shijiazhuang, Science of The Total Environment, 745, 141025, https://doi.org/10.1016/j.scitotenv.2020.141025, 2020b.

Liu, Y., Zhang, Y., Lian, C., Yan, C., Feng, Z., Zheng, F., Fan, X., Chen, Y., Wang, W., Chu, B., Wang, Y., Cai, J., Du, W., Daellenbach, K. R., Kangasluoma, J., Bianchi, F., Kujansuu, J., Petäjä, T., Wang, X., Hu, B., Wang, Y., Ge, M., He, H., and Kulmala, M.: The promotion effect of nitrous acid on aerosol formation in wintertime in Beijing: the possible contribution of traffic-related emissions, Atmos. Chem. Phys., 20, 13023-13040, https://doi.org/10.5194/acp-20-13023-2020, 2020c.

Lou, S., Holland, F., Rohrer, F., Lu, K., Bohn, B., Brauers, T., Chang, C. C., Fuchs, H., Häseler, R., Kita, K., Kondo, Y., Li, X., Shao, M., Zeng, L., Wahner, A., Zhang, Y., Wang, W., and Hofzumahaus, A.: Atmospheric OH reactivities in the Pearl River Delta – China in summer 2006: measurement and model results, Atmos. Chem. Phys., 10, 11243-11260, https://doi.org/10.5194/acp-10-11243-2010, 2010.

Lu, K. D., Rohrer, F., Holland, F., Fuchs, H., Bohn, B., Brauers, T., Chang, C. C., Häseler, R., Hu, M., Kita, K., Kondo, Y., Li, X., Lou, S. R., Nehr, S., Shao, M., Zeng, L. M., Wahner, A., Zhang, Y. H., and Hofzumahaus, A.: Observation and

modelling of OH and HO_2 concentrations in the Pearl River Delta 2006: a missing OH source in a VOC rich atmosphere, Atmos. Chem. Phys., 12, 1541-1569, https://doi.org/10.5194/acp-12-1541-2012, 2012.

Lu, K. D., Hofzumahaus, A., Holland, F., Bohn, B., Brauers, T., Fuchs, H., Hu, M., Häseler, R., Kita, K., Kondo, Y., Li, X., Lou, S. R., Oebel, A., Shao, M., Zeng, L. M., Wahner, A., Zhu, T., Zhang, Y. H., and Rohrer, F.: Missing OH source in a suburban environment near Beijing: observed and modelled OH and HO_2 concentrations in summer 2006, Atmos. Chem. Phys., 13, 1057-1080, https://doi.org/10.5194/acp-13-1057-2013, 2013.

Lu, K. D., Rohrer, F., Holland, F., Fuchs, H., Brauers, T., Oebel, A., Dlugi, R., Hu, M., Li, X., Lou, S. R., Shao, M., Zhu, T., Wahner, A., Zhang, Y. H., and Hofzumahaus, A.: Nighttime observation and chemistry of HOx in the Pearl River Delta and Beijing in summer 2006, Atmos. Chem. Phys., 14, 4979-4999, https://doi.org/10.5194/acp-14-4979-2014, 2014.

Lu, X., Hong, J., Zhang, L., Cooper, O. R., Schultz, M. G., Xu, X., Wang, T., Gao, M., Zhao, Y., and Zhang, Y.: Severe Surface Ozone Pollution in China: A Global Perspective, Environmental Science & Technology Letters, 5, 487-494, https://doi.org/10.1021/acs.estlett.8b00366, 2018.

Maljanen, M., Yli-Pirilä, P., Hytönen, J., Joutsensaari, J., and Martikainen, P. J.: Acidic northern soils as sources of atmospheric nitrous acid (HONO), Soil Biology and Biochemistry, 67, 94-97, https://doi.org/10.1016/j.soilbio.2013.08.013, 2013.

Malkin, T. L., Heard, D. E., Hood, C., Stocker, J., Carruthers, D., MacKenzie, I. A., Doherty, R. M., Vieno, M., Lee, J., Kleffmann, J., Laufs, S., and Whalley, L. K.: Assessing chemistry schemes and constraints in air quality models used to predict ozone in London against the detailed Master Chemical Mechanism, Faraday Discuss, 189, 589-616, https://doi.org/10.1039/C5FD00218D, 2016.

Marion, A., Morin, J., Gandolfo, A., Ormeño, E., D'Anna, B., and Wortham, H.: Nitrous acid formation on Zea mays leaves by heterogeneous reaction of nitrogen dioxide in the laboratory, Environmental Research, 193, 110543, https://doi.org/10.1016/j.envres.2020.110543, 2021.

Martinez, M., Harder, H., Kovacs, T. A., Simpas, J. B., Bassis, J., Lesher, R., Brune, W. H., Frost, G. J., Williams, E. J., Stroud, C. A., Jobson, B. T., Roberts, J. M., Hall, S. R., Shetter, R. E., Wert, B., Fried, A., Alicke, B., Stutz, J., Young, V. L., White, A. B., and Zamora, R. J.: OH and HO_2 concentrations, sources, and loss rates during the Southern Oxidants Study in Nashville, Tennessee, summer 1999, Journal of Geophysical Research: Atmospheres, 108, https://doi.org/10.1029/2003JD003551, 2003.

Mebel, A. M., Lin, M. C., and Melius, C. F.: Rate Constant of the HONO + HONO $\rightarrow$ H_2O + NO + NO_2 Reaction from ab Initio MO and TST Calculations, The Journal of Physical Chemistry A, 102, 1803-1807, https://doi.org/10.1021/jp973449w, 1998.

Meng, F., Qin, M., Tang, K., Duan, J., Fang, W., Liang, S., Ye, K., Xie, P., Sun, Y., Xie, C., Ye, C., Fu, P., Liu, J., and Liu, W.: High-resolution vertical distribution and sources of HONO and NO_2 in the nocturnal boundary layer in urban Beijing, China, Atmos. Chem. Phys., 20, 5071-5092, https://doi.org/10.5194/acp-20-5071-2020, 2020.

Meusel, H., Kuhn, U., Reiffs, A., Mallik, C., Harder, H., Martinez, M., Schuladen, J., Bohn, B., Parchatka, U., Crowley, J. N., Fischer, H., Tomsche, L., Novelli, A., Hoffmann, T., Janssen, R. H. H., Hartogensis, O., Pikridas, M., Vrekoussis, M., Bourtsoukidis, E., Weber, B., Lelieveld, J., Williams, J., Pöschl, U., Cheng, Y., and Su, H.: Daytime formation of nitrous acid at a coastal remote site in Cyprus indicating a common ground source of atmospheric HONO and NO, Atmos. Chem. Phys., 16, 14475-14493, https://doi.org/10.5194/acp-16-14475-2016, 2016.

Meusel, H., Tamm, A., Kuhn, U., Wu, D., Leifke, A. L., Fiedler, S., Ruckteschler, N., Yordanova, P., Lang-Yona, N., Pöhlker, M., Lelieveld, J., Hoffmann, T., Pöschl, U., Su, H., Weber, B., and Cheng, Y.: Emission of nitrous acid from soil and biological soil crusts represents an important source of HONO in the remote atmosphere in Cyprus, Atmos. Chem. Phys., 18, 799-813, https://doi.org/10.5194/acp-18-799-2018, 2018.

Michoud, V., Kukui, A., Camredon, M., Colomb, A., Borbon, A., Miet, K., Aumont, B., Beekmann, M., Durand-Jolibois, R., Perrier, S., Zapf, P., Siour, G., Ait-Helal, W., Locoge, N., Sauvage, S., Afif, C., Gros, V., Furger, M., Ancellet, G., and Doussin, J. F.: Radical budget analysis in a suburban European site during the MEGAPOLI summer field campaign, Atmos. Chem. Phys., 12, 11951-11974, https://doi.org/10.5194/acp-12-11951-2012, 2012.

Michoud, V., Colomb, A., Borbon, A., Miet, K., Beekmann, M., Camredon, M., Aumont, B., Perrier, S., Zapf, P., Siour, G., Ait-Helal, W., Afif, C., Kukui, A., Furger, M., Dupont, J. C., Haeffelin, M., and Doussin, J. F.: Study of the unknown HONO daytime source at a European suburban site during the MEGAPOLI summer and winter field campaigns, Atmos. Chem. Phys., 14, 2805-2822, https://doi.org/10.5194/acp-14-2805-2014, 2014.

Ndour, M., D'Anna, B., George, C., Ka, O., Balkanski, Y., Kleffmann, J., Stemmler, K., and Ammann, M.: Photoenhanced uptake of NO_2 on mineral dust: Laboratory experiments and model simulations, Geophysical Research Letters, 35, https://doi.org/10.1029/2007GL032006, 2008.

Neuman, J. A., Trainer, M., Brown, S. S., Min, K.-E., Nowak, J. B., Parrish, D. D., Peischl, J., Pollack, I. B., Roberts, J. M., Ryerson, T. B., and Veres, P. R.: HONO emission and production determined from airborne measurements over the Southeast U.S, Journal of Geophysical Research: Atmospheres, 121, 9237-9250, https://doi.org/10.1002/2016JD025197, 2016.

Nie, W., Ding, A. J., Xie, Y. N., Xu, Z., Mao, H., Kerminen, V. M., Zheng, L. F., Qi, X. M., Huang, X., Yang, X. Q., Sun, J. N., Herrmann, E., Petäjä, T., Kulmala, M., and Fu, C. B.: Influence of biomass burning plumes on HONO chemistry in eastern China, Atmos. Chem. Phys., 15, 1147-1159, https://doi.org/10.5194/acp-15-1147-2015, 2015.

Oswald, R., Behrendt, T., Ermel, M., Wu, D., Su, H., Cheng, Y., Breuninger, C., Moravek, A., Mougin, E., Delon, C., Loubet, B., Pommerening-Röser, A., Sörgel, M., Pöschl, U., Hoffmann, T., Andreae, M. O., Meixner, F. X., and Trebs, I.: HONO Emissions from Soil Bacteria as a Major Source of Atmospheric Reactive Nitrogen, Science, 341, 1233-1235, https://doi.org/10.1126/science.1242266, 2013.

Pagsberg, P., Bjergbakke, E., Ratajczak, E., and Sillesen, A.: Kinetics of the gas phase reaction OH + NO(+M)→HONO(+M) and the determination of the UV absorption cross sections of HONO, Chemical Physics Letters, 272, 383-390, https://doi.org/10.1016/S0009-2614(97)00576-9, 1997.

Porada, P., Tamm, A., Raggio, J., Cheng, Y., Kleidon, A., Pöschl, U., and Weber, B.: Global NO and HONO emissions of biological soil crusts estimated by a process-based non-vascular vegetation model, Biogeosciences, 16, 2003-2031, https://doi.org/10.5194/bg-16-2003-2019, 2019.

Qin, M., Xie, P., Su, H., Gu, J., Peng, F., Li, S., Zeng, L., Liu, J., Liu, W., and Zhang, Y.: An observational study of the HONO–NO2 coupling at an urban site in Guangzhou City, South China, Atmospheric Environment, 43, 5731-5742, https://doi.org/10.1016/j.atmosenv.2009.08.017, 2009.

Ren, X., Harder, H., Martinez, M., Lesher, R. L., Oliger, A., Simpas, J. B., Brune, W. H., Schwab, J. J., Demerjian, K. L., He, Y., Zhou, X., and Gao, H.: OH and HO2 Chemistry in the urban atmosphere of New York City, Atmospheric Environment, 37, 3639-3651, https://doi.org/10.1016/S1352-2310(03)00459-X, 2003.

Ren, X., van Duin, D., Cazorla, M., Chen, S., Mao, J., Zhang, L., Brune, W. H., Flynn, J. H., Grossberg, N., Lefer, B. L., Rappenglück, B., Wong, K. W., Tsai, C., Stutz, J., Dibb, J. E., Thomas Jobson, B., Luke, W. T., and Kelley, P.: Atmospheric oxidation chemistry and ozone production: Results from SHARP 2009 in Houston, Texas, Journal of Geophysical Research: Atmospheres, 118, 5770-5780, https://doi.org/10.1002/jgrd.50342, 2013.

Rohrer, F., and Berresheim, H.: Strong correlation between levels of tropospheric hydroxyl radicals and solar ultraviolet radiation, Nature, 442, 184-187, https://doi.org/10.1038/nature04924, 2006.

Saliba, N. A., Yang, H., and Finlayson-Pitts, B. J.: Reaction of Gaseous Nitric Oxide with Nitric Acid on Silica Surfaces in the Presence of Water at Room Temperature, The Journal of Physical Chemistry A, 105, 10339-10346, https://doi.org/10.1021/jp012330r, 2001.

Sarwar, G., Roselle, S. J., Mathur, R., Appel, W., Dennis, R. L., and Vogel, B.: A comparison of CMAQ HONO predictions with observations from the Northeast Oxidant and Particle Study, Atmospheric Environment, 42, 5760-5770, https://doi.org/10.1016/j.atmosenv.2007.12.065, 2008.

Seinfeld, J. H., and Pandis, S. N.: Atmospheric chemistry and physics: from air pollution to climate change, John Wiley & Sons, 2016.

Shao, M., Ren, X., Wang, H., Zeng, L., Zhang, Y., and Tang, X.: Quantitative relationship between production and removal of OH and HO2 radicals in urban atmosphere, Chinese Science Bulletin, 49, 2253-2258, https://doi.org/10.1360/04wb0006, 2004.

Shi, X., Ge, Y., Zhang, Y., Ma, Y., and Zheng, J.: HONO observation and assessment of the effects of atmospheric oxidation capacity in Changzhou during the springtime of 2017, Environmental Science, v.41, 113-121, DOI: 10. 13227/j. hjkx. 201909032, 2020a.

Shi, X., Ge, Y., Zheng, J., Ma, Y., Ren, X., and Zhang, Y.: Budget of nitrous acid and its impacts on atmospheric oxidative capacity at an urban site in the central Yangtze River Delta region of China, Atmospheric Environment, 238, 117725, https://doi.org/10.1016/j.atmosenv.2020.117725, 2020b.

Slater, E. J., Whalley, L. K., Woodward-Massey, R., Ye, C., Lee, J. D., Squires, F., Hopkins, J. R., Dunmore, R. E., Shaw, M., Hamilton, J. F., Lewis, A. C., Crilley, L. R., Kramer, L., Bloss, W., Vu, T., Sun, Y., Xu, W., Yue, S., Ren, L., Acton, W. J. F., Hewitt, C. N., Wang, X., Fu, P., and Heard, D. E.: Elevated levels of OH observed in haze events during wintertime in central Beijing, Atmos. Chem. Phys., 20, 14847-14871, https://doi.org/10.5194/acp-20-14847-2020, 2020.

Song, L., Deng, T., and Wu, D.: Study on planetary boundary layer height in a typical haze period and different weather types over Guangzhou, Acta Scientiae Circumstantiae, 39(5), 1381-1391, DOI: 10.13671/j.hjkxxb.2019.0080, 2019.

Sörgel, M., Regelin, E., Bozem, H., Diesch, J. M., Drewnick, F., Fischer, H., Harder, H., Held, A., Hosaynali-Beygi, Z., Martinez, M., and Zetzsch, C.: Quantification of the unknown HONO daytime source and its relation to NO_2, Atmos. Chem. Phys., 11, 10433-10447, https://doi.org/10.5194/acp-11-10433-2011, 2011a.

Sörgel, M., Trebs, I., Serafimovich, A., Moravek, A., Held, A., and Zetzsch, C.: Simultaneous HONO measurements in and above a forest canopy: influence of turbulent exchange on mixing ratio differences, Atmos. Chem. Phys., 11, 841-855, https://doi.org/10.5194/acp-11-841-2011, 2011b.

Sosedova, Y., Rouvière, A., Bartels-Rausch, T., and Ammann, M.: UVA/Vis-induced nitrous acid formation on polyphenolic films exposed to gaseous NO_2, Photochemical & Photobiological Sciences, 10, 1680-1690, http://dx.doi.org/10.1039/C1PP05113J, 2011.

Spindler, G., Brüggemann, E., and Herrmann, H.: Nitrous acid (HNO_2) concentration measurements and estimation of dry deposition over grassland in eastern Germany, Proceedings of the EUROTRAC Symposium 1998, Vol. 2, WITpress, Southampton, UK, 218–222, 1999.

Stemmler, K., Ammann, M., Donders, C., Kleffmann, J., and George, C.: Photosensitized reduction of nitrogen dioxide on humic acid as a source of nitrous acid, Nature, 440, 195-198, https://doi.org/10.1038/nature04603, 2006.

Stutz, J., Kim, E. S., Platt, U., Bruno, P., Perrino, C., and Febo, A.: UV-visible absorption cross sections of nitrous acid, Journal of Geophysical Research: Atmospheres, 105, 14585-14592, https://doi.org/10.1029/2000JD900003, 2000.

Stutz, J., Alicke, B., and Neftel, A.: Nitrous acid formation in the urban atmosphere: Gradient measurements of NO_2 and HONO over grass in Milan, Italy, Journal of Geophysical Research: Atmospheres, 107, 8192, https://doi.org/10.1029/2001JD000390, 2002.

Stutz, J., Alicke, B., Ackermann, R., Geyer, A., Wang, S., White, A. B., Williams, E. J., Spicer, C. W., and Fast, J. D.: Relative humidity dependence of HONO chemistry in urban areas, Journal of Geophysical Research: Atmospheres, 109, https://doi.org/10.1029/2003JD004135, 2004.

Su, H.: HONO: a study to its sources and impacts from field measurements at the sub-urban areas of PRD region, Ph.D. thsis, College of Environmental Sciences and Engineering, Peking University, China, 2008.

Su, H., Cheng, Y. F., Cheng, P., Zhang, Y. H., Dong, S., Zeng, L. M., Wang, X., Slanina, J., Shao, M., and Wiedensohler, A.: Observation of nighttime nitrous acid (HONO) formation at a non-urban site during PRIDE-PRD2004 in China, Atmospheric Environment, 42, 6219-6232, https://doi.org/10.1016/j.atmosenv.2008.04.006, 2008a.

Su, H., Cheng, Y. F., Shao, M., Gao, D. F., Yu, Z. Y., Zeng, L. M., Slanina, J., Zhang, Y. H., and Wiedensohler, A.: Nitrous acid (HONO) and its daytime sources at a rural site during the 2004 PRIDE-PRD experiment in China, Journal of Geophysical Research, 113, https://doi.org/10.1029/2007JD009060, 2008b.

Su, H., Cheng, Y., Oswald, R., Behrendt, T., Trebs, I., Meixner, F. X., Andreae, M. O., Cheng, P., Zhang, Y., and Pöschl, U.: Soil Nitrite as a Source of Atmospheric HONO and OH Radicals, Science, 333, 1616-1618, https://doi.org/10.1126/science.1207687, 2011.

Tan, Z., Fuchs, H., Lu, K., Hofzumahaus, A., Bohn, B., Broch, S., Dong, H., Gomm, S., Häseler, R., He, L., Holland, F., Li, X., Liu, Y., Lu, S., Rohrer, F., Shao, M., Wang, B., Wang, M., Wu, Y., Zeng, L., Zhang, Y., Wahner, A., and Zhang, Y.: Radical chemistry at a rural site (Wangdu) in the North China Plain: observation and model calculations of OH, HO_2 and RO_2 radicals, Atmos. Chem. Phys., 17, 663-690, https://doi.org/10.5194/acp-17-663-2017, 2017.

Tan, Z., Rohrer, F., Lu, K., Ma, X., Bohn, B., Broch, S., Dong, H., Fuchs, H., Gkatzelis, G. I., Hofzumahaus, A., Holland, F., Li, X., Liu, Y., Liu, Y., Novelli, A., Shao, M., Wang, H., Wu, Y., Zeng, L., Hu, M., Kiendler-Scharr, A., Wahner, A., and Zhang, Y.: Wintertime photochemistry in Beijing: observations of ROx radical concentrations in the North China Plain during the BEST-ONE campaign, Atmos. Chem. Phys., 18, 12391-12411, https://doi.org/10.5194/acp-18-12391-2018, 2018.

Tan, Z., Lu, K., Hofzumahaus, A., Fuchs, H., Bohn, B., Holland, F., Liu, Y., Rohrer, F., Shao, M., Sun, K., Wu, Y., Zeng, L., Zhang, Y., Zou, Q., Kiendler-Scharr, A., Wahner, A., and Zhang, Y.: Experimental budgets of OH, HO2, and RO2 radicals

and implications for ozone formation in the Pearl River Delta in China 2014, Atmos. Chem. Phys., 19, 7129-7150, https://doi.org/10.5194/acp-19-7129-2019, 2019a.

Tan, Z., Lu, K., Jiang, M., Su, R., Wang, H., Lou, S., Fu, Q., Zhai, C., Tan, Q., Yue, D., Chen, D., Wang, Z., Xie, S., Zeng, L., and Zhang, Y.: Daytime atmospheric oxidation capacity in four Chinese megacities during the photochemically polluted season: a case study based on box model simulation, Atmos. Chem. Phys., 19, 3493-3513, https://doi.org/10.5194/acp-19-3493-2019, 2019b.

Tang, X. Y.: The characteristics of urban air pollution in China, in Urbanization, energy, and air pollution in China: The challenges ahead, Proceedings of A Symposium, 47-54, DOI : 10.17226/11192, 2004.

Tang, Y., An, J., Wang, F., Li, Y., Qu, Y., Chen, Y., and Lin, J.: Impacts of an unknown daytime HONO source on the mixing ratio and budget of HONO, and hydroxyl, hydroperoxyl, and organic peroxy radicals, in the coastal regions of China, Atmos. Chem. Phys., 15, 9381-9398, https://doi.org/10.5194/acp-15-9381-2015, 2015.

Tian, Z., Yang, W., Yu, X., Zhang, M., Zhang, H., Cheng, D., Cheng, P., and Wang, B.: HONO pollution characteristics and nighttime sources during autumn in Guangzhou, China Environmental Science, 39 (05), 2000-2009, DOI: 10. 13227/j. hjkx. 201709269, 2018.

Tong, S., Hou, S., Zhang, Y., Chu, B., Liu, Y., He, H., Zhao, P., and Ge, M.: Comparisons of measured nitrous acid (HONO) concentrations in a pollution period at urban and suburban Beijing, in autumn of 2014, Science China Chemistry, 58, 1393-1402, https://doi.org/10.1007/s11426-015-5454-2, 2015.

Tong, S., Hou, S., Zhang, Y., Chu, B., Liu, Y., He, H., Zhao, P., and Ge, M.: Exploring the nitrous acid (HONO) formation mechanism in winter Beijing: direct emissions and heterogeneous production in urban and suburban areas, Faraday Discuss, 189, 213-230, https://doi.org/10.1039/C5FD00163C, 2016.

VandenBoer, T. C., Brown, S. S., Murphy, J. G., Keene, W. C., Young, C. J., Pszenny, A. A. P., Kim, S., Warneke, C., de Gouw, J. A., Maben, J. R., Wagner, N. L., Riedel, T. P., Thornton, J. A., Wolfe, D. E., Dubé, W. P., Öztürk, F., Brock, C. A., Grossberg, N., Lefer, B., Lerner, B., Middlebrook, A. M., and Roberts, J. M.: Understanding the role of the ground surface in HONO vertical structure: High resolution vertical profiles during NACHTT-11, Journal of Geophysical Research: Atmospheres, 118, 10,155-110,171, https://doi.org/10.1002/jgrd.50721, 2013.

VandenBoer, T. C., Young, C. J., Talukdar, R. K., Markovic, M. Z., Brown, S. S., Roberts, J. M., and Murphy, J. G.: Nocturnal loss and daytime source of nitrous acid through reactive uptake and displacement, Nature Geoscience, 8, 55-60, https://doi.org/10.1038/ngeo2298, 2015.

Villena, G., Kleffmann, J., Kurtenbach, R., Wiesen, P., Lissi, E., Rubio, M. A., Croxatto, G., and Rappenglück, B.: Vertical gradients of HONO, NOx and O_3 in Santiago de Chile, Atmospheric Environment, 45, 3867-3873, https://doi.org/10.1016/j.atmosenv.2011.01.073, 2011.

Wang, G., Zhang, R., Gomez, M. E., Yang, L., Levy Zamora, M., Hu, M., Lin, Y., Peng, J., Guo, S., Meng, J., Li, J., Cheng, C., Hu, T., Ren, Y., Wang, Y., Gao, J., Cao, J., An, Z., Zhou, W., Li, G., Wang, J., Tian, P., Marrero-Ortiz, W., Secrest, J., Du, Z., Zheng, J., Shang, D., Zeng, L., Shao, M., Wang, W., Huang, Y., Wang, Y., Zhu, Y., Li, Y., Hu, J., Pan, B., Cai, L., Cheng, Y., Ji, Y., Zhang, F., Rosenfeld, D., Liss, P. S., Duce, R. A., Kolb, C. E., and Molina, M. J.: Persistent sulfate formation from London Fog to Chinese haze, Proceedings of the National Academy of Sciences, 113, 13630-13635, https://doi.org/10.1073/pnas.1616540113, 2016.

Wang, G., Ma, S., Niu, X., Chen, X., Liu, F., Li, X., Li, L., Shi, G., and Wu, Z.: Barrierless HONO and HOS(O)2-NO2 Formation via NH3-Promoted Oxidation of SO2 by NO2, The Journal of Physical Chemistry A, 125, 2666-2672, https://doi.org/10.1021/acs.jpca.1c00539, 2021.

Wang, J., Zhang, X., Guo, J., Wang, Z., and Zhang, M.: Observation of nitrous acid (HONO) in Beijing, China: Seasonal variation, nocturnal formation and daytime budget, Science of The Total Environment, 587-588, 350-359, https://doi.org/10.1016/j.scitotenv.2017.02.159, 2017a.

Wang, S., Zhou, R., Zhao, H., Wang, Z., Chen, L., and Zhou, B.: Long-term observation of atmospheric nitrous acid (HONO) and its implication to local NO_2 levels in Shanghai, China, Atmospheric Environment, 77, 718-724, https://doi.org/10.1016/j.atmosenv.2013.05.071, 2013.

Wang, T., Wei, X. L., Ding, A. J., Poon, C. N., Lam, K. S., Li, Y. S., Chan, L. Y., and Anson, M.: Increasing surface ozone concentrations in the background atmosphere of Southern China, 1994–2007, Atmos. Chem. Phys., 9, 6217-6227, https://doi.org/10.5194/acp-9-6217-2009, 2009.

Wang, T., Xue, L., Brimblecombe, P., Lam, Y. F., Li, L., and Zhang, L.: Ozone pollution in China: A review of concentrations, meteorological influences, chemical precursors, and effects, Science of The Total Environment, 575, 1582-1596, https://doi.org/10.1016/j.scitotenv.2016.10.081, 2017b.

Weber, B., Wu, D., Tamm, A., Ruckteschler, N., Rodriguez-Caballero, E., Steinkamp, J., Meusel, H., Elbert, W., Behrendt, T., Sorgel, M., Cheng, Y., Crutzen, P. J., Su, H., and Poschl, U.: Biological soil crusts accelerate the nitrogen cycle through large NO and HONO emissions in drylands, Proceedings of the National Academy of Sciences, 112, 15384-15389, https://doi.org/10.1073/pnas.1515818112, 2015.

Wen, L., Chen, T., Zheng, P., Wu, L., Wang, X., Mellouki, A., Xue, L., and Wang, W.: Nitrous acid in marine boundary layer over eastern Bohai Sea, China: Characteristics, sources, and implications, Science of The Total Environment, 670, 282-291, https://doi.org/10.1016/j.scitotenv.2019.03.225, 2019.

Wojtal, P., Halla, J. D., and McLaren, R.: Pseudo steady states of HONO measured in the nocturnal marine boundary layer: a conceptual model for HONO formation on aqueous surfaces, Atmos. Chem. Phys., 11, 3243-3261, https://doi.org/10.5194/acp-11-3243-2011, 2011.

Wolfe, G. M., Marvin, M. R., Roberts, S. J., Travis, K. R., and Liao, J.: The Framework for 0-D Atmospheric Modeling (F0AM) v3.1, Geosci. Model Dev., 9, 3309-3319, https://doi.org/10.5194/gmd-9-3309-2016, 2016.

Wong, K. W., Oh, H. J., Lefer, B. L., Rappenglück, B., and Stutz, J.: Vertical profiles of nitrous acid in the nocturnal urban atmosphere of Houston, TX, Atmos. Chem. Phys., 11, 3595-3609, https://doi.org/10.5194/acp-11-3595-2011, 2011.

Wong, K. W., Tsai, C., Lefer, B., Haman, C., Grossberg, N., Brune, W. H., Ren, X., Luke, W., and Stutz, J.: Daytime HONO vertical gradients during SHARP 2009 in Houston, TX, Atmos. Chem. Phys., 12, 635-652, https://doi.org/10.5194/acp-12-635-2012, 2012.

Wu, C., Wu, D., and Yu, J. Z.: Quantifying black carbon light absorption enhancement with a novel statistical approach, Atmos. Chem. Phys., 18, 289-309, https://doi.org/10.5194/acp-18-289-2018, 2018.

Wu, D., Horn, M. A., Behrendt, T., Muller, S., Li, J., Cole, J. A., Xie, B., Ju, X., Li, G., Ermel, M., Oswald, R., Frohlich-Nowoisky, J., Hoor, P., Hu, C., Liu, M., Andreae, M. O., Poschl, U., Cheng, Y., Su, H., Trebs, I., Weber, B., and Sorgel, M.: Soil HONO emissions at high moisture content are driven by microbial nitrate reduction to nitrite: tackling the HONO puzzle, ISME J, 13, 1688-1699, https://doi.org/10.1038/s41396-019-0379-y, 2019.

Wu, Y., Li, S., and Yu, S.: Monitoring urban expansion and its effects on land use and land cover changes in Guangzhou city, China, Environmental Monitoring and Assessment, 188, 54, https://doi.org/10.1007/s10661-015-5069-2, 2015.

Xing, L., Wu, J., Elser, M., Tong, S., Liu, S., Li, X., Liu, L., Cao, J., Zhou, J., El-Haddad, I., Huang, R., Ge, M., Tie, X., Prévôt, A. S. H., and Li, G.: Wintertime secondary organic aerosol formation in Beijing–Tianjin–Hebei (BTH): contributions of HONO sources and heterogeneous reactions, Atmos. Chem. Phys., 19, 2343-2359, https://doi.org/10.5194/acp-19-2343-2019, 2019.

Xu, W., Kuang, Y., Zhao, C., Tao, J., Zhao, G., Bian, Y., Yang, W., Yu, Y., Shen, C., Liang, L., Zhang, G., Lin, W., and Xu, X.: NH3-promoted hydrolysis of NO2 induces explosive growth in HONO, Atmos. Chem. Phys., 19, 10557-10570, https://doi.org/10.5194/acp-19-10557-2019, 2019.

Xu, Z., Wang, T., Xue, L. K., Louie, P. K. K., Luk, C. W. Y., Gao, J., Wang, S. L., Chai, F. H., and Wang, W. X.: Evaluating the uncertainties of thermal catalytic conversion in measuring atmospheric nitrogen dioxide at four differently polluted sites in China, Atmospheric Environment, 76, 221-226, https://doi.org/10.1016/j.atmosenv.2012.09.043, 2013.

Xu, Z., Wang, T., Wu, J., Xue, L., Chan, J., Zha, Q., Zhou, S., Louie, P. K. K., and Luk, C. W. Y.: Nitrous acid (HONO) in a polluted subtropical atmosphere: Seasonal variability, direct vehicle emissions and heterogeneous production at ground surface, Atmospheric Environment, 106, 100-109, https://doi.org/10.1016/j.atmosenv.2015.01.061, 2015.

Xue, C., Zhang, C., Ye, C., Liu, P., Catoire, V., Krysztofiak, G., Chen, H., Ren, Y., Zhao, X., Wang, J., Zhang, F., Zhang, C., Zhang, J., An, J., Wang, T., Chen, J., Kleffmann, J., Mellouki, A., and Mu, Y.: HONO Budget and Its Role in Nitrate Formation in the Rural North China Plain, Environ Sci Technol, 54, 11048-11057, https://doi.org/10.1021/acs.est.0c01832, 2020.

Xue, L., Gu, R., Wang, T., Wang, X., Saunders, S., Blake, D., Louie, P. K. K., Luk, C. W. Y., Simpson, I., Xu, Z., Wang, Z., Gao, Y., Lee, S., Mellouki, A., and Wang, W.: Oxidative capacity and radical chemistry in the polluted atmosphere of Hong Kong and Pearl River Delta region: analysis of a severe photochemical smog episode, Atmos. Chem. Phys., 16, 9891-9903, https://doi.org/10.5194/acp-16-9891-2016, 2016.

Xue, L. K., Wang, T., Gao, J., Ding, A. J., Zhou, X. H., Blake, D. R., Wang, X. F., Saunders, S. M., Fan, S. J., Zuo, H. C., Zhang, Q. Z., and Wang, W. X.: Ground-level ozone in four Chinese cities: precursors, regional transport and heterogeneous processes, Atmos. Chem. Phys., 14, 13175-13188, https://doi.org/10.5194/acp-14-13175-2014, 2014.

Yang, J., Shen, H., Guo, M.-Z., Zhao, M., Jiang, Y., Chen, T., Liu, Y., Li, H., Zhu, Y., Meng, H., Wang, W., and Xue, L.: Strong marine-derived nitrous acid (HONO) production observed in the coastal atmosphere of northern China, Atmospheric Environment, 244, 117948, https://doi.org/10.1016/j.atmosenv.2020.117948, 2021a.

Yang, Q.: Observations and sources analysis of gaseous nitrous acid — A case study in Beijing and Pearl River Delta area, Ph.D. thsis, College of Environmental Sciences and Engineering, Peking University, China, 2014.

Yang, Q., Su, H., Li, X., Cheng, Y., Lu, K., Cheng, P., Gu, J., Guo, S., Hu, M., Zeng, L., Zhu, T., and Zhang, Y.: Daytime HONO formation in the suburban area of the megacity Beijing, China, Science China Chemistry, 57, 1032-1042, https://doi.org/10.1007/s11426-013-5044-0, 2014.

Yang, W., Cheng, P., Tian, Z., Zhang, H., Zhang, M., and Wang, B.: Study on HONO pollution characteristics and daytime unknown sources during summer and autumn in Guangzhou, China., China Environmental Science, 37 (006), 2029-2039, DOI: 10.3969/j.issn.1000-6923.2017.06.005, 2017a.

Yang, W., Han, C., Zhang, T., Tang, N., Yang, H., and Xue, X.: Heterogeneous photochemical uptake of NO2 on the soil surface as an important ground-level HONO source, Environmental Pollution, 271, 116289, https://doi.org/10.1016/j.envpol.2020.116289, 2021b.

Yang, Y., Shao, M., Keßel, S., Li, Y., Lu, K., Lu, S., Williams, J., Zhang, Y., Zeng, L., Nölscher, A. C., Wu, Y., Wang, X., and Zheng, J.: How the OH reactivity affects the ozone production efficiency: case studies in Beijing and Heshan, China, Atmos. Chem. Phys., 17, 7127-7142, https://doi.org/10.5194/acp-17-7127-2017, 2017b.

Yang, Y., Li, X., Zu, K., Lian, C., Chen, S., Dong, H., Feng, M., Liu, H., Liu, J., Lu, K., Lu, S., Ma, X., Song, D., Wang, W., Yang, S., Yang, X., Yu, X., Zhu, Y., Zeng, L., Tan, Q., and Zhang, Y.: Elucidating the effect of HONO on O_3 pollution by a case study in southwest China, Science of The Total Environment, 756, 144127, https://doi.org/10.1016/j.scitotenv.2020.144127, 2021c.

Ye, C., Zhou, X., Pu, D., Stutz, J., Festa, J., Spolaor, M., Cantrell, C., Mauldin, R. L., Weinheimer, A., and Haggerty, J.: ATMOSPHERIC SCIENCE. Comment on "Missing gas-phase source of HONO inferred from Zeppelin measurements in the troposphere", Science, 348, 1326, DOI: 10.1126/science.aaa1992, 2015.

Ye, C., Gao, H., Zhang, N., and Zhou, X.: Photolysis of Nitric Acid and Nitrate on Natural and Artificial Surfaces, Environ Sci Technol, 50, 3530-3536, https://doi.org/10.1021/acs.est.5b05032, 2016.

Ye, C., Zhang, N., Gao, H., and Zhou, X.: Photolysis of Particulate Nitrate as a Source of HONO and NOx, Environmental Science & Technology, 51, 6849-6856, https://doi.org/10.1021/acs.est.7b00387, 2017.

Yue, D. L., Hu, M., Wu, Z. J., Guo, S., Wen, M. T., Nowak, A., Wehner, B., Wiedensohler, A., Takegawa, N., Kondo, Y., Wang, X. S., Li, Y. P., Zeng, L. M., and Zhang, Y. H.: Variation of particle number size distributions and chemical compositions at the urban and downwind regional sites in the Pearl River Delta during summertime pollution episodes, Atmos. Chem. Phys., 10, 9431-9439, https://doi.org/10.5194/acp-10-9431-2010, 2010.

Yue, D. L., Zhong, L., Shen, J., Zhang, T., Zhou, Y., Zeng, L., and Dong, H.: Pollution properties of atmospheric HNO_2 and its effect on OH radical formation in the PRD region in autumn, Environmental Science & Technology, 162-166, DOI: 10.3969/j.issn.1003-6504.2016.02.030, 2016.

Yun, H., Wang, Z., Zha, Q., Wang, W., Xue, L., Zhang, L., Li, Q., Cui, L., Lee, S., Poon, S. C. N., and Wang, T.: Nitrous acid in a street canyon environment: Sources and contributions to local oxidation capacity, Atmospheric Environment, 167, 223-234, https://doi.org/10.1016/j.atmosenv.2017.08.018, 2017.

Yun, H.: Reactive nitrogen ocides (HONO, N_2O_5 and $ClNO_2$) in different atmospheric environment in China: concentrations formation and the impact on atmospheric oxidation capacity, Ph.D. thsis. Department of Civil and Environmental Engineering, The Hong Kong Polytechnic University, China, 2018.

Zha, Q., Xue, L., Wang, T., Xu, Z., Yeung, C., Louie, P. K. K., and Luk, C. W. Y.: Large conversion rates of NO_2 to HNO_2 observed in air masses from the South China Sea: Evidence of strong production at sea surface?, Geophysical Research Letters, 41, 7710-7715, https://doi.org/10.1002/2014GL061429, 2014.

Zhang, B., and Tao, F.-M.: Direct homogeneous nucleation of NO_2, H_2O, and NH_3 for the production of ammonium nitrate particles and HONO gas, Chemical Physics Letters, 489, 143-147, https://doi.org/10.1016/j.cplett.2010.02.059, 2010.

Zhang, J., An, J., Qu, Y., Liu, X., and Chen, Y.: Impacts of potential HONO sources on the concentrations of oxidants and secondary organic aerosols in the Beijing-Tianjin-Hebei region of China, Science of The Total Environment, 647, 836-852, https://doi.org/10.1016/j.scitotenv.2018.08.030, 2019a.

Zhang, L., Wang, T., Zhang, Q., Zheng, J., Xu, Z., and Lv, M.: Potential sources of nitrous acid (HONO) and their impacts on ozone: A WRF-Chem study in a polluted subtropical region, Journal of Geophysical Research: Atmospheres, 121, 3645-3662, https://doi.org/10.1002/2015JD024468, 2016.

Zhang, N., Zhou, X., Shepson, P. B., Gao, H., Alaghmand, M., and Stirm, B.: Aircraft measurement of HONO vertical profiles over a forested region, Geophysical Research Letters, 36, https://doi.org/10.1029/2009GL038999, 2009.

Zhang, W., Tong, S., Ge, M., An, J., Shi, Z., Hou, S., Xia, K., Qu, Y., Zhang, H., Chu, B., Sun, Y., and He, H.: Variations and sources of nitrous acid (HONO) during a severe pollution episode in Beijing in winter 2016, Science of The Total Environment, 648, 253-262, https://doi.org/10.1016/j.scitotenv.2018.08.133, 2019b.

Zheng, J., Zhong, L., Wang, T., Louie, P. K. K., and Li, Z.: Ground-level ozone in the Pearl River Delta region: Analysis of data from a recently established regional air quality monitoring network, Atmospheric Environment, 44, 814-823, https://doi.org/10.1016/j.atmosenv.2009.11.032, 2010.

Zheng, J., Shi, X., Ma, Y., Ren, X., Jabbour, H., Diao, Y., Wang, W., Ge, Y., Zhang, Y., and Zhu, W.: Contribution of nitrous acid to the atmospheric oxidation capacity in an industrial zone in the Yangtze River Delta region of China, Atmos. Chem. Phys., 20, 5457-5475, https://doi.org/10.5194/acp-20-5457-2020, 2020.

Zhong, L., Louie, P. K. K., Zheng, J., Yuan, Z., Yue, D., Ho, J. W. K., and Lau, A. K. H.: Science–policy interplay: Air quality management in the Pearl River Delta region and Hong Kong, Atmospheric Environment, 76, 3-10, https://doi.org/10.1016/j.atmosenv.2013.03.012, 2013.

Zhou, X., Civerolo, K., Dai, H., Huang, G., Schwab, J., and Demerjian, K.: Summertime nitrous acid chemistry in the atmospheric boundary layer at a rural site in New York State, Journal of Geophysical Research: Atmospheres, 107, ACH 13-11-ACH 13-11, https://doi.org/10.1029/2001JD001539, 2002a.

Zhou, X., He, Y., Huang, G., Thornberry, T. D., Carroll, M. A., and Bertman, S. B.: Photochemical production of nitrous acid on glass sample manifold surface, Geophysical Research Letters, 29, 26-21-26-24, https://doi.org/10.1029/2002GL015080, 2002b.

Zhou, X., Gao, H., He, Y., Huang, G., Bertman, S. B., Civerolo, K., and Schwab, J.: Nitric acid photolysis on surfaces in low-NOx environments: Significant atmospheric implications, Geophysical Research Letters, 30, https://doi.org/10.1029/2003GL018620, 2003.

Zhou, X., Huang, G., Civerolo, K., Roychowdhury, U., and Demerjian, K. L.: Summertime observations of HONO, HCHO, and O3 at the summit of Whiteface Mountain, New York, Journal of Geophysical Research: Atmospheres, 112, https://doi.org/10.1029/2006JD007256, 2007.

Zhou, X., Zhang, N., TerAvest, M., Tang, D., Hou, J., Bertman, S., Alaghmand, M., Shepson, P. B., Carroll, M. A., Griffith, S., Dusanter, S., and Stevens, P. S.: Nitric acid photolysis on forest canopy surface as a source for tropospheric nitrous acid, Nature Geoscience, 4, 440-443, https://doi.org/10.1038/ngeo1164, 2011.

Ziemba, L. D., Dibb, J. E., Griffin, R. J., Anderson, C. H., Whitlow, S. I., Lefer, B. L., Rappenglück, B., and Flynn, J.: Heterogeneous conversion of nitric acid to nitrous acid on the surface of primary organic aerosol in an urban atmosphere, Atmospheric Environment, 44, 4081-4089, https://doi.org/10.1016/j.atmosenv.2008.12.024, 2010.

Supplement of

Budget of nitrous acid (HONO) and its impacts on atmospheric oxidation capacity at an urban site in the fall season of Guangzhou, China

Yihang Yu[1,2,†], Peng Cheng[1,2,*,†], Huirong Li[1,2], Wenda Yang[1,2], Baobin Han[1,2], Wei Song[3], Weiwei Hu[3], Xinming Wang[3], Bin Yuan[4,5], Min Shao[4,5], Zhijiong Huang[4], Zhen Li[4], Junyu Zheng[4,5], Haichao Wang[6] and Xiaofang Yu[1,2]

[1]Institute of Mass Spectrometry and Atmospheric Environment, Jinan University, Guangzhou 510632, China
[2]Guangdong Provincial Engineering Research Center for Online Source Apportionment System of Air Pollution, Guangzhou 510632, China
[3]State Key Laboratory of Organic Geochemistry, Guangzhou Institute of Geochemistry, Chinese Academy of Sciences, Guangzhou 510640, China
[4]Institute for Environmental and Climate Research, Jinan University, Guangzhou 511443, China
[5]Guangdong-Hongkong-Macau Joint Laboratory of Collaborative Innovation for Environmental Quality, Guangzhou 511443, China
[6]School of Atmospheric Sciences, Sun Yat-Sen University, Zhuhai, China.

† These authors contribute equally to this paper.

∗ *Correspondence to:* Peng Cheng (chengp@jnu.edu.cn)

Evaluation of model performance

The index of agreement (IOA) can be calculated by E S1 to further evaluate the performance of O_3 simulation against the measurement.

$$IOA = 1 - \frac{\sum_{i=1}^{n} (O_i - S_i)^2}{\sum_{i=1}^{n} (|O_i - \bar{O}| + |S_i - \bar{O}|)^2} \quad \text{(E S1)}$$

where n is a number of data points, and Si and Oi denote box model simulated and observed concentrations, respectively. The IOA ranges from 0 to 1, and a larger IOA value suggests better agreement between model and observation. The IOA of O_3 simulation is 0.78, showing the good performance of model in this study.

The introduction of our custom-built LOPAP

The LOPAP instrument was first developed by Heland et al. (2001), which is based on wet chemical sampling and photometric detection. Ambient air is sampled into an external sampling unit consisting of two similar stripping coils in series. Almost all the HONO and a small fraction of interfering substances (PAN, HNO_3, NO_2, etc.) are absorbed in solution in the first stripping coil, while in the second stripping coil only the interfering species are absorbed. To minimize the potential interferences, we assume the interferences absorbed in the first and the second coil are the same, so the real HONO concentration in the atmosphere is determined by subtracting the measured signal of the second coil from the measured signal of the first coil. The absorption solution R1 is a mixture reagent of 1 L hydrochloric acid (HCl) (37% volume fraction) and 100 g sulfanilamide dissolved in 9 L pure water. The dye solution R2, 2 g n-(1-naphtyl)-ethylendiamine-dihydrchloride (NEDA) dissolved in 10 L pure water, is then reacted with the absorption solution from two stripping coils pumped by a peristaltic pump to form colored azo dye. The light-absorbing colored azo dye is then pumped through a debubbler by the peristaltic pump and flows into the detection unit, which consists of two liquid waveguide capillary cells (World Precision Instrument, LWCC), one LED light source (Ocean Optics), two miniature spectrometers (Ocean Optics, Maya2000Pro) and several optical fibers. To correct for the small zero-drifts in the instrument's baseline, the zero measurements were conducted every 12 h by introducing zero air (highly pure nitrogen). During the instrument's operation, the instrument calibration was performed every week using the standard sodium nitrite ($NaNO_2$) solution.

Detection limit is defined as 3σ of HONO concentration measured in zero air measurement. The detection limit of 5 pptv for this campaign was determined by zero air measurement. This 5 pptv also serves as the precision of the instrument. Time resolution is defined as the time interval between HONO signal decreases from 90% of the signal when start zero air running to 10% higher than the zero signal. It also relates to the liquid flow. The determined time resolution during the campaign is about 15 min considering the air flow of 1 L min^{-1} and liquid flow of 0.4 mL min^{-1}. Measurement error is the sum of statistic error and systematic error. Statistic error is defined as 1σ of HONO signal in zero air measurement. Systematic error is coming from the uncertainties of air flow rate, liquid flow rate and calibration factor, and is about 8% of measured HONO by applying "Gaussian Error Propagation" method (Trebs et al., 2004). The instrument parameters are listed in Table S1.

A commercial LOPAP (QUMA, Germany) operated by the Guangzhou Institute of Geochemistry Chinese Academy of Sciences (GIGCAS) also measured HONO during the observation. Unfortunately, only less than 10 days data were obtained by the commercial LOPAP due to malfunction. Our custom-built LOPAP was validated against the commercial LOPAP instrument with good agreement ($R^2 = 0.910$) (see Fig. S2), which further demonstrated the reliability of our instrument.

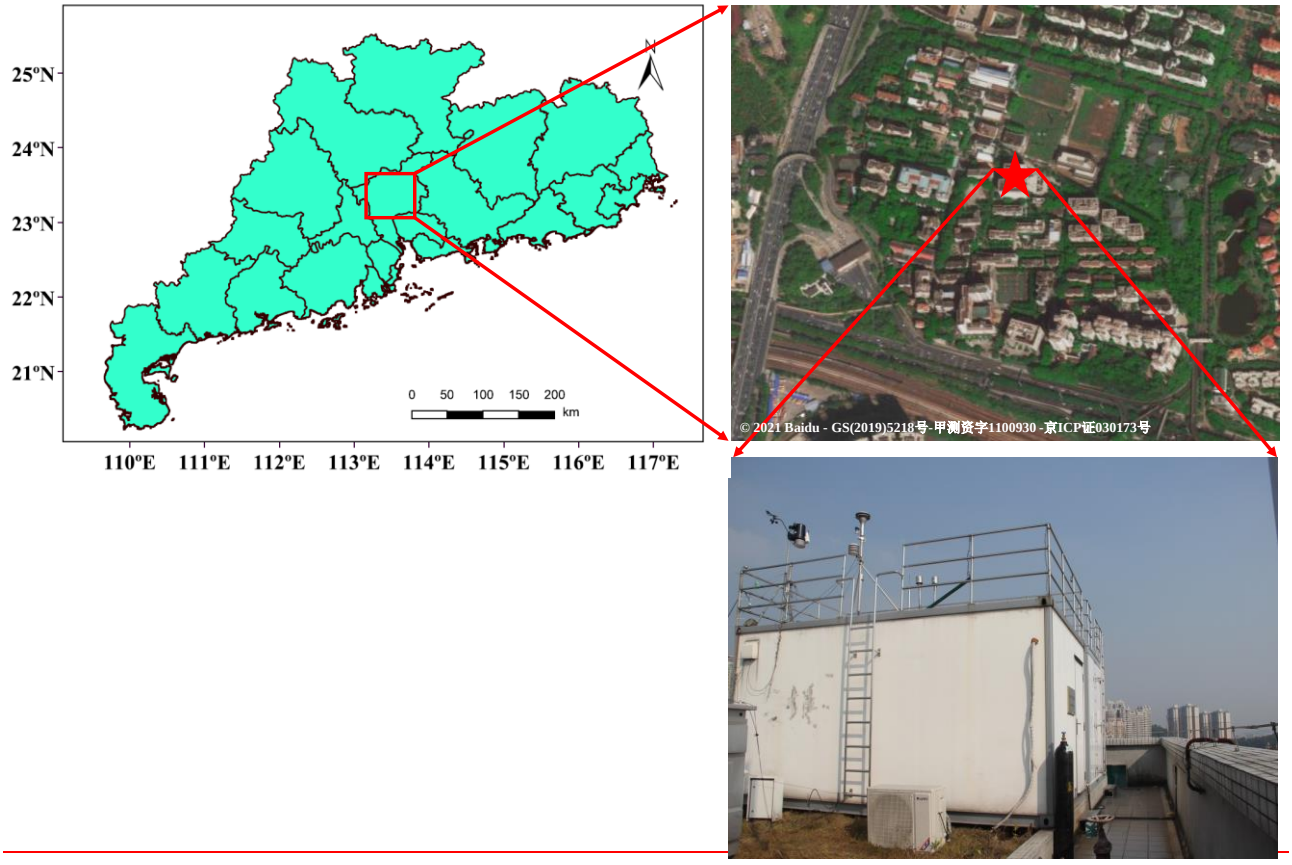
25°N
24°N
23°N
22°N
21°N
110°E
111°E
112°E
113°E
114°E
115°E
116°E
117°E
0 50 100 150 200
km
© 2021 Baidu - GS(2019)5218号-甲测资字1100930 -京ICP证030173号

65

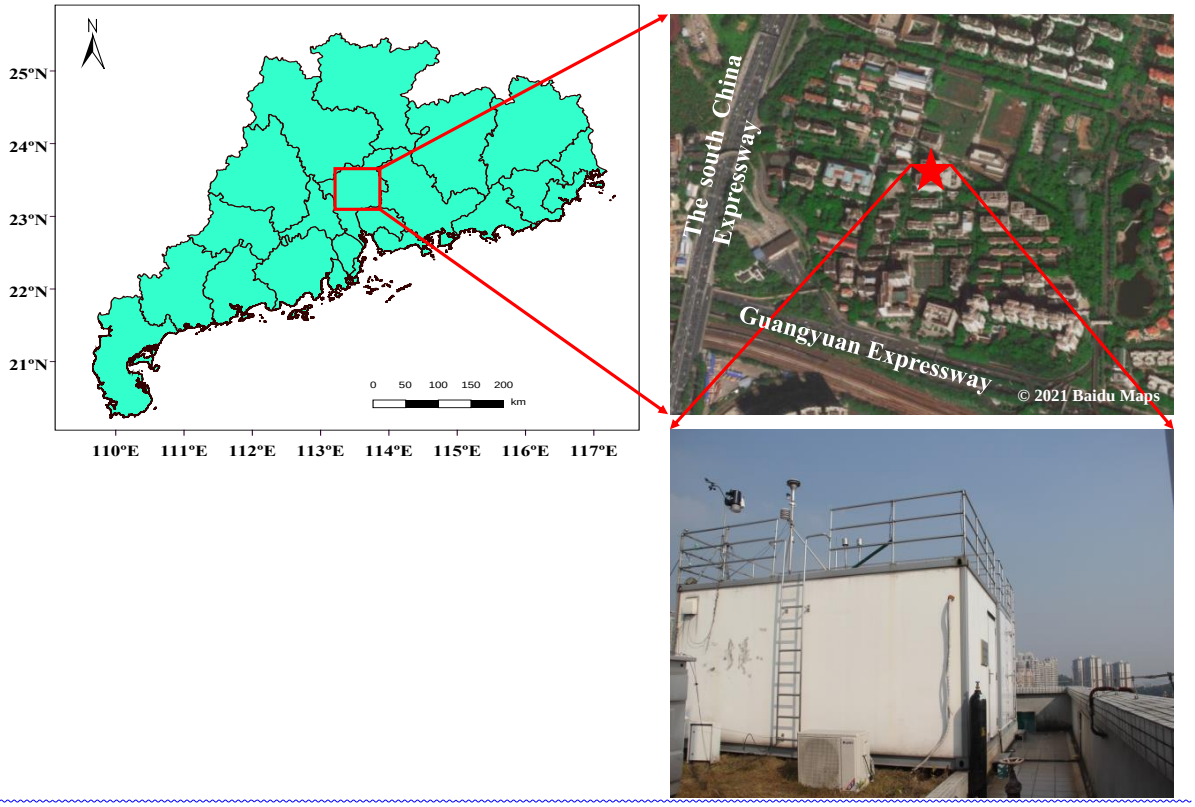

Figure S1. Schematic map of the measurement site in Guangzhou. The red star represents specimen building of the Guangzhou Institute of Geochemistry, Chinese Academy of Sciences (GIGCAS).

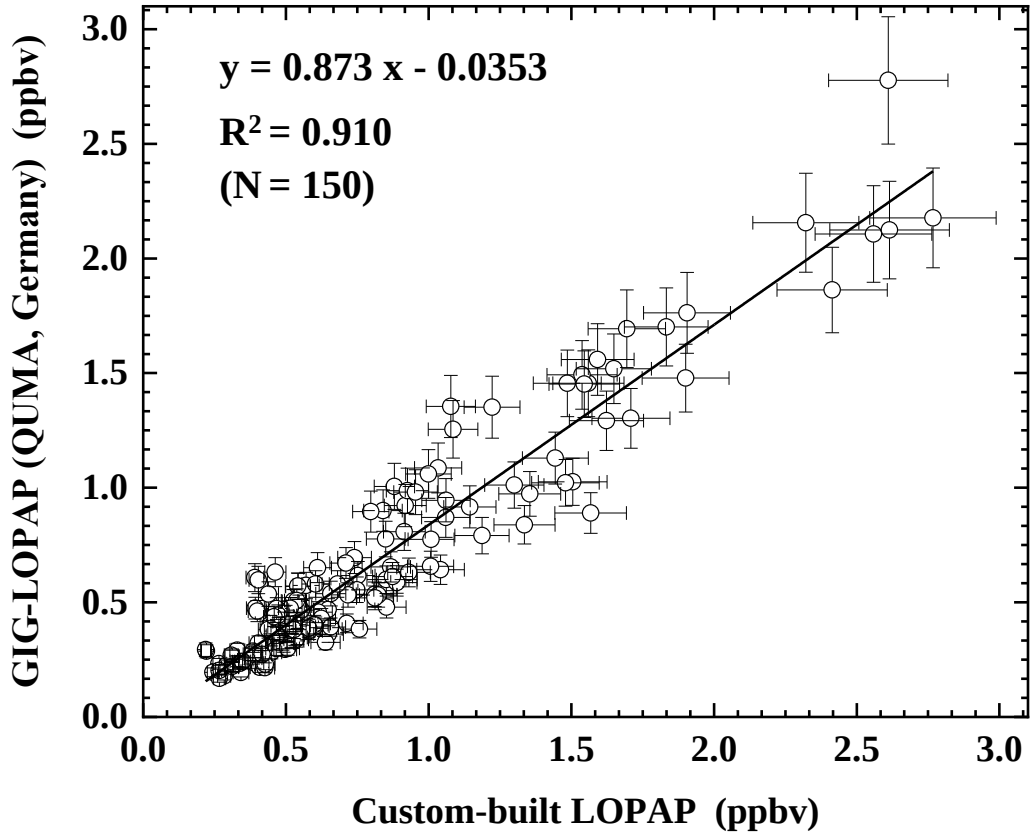

Figure S2. Intercomparison between the custom-built LOPAP with the commercial LOPAP (QUMA, Germany). The linear fitting line has an intercept of A = -0.035 ± 0.022, a slope of B = 0.873 ± 0.023 and R^2 = 0.910 (N = 150). The error bars represent the uncertainties of our custom-built LOPAP (8%) and commercial LOPAP data (QUMA, Germany) (10%). The data from October 15-18 and November 1-6, 2018 was used for comparison.

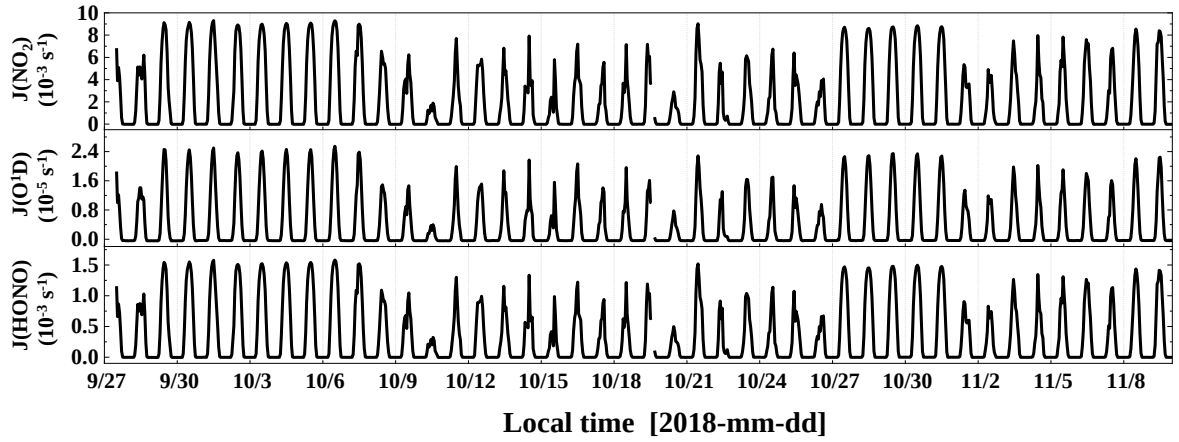

Figure S~~2~~3. Temporal variations of photolysis rates J(HONO), J(O^1D) and J(NO_2) during the observation period.

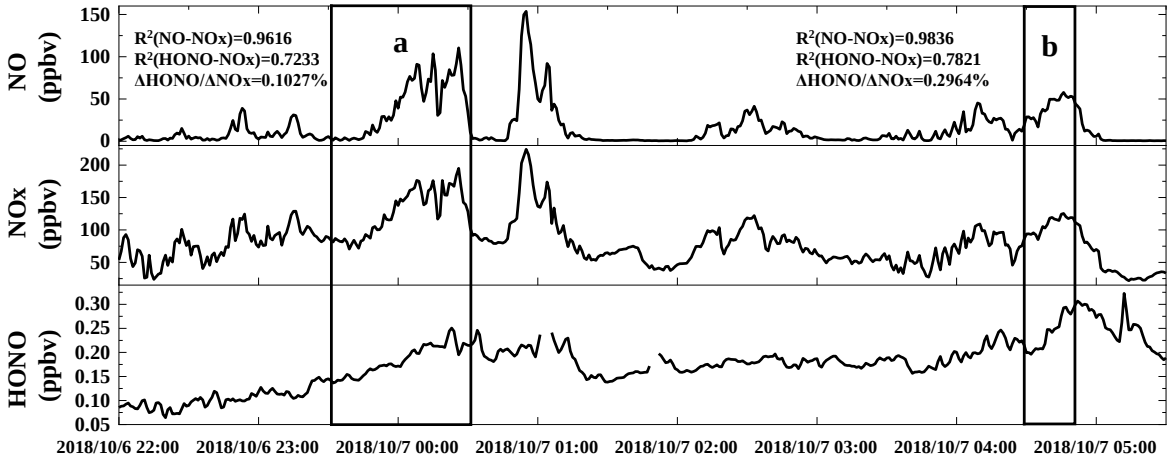

Figure S~~3~~4. Temporal variations of nocturnal HONO, NOx and NO on October 6–7, 2018. The HONO emission factors were obtained according to the data in the black frames a and b.

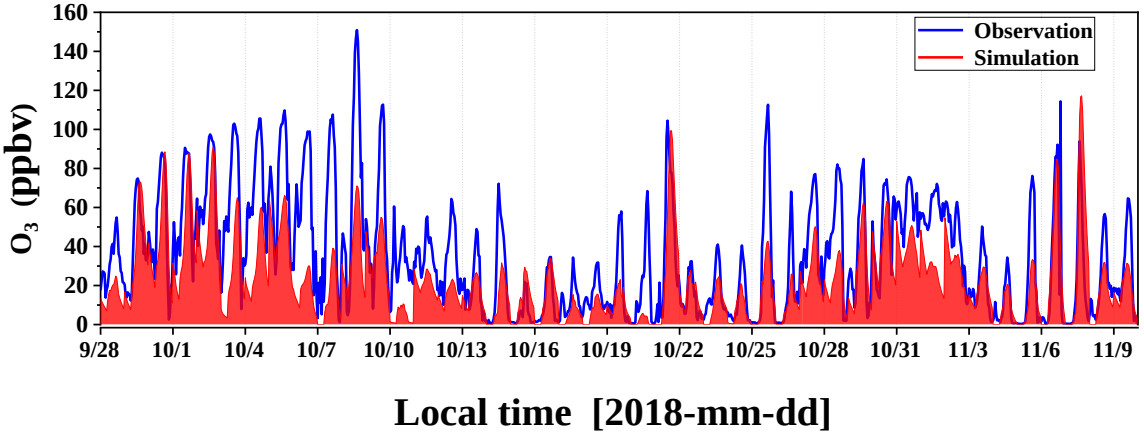

Figure S45. The time series of measured and simulated O_3 values.

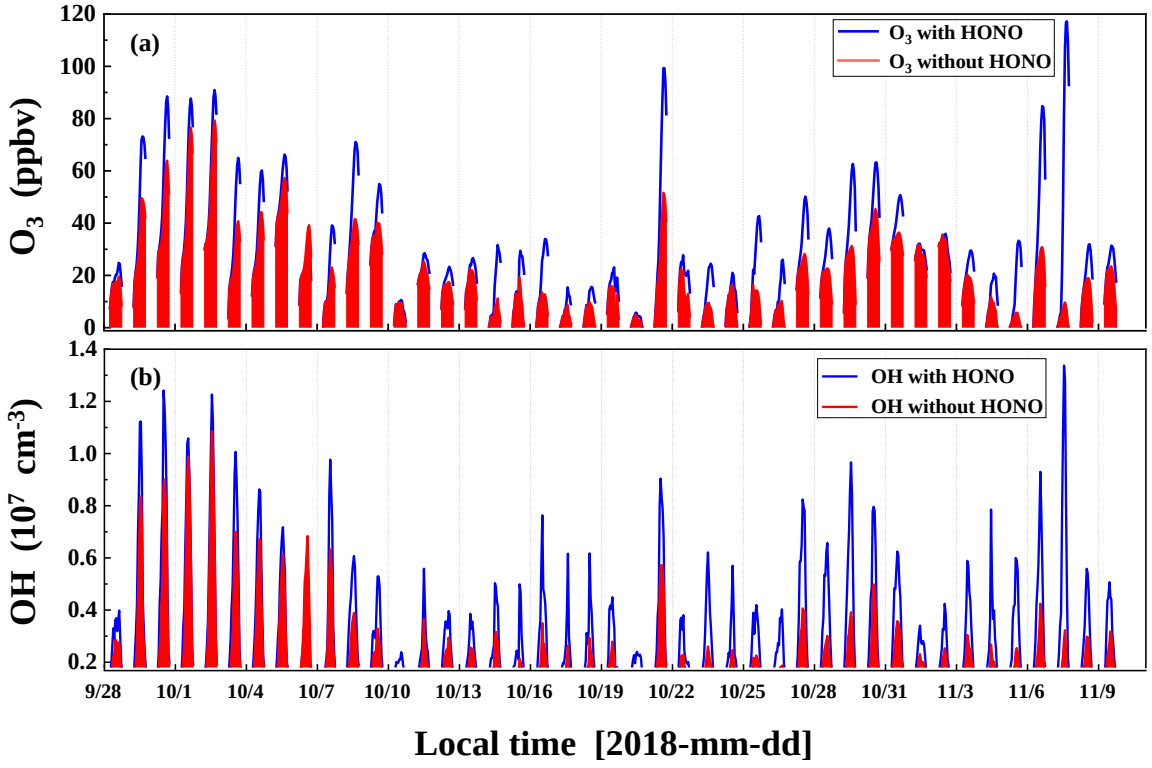

Figure S56. The time series of simulation results of O_3 and OH.

Table S1. The parameters of our custom-built LOPAP.

Parameters	Values
Air flow	1 L min^{-1}
Liquid flow	0.4 mL min^{-1}
Length of LWCC	100 cm
Detection limit	5 pptv
Detection range	5 pptv–10 ppbv
Time resolution	15 min
Uncertainty	8%

Table S2. The VOCs species constrained in the F0AM model.

Classification	Measured hydrocarbons
Alkane	CYCLOHEXANE, ETHANE, N-BUTANE, N-DECANE, N-NONANE, N-OCTANE, PROPANE, 2-METHYLHEXANE, 2-METHYLPENTANE, 3-METHYLHEXANE, 3-METHYLPENTANE, 2-METHYLPROPANE, 2-METHYLBUTANE, PENTANE, HEXANE, HEPTANE, HENDECANE
Alkene	PROPENE, TRANS-2-BUTENE, TRANS-2-PENTENE, 1-BUTENE, 1-PENTENE, 1-HEXENE, CIS-2-BUTENE, CIS-2-PENTENE, STYRENE
ISO	ISOPRENE
Alkyne	ETHYNE
Aromatic	BENZENE, N-PROPYLBENZENE, 1-2-3-TRIMETHYLBENZENE, 1-2-4-TRIMETHYLBENZENE, 1-3-5-TRIMETHYLBENZENE, METHYLBENZENE, ETHYLBENZENE, 1,4-DIMETHYLBENZENE, 1,2-DIMETHYLBENZENE, I-PROPYLBENZENE, 1-ETHYL-3-METHYLBENZENE, 1-ETHYL-4-METHYLBENZENE, 1-ETHYL-2-METHYLBENZENE

Table S~~1~~3. Emission factors (ΔHONO/ΔNOx) and other information in 11 fresh plumes.

Starting time	Duration (min)	R^2 (NO-NOx)	R^2 (HONO-NOx)	ΔNO/ΔNOx	HONO/NOx	ΔHONO/ΔNOx
2018/10/6 23:29	62	0.9616	0.7233	0.90	0.002	0.001
2018/10/7 4:29	22	0.9836	0.7821	0.97	0.002	0.003
2018/10/7 20:44	34	0.9559	0.7054	0.88	0.011	0.010
2018/10/7 22:49	22	0.9904	0.8051	1.05	0.013	0.008
2018/10/20 0:33	24	0.9621	0.7826	0.96	0.020	0.007
2018/10/21 6:28	40	0.9959	0.9403	0.89	0.021	0.014
2018/10/25 6:55	20	0.9615	0.7291	1.04	0.024	0.014
2018/11/4 19:04	22	0.9761	0.8148	1.05	0.022	0.011
2018/11/4 22:01	78	0.9892	0.7684	1.02	0.016	0.007
2018/11/6 7:31	29	0.9835	0.7902	1.03	0.029	0.009
2018/11/7 4:56	30	0.9750	0.7007	0.93	0.027	0.015

Table S4. The overview of percentage of nighttime primary emissions of HONO from urban sites in China.

Location	Date	Nighttime NOx (ppbv)	$[HONO]_{emis}/[HONO]$ (%)	Emission ratio HONO/NOx (%)	Reference
Guangzhou	Oct 2015	57.9	15.1	0.65	1
Guangzhou	Sep–Nov 2018	47.7	47	0.9	2
Shanghai	May 2016	–	12.5	0.65	3
Changzhou	Apr 2017	–	31.4	0.69	4
Zhengzhou	Jan 2019	41 68.7 107.3	17[a] 16[b] 16[c]	0.65	5
Ji'nan	Nov 2013–Jan 2014	–	42	0.58	6
Ji'nan	Sep–Nov 2015 Dec 2015–Feb 2016 Mar–May 2016 Jun–Aug 2016	38 78.5 47.3 29.1	18 21 12 15	0.53	7
Beijing	Jan–Feb 2007 Aug 2007	– –	20.59 11.68	0.65	8
Beijing	Oct–Nov 2014	94.5	39.6	0.65	9
Beijing	Dec 2015	–	48.8	0.8	10
Beijing	Dec 2015	– –	52[b] 40[c]	1.3	11
Beijing	Dec 2016	–	29.3	0.78	12
Beijing	May–Jul 2018 Nov 2018–Jan 2019	– –	14.21 30.79	0.78	13

[a]: clean; [b]: polluted; [c]: severely polluted. Reference: 1. Tian et al. (2018); 2. This work; 3. Cui et al. (2018); 4. Shi et al. (2020); 5. Hao et al. (2020); 6. Wang et al. (2015); 7. Li et al. (2018); 8. Spataro et al. (2013); 9. Tong et al. (2015); 10. Tong et al. (2016); 11. Zhang et al. (2019); 12. Meng et al. (2020); 13. Liu et al. (2021).

Table S25. The OH concentration is assumed of 1.0 × 10^6 molecules cm^{-3}. The integrated P_{net} of homogeneous reaction of NO + OH from 18:00 to 6:00.

OH/molecules cm^{-3}	Integrated P_{net}/ppbv	Measured HONO/ppbv
1×10^5	0.34	0.26
5×10^5	1.54	
1×10^6	3.24	
2×10^6	6.17	

Table S6. Ozonolysis reaction rate constants and OH formation yields of the volatile organic compounds (VOC) used in the calculation.

VOC	k (298 K)/($\times 10^{-18}$ cm^3 molec.$^{-1}$ s^{-1})[a]	OH yield
PROPENE	10.1	0.34[b]
TRANS-2-BUTENE	190	0.59[b]
TRANS-2-PENTENE	160	0.47[c]
1-BUTENE	9.64	0.41[b]
1-HEXENE	11.3	0.32[b]
1-PENTENE	10.6	0.37[b]
CIS-2-BUTENE	125	0.37[b]
CIS-2-PENTENE	130	0.3[c]
STYRENE	17	0.07[c]
ISOPRENE	12.8[c]	0.13 ± 0.03[c]

[a] Atkinson and Arey (2003); [b] Rickard et al. (1999); [c] Alicke et al. (2002)

References

Alicke, B., Platt, U., and Stutz, J.: Impact of nitrous acid photolysis on the total hydroxyl radical budget during the Limitation of Oxidant Production/Pianura Padana Produzione di Ozono study in Milan, Journal of Geophysical Research: Atmospheres, 107, 8196, https://doi.org/10.1029/2000JD000075, 2002.

Atkinson, R., and Arey, J.: Atmospheric Degradation of Volatile Organic Compounds, Chemical Reviews, 103, 4605-4638, https://doi.org/10.1021/cr0206420, 2003.

Cui, L., Li, R., Zhang, Y., Meng, Y., Fu, H., and Chen, J.: An observational study of nitrous acid (HONO) in Shanghai, China: The aerosol impact on HONO formation during the haze episodes, Science of The Total Environment, 630, 1057-1070, https://doi.org/10.1016/j.scitotenv.2018.02.063, 2018.

Hao, Q., Jiang, N., Zhang, R., Yang, L., and Li, S.: Characteristics, sources, and reactions of nitrous acid during winter at an urban site in the Central Plains Economic Region in China, Atmos. Chem. Phys., 20, 7087-7102, https://doi.org/10.5194/acp-20-7087-2020, 2020.

Heland, J., Kleffmann, J., Kurtenbach, R., and Wiesen, P.: A New Instrument To Measure Gaseous Nitrous Acid (HONO) in the Atmosphere, Environmental Science & Technology, 35, 3207-3212, https://doi.org/10.1021/es000303t, 2001.

Li, D., Xue, L., Wen, L., Wang, X., Chen, T., Mellouki, A., Chen, J., and Wang, W.: Characteristics and sources of nitrous acid in an urban atmosphere of northern China: Results from 1-yr continuous observations, Atmospheric Environment, 182, 296-306, https://doi.org/10.1016/j.atmosenv.2018.03.033, 2018.

Liu, J., Liu, Z., Ma, Z., Yang, S., Yao, D., Zhao, S., Hu, B., Tang, G., Sun, J., Cheng, M., Xu, Z., and Wang, Y.: Detailed budget analysis of HONO in Beijing, China: Implication on atmosphere oxidation capacity in polluted megacity, Atmospheric Environment, 244, 117957, https://doi.org/10.1016/j.atmosenv.2020.117957, 2021.

Meng, F., Qin, M., Tang, K., Duan, J., Fang, W., Liang, S., Ye, K., Xie, P., Sun, Y., Xie, C., Ye, C., Fu, P., Liu, J., and Liu, W.: High-resolution vertical distribution and sources of HONO and NO_2 in the nocturnal boundary layer in urban Beijing, China, Atmos. Chem. Phys., 20, 5071-5092, https://doi.org/10.5194/acp-20-5071-2020, 2020.

Rickard, A. R., Johnson, D., McGill, C. D., and Marston, G.: OH Yields in the Gas-Phase Reactions of Ozone with Alkenes, The Journal of Physical Chemistry A, 103, 7656-7664, https://doi.org/10.1021/jp9916992, 1999.

Shi, X., Ge, Y., Zheng, J., Ma, Y., Ren, X., and Zhang, Y.: Budget of nitrous acid and its impacts on atmospheric oxidative capacity at an urban site in the central Yangtze River Delta region of China, Atmospheric Environment, 238, 117725, https://doi.org/10.1016/j.atmosenv.2020.117725, 2020.

Spataro, F., Ianniello, A., Esposito, G., Allegrini, I., Zhu, T., and Hu, M.: Occurrence of atmospheric nitrous acid in the urban area of Beijing (China), Science of The Total Environment, 447, 210-224, https://doi.org/10.1016/j.scitotenv.2012.12.065, 2013.

Tian, Z., Yang, W., Yu, X., Zhang, M., Zhang, H., Cheng, D., Cheng, P., and Wang, B.: HONO pollution characteristics and nighttime sources during autumn in Guangzhou, China Environmental Science, 39 (05), 2000-2009, DOI: 10. 13227/j. hjkx. 201709269, 2018.

Tong, S., Hou, S., Zhang, Y., Chu, B., Liu, Y., He, H., Zhao, P., and Ge, M.: Comparisons of measured nitrous acid (HONO) concentrations in a pollution period at urban and suburban Beijing, in autumn of 2014, Science China Chemistry, 58, 1393-1402, https://doi.org/10.1007/s11426-015-5454-2, 2015.

Tong, S., Hou, S., Zhang, Y., Chu, B., Liu, Y., He, H., Zhao, P., and Ge, M.: Exploring the nitrous acid (HONO) formation mechanism in winter Beijing: direct emissions and heterogeneous production in urban and suburban areas, Faraday Discuss, 189, 213-230, https://doi.org/10.1039/C5FD00163C, 2016.

Trebs, I., Meixner, F. X., Slanina, J., Otjes, R., Jongejan, P., and Andreae, M. O.: Real-time measurements of ammonia, acidic trace gases and water-soluble inorganic aerosol species at a rural site in the Amazon Basin, Atmos. Chem. Phys., 4, 967-987, https://doi.org/10.5194/acp-4-967-2004, 2004.

Wang, L., Wen, L., Xu, C., Chen, J., Wang, X., Yang, L., Wang, W., Yang, X., Sui, X., Yao, L., and Zhang, Q.: HONO and its potential source particulate nitrite at an urban site in North China during the cold season, Science of The Total Environment, 538, 93-101, https://doi.org/10.1016/j.scitotenv.2015.08.032, 2015.

Zhang, W., Tong, S., Ge, M., An, J., Shi, Z., Hou, S., Xia, K., Qu, Y., Zhang, H., Chu, B., Sun, Y., and He, H.: Variations and sources of nitrous acid (HONO) during a severe pollution episode in Beijing in winter 2016, Science of The Total Environment, 648, 253-262, https://doi.org/10.1016/j.scitotenv.2018.08.133, 2019.